Deltares

Long-term morphological modelling of the Mouth of the Columbia River

E.Moerman
1158538

Deltares

Long-term morphological modelling of the Mouth of the Columbia River

E.Moerman
1158538

Deltares

Title
Long-term morphological modelling
of the Mouth of the Columbia River

Pages
155

Abstract
With the construction of a process-based long-term morphological model (Delft3D) for the Mouth of the Columbia River (MCR), a first approach is made in trying to simulating the long-term morphodynamics of the MCR. Focus is on simulating the observed morphological changes for the post-jetty period of 1926-1958. The model is supplied with a high-resolution schematisation of river discharge and wave conditions in combination with a representative tide. Seasonal variations of the forcing conditions and their joint probability of occurrence are accounted for. Morphological acceleration techniques allow the simulations to stay with acceptable computation times. General patterns of erosion and sedimentation as a result of jetty construction as well as general bed level developments are represented by the model. Both the model and the observations show that jetty construction pre-dominantly pushed sediments from the inlet and the inner delta onto the outer delta. Differences in quantity and orientation are however present between the observations and the model. Despite the application of lower limit sediment transport calibration factors, a general overestimation of the morphological change is computed. Also, a wider and shallower inlet channel develops in the model. The interaction of the MCR with the adjacent coast is modelled to a limited extent only. Certain morphologically important physical processes may still be missing in the model. The representation of forcing conditions responsible for morphological change at the MCR allows for optimization. Even though model results in this study do not fully simulate the observed morphological changes of the MCR yet, an important first step has been taken in the goal of simulating the long-term morphological change of the complex coastal area of the MCR. The products of this study provide a valuable base for continuing research.

Keywords
Delft3D, long-term morphodynamics, tidal delta, jetty construction, Columbia River

Supervising committee

Prof. dr. ir. M.J.F. Stive	(TU Delft)
ir. A.P. Luijendijk	(Deltares)
dr. ir. E. Elias	(Deltares/USGS)
ir. M. van Ormondt	(Deltares)
dr. G. Gelfenbaum	(USGS)
dr. ir. J.E.A. Storms	(TU Delft)

Version	Date	Author	Initials	Review	Initials	Approval	Initials
1	19-01-2011	E. Moerman	EM	A.P. Luijendijk	APL	M.J.F. Stive	MJFS
				E. Elias	EE		
				M. van Ormondt	MvO		
				G. Gelfenbaum	GG		
				J.E.A. Storms	JEAS		

State
final

Preface

"The world is round and the place which may seem like the end may also be the beginning"
-Ivy Baker Priest, Amerikaans politicus, eind jaren '50.

This thesis is written to complete my Master of Science in Coastal Engineering at the faculty of Civil Engineering and Geosciences of Delft University of Technology, the Netherlands. It brings me at an important checkpoint in life: the finalization of my academic career and the beginning of my professional career.

The thesis describes the development and results of a process-based numerical model in the application of long-term morphodynamic modelling of the Mouth of the Columbia River (MCR) in the United States of America. A cooperation between Deltares, United States Geological Survey (USGS) and Delft University of Technology made the thesis possible.

I would like to thank the members of my supervising committee. Professor Marcel Stive, for putting me in contact with Deltares, for his motivating lectures, experience and insights within the committee as well a during my Masters in general. Arjen Luijendijk, for being my daily supervisor at Deltares, for always being available for another problem with modelling, for having quick solutions ready at the minute and his constant enthousiasm during the length of my thesis. Edwin Elias for being my supervisor during my stay at USGS, Menlo Park, for his knowledge on the Columbia River, for adressing the importance of being critical, and general devotion. Guy Gelfenbaum, for making my stay in the United States even better and for his experience and enthousiasm. Furthermore I would like to thank Maarten van Ormondt and Joep Storms for completing the committee. Dirk-Jan Walstra for providing the thesis subject, Andrew Stevens for his help with Matlab and all of the other colleagues at Deltares and USGS.

Emiel Moerman

Delft, January, 2011

Summary

Construction of entrance jetties at the end of the 19th century has been the dominant driver of coastal change at the Mouth of the Columbia River (United States of America). Jetty construction confined the entrance and increased tidal currents deepened and stabilized the main inlet channel and eroded the existing tidal delta. Over decades, sand from the scoured delta accumulated in a new ebb-tidal delta further offshore and wave and current processes distributed the sediment onto the adjacent shores, causing beaches near the jetties to rapidly grow and form new land. An over time, decreasing availability of sediment at the mouth however, recently caused several former strongly accreting beaches to erode. With sediment in short supply, the system may be entering a long-term period of erosion.

The problem of erosion called for a better understanding of the hydrodynamic and morphodynamic behaviour of the area. Evaluation of long-term morphological change at the Mouth of the Columbia River (MCR) using process-based numerical modelling (Delft3D) could provide a valuable insight in processes driving morphological change. A better understanding of the morphodynamic behaviour of the MCR can ultimately lead to predictive modelling and support management dredging and coastal planning.

The MCR is a complex area where saline ocean tides, strong fresh river flows with high sediment carrying capacities, and a high-energy wave climate meet. An important task in long-term morphological modelling of the MCR is therefore the schematizations of these forcing conditions. The strong seasonal variation of the forcing conditions should herein be accounted for. Furthermore, input reduction and morphological acceleration techniques need to be applied to keep the computations within practical time limits, in which the scale of interest of the model needs to be kept in mind at all times.

The main goal of this thesis was to develop a long-term morphological model for the MCR and investigate methods and modelling approaches in simulating the complex morphodynamics of the MCR. Focus is on simulating the observed changes for the post-jetty construction period of 1926-1958. However, verification of the model performance in simulating the observed morphological performance of the consectutive era from 1958-1999 is also done. The model is forced with a representative tide and a high-resolution schematization of the river discharge and wave conditions that accounts for the seasonal joint probability between the two.

As a first approach in simulating the long-term morphodynamics for the MCR, the model is considered to have an acceptable performance. Computational times stay within acceptable limits (about 8 days for 30 years of morphological simulation). The general patterns of erosion and sedimentation as a result of jetty construction as well as general bed levels are represented reasonably well by the model. Both the model and observations show that jetty construction predominantly pushed sediments from the inlet and inner delta onto the outer delta.

The model results are however not perfect yet. Differences in both quantity and orientation are present between the observed and computed morphological changes. Despite the application of strongly reduced sediment transport calibration factors, a general overestimation of the morphological change is computed. This may imply that certain morphologically important physical processes may still be missing in the model. A limited interaction of the model with the adjacent coasts is an example. Optimization of the

representation of the forcing conditions responsible for long-term morphological change at the MCR might therefore still be possible. Furthermore, a general wider, shallower and more southern orientated inlet channel develops in the model. Model shortcomings as relative large grid cell dimensions within the area of the inlet, as well as user-imposed deficiencies as the omission of several small-scale structures (groynes) and dredging activities are considered to be the reason for the less pronounced channel formation in the model.

Limited performance of the model in simulating the morphological change of the consecutive era of 1958-1999 was reached under the same model settings. Incomplete available bathymetric coverage and significant change in forcing conditions as the introduction of severe dredging activities and regulated river flows as a result of dam construction are addressed as reasons.

Model simulations based on lower level of detail of forcing conditions schematizations (mean river discharge and basic wave climate schematization versus variable river discharge and high-resolution wave climate schematization) showed to be capable of simulating the general morphological change to a certain degree (relative difference of less than 20%). The dominance of the tide in the morphological development seems to allow for a reduction of the level of detail in the schematization of especially the river discharge and to a limited extent also of the wave conditions. However, with the model not fully representing the observed morphological changes in the simulation with the higher level of detail of schematization of forcing conditions, a lower level of detail seems not at place.

Even though model results in this study do not fully simulate the observed morphological changes of the MCR, it is felt that an important first step has been taken in the goal of simulating the long-term morphological change of the complex coastal area of the MCR. The products of this study will provide a valuable base for continuing research.

With the model not capturing the long-term morphological change to its full extent, improvement of the model results may be reached by the optimization of the forcing conditions. In particular forcing conditions responsible for sediment transport to the adjacent coasts are represented to a limited extent only. Furthermore, it is recommended that in the simulation of more present day conditions, dredging activities should be accounted for by the model since the morphological impact of dreding activities becomes more significant.

Contents

List of Tables

List of Figures

1 Introduction

1.1 Background

Throughout the Holocene, the Columbia River Littoral Cell (CRLC) has been an area of constant coastal change. Various drivers such as changing rates of sea-level rise, co-seismic subsidence events, inter-annual climatic fluctuations (El Niño cycles), a seasonally varying wave climate, and numerous anthropogenic influences such as the construction of over 400 dams within the Columbia River drainage basin, dredging of navigation channels, and the constructions of entrance jetties at the mouth of both the Grays Harbor and Columbia River estuary are the reason for the dynamic behaviour of the system. The construction of the entrance jetties at the end of the 19th century has been the dominant driver of coastal change throughout most of the littoral cell over the last century (Gelfenbaum and Kaminsky, 2010).

The major supplier of sediment to the CRLC is the Columbia River. At the mouth, sediments from the river are temporarily stored in the ebb-tidal delta and wave and current processes are responsible for distributing the sediment from the ebb-delta both north and southward into the littoral cell and onto the adjacent beaches. Jetty construction had an effect of confining the entrance and of deepening and stabilizing the main inlet channels in which the entrance channel as well as the ebb-tidal delta eroded. Over decades, sand from the scoured delta accumulated in a new area further offshore and the littoral drift distributed this sediment onshore causing beaches near the jetties to rapidly grow and form new land. The decreasing availability of sediment from the scoured ebb-tidal delta at the mouth over time as a result of the dispersive behaviour of the waves and general littoral drift together with the reduced overall sediment supply from the river to the mouth due to severe damming of the Columbia River basin recently caused several former strongly accreting beaches in the CRLC to erode (Figure 1.1). The need to obtain a broader understanding of the system's coastal erosion problem and the desire to be able to describe and quantify the processes responsible for this morphological change have been the initiators of this study.

1.2 Area description

1.2.1 Location

The Columbia River Littoral Cell is located at the Northwest coast of the United States of America. It is 165 km in length and takes up the coastal area between the rocky headlands of Point Grenville, Washington and Tillamook Head, Oregon (Figure 1.1). Within the littoral cell three large estuaries, Grays Harbor, Willapa Bay and the Columbia River are present. The presence of the two headlands and the estuaries subdivide the CRLC into four sub-cells, from north to south denoted as: North Beach, Grayland Plains, Long Beach Peninsula, and Clatsop Plains.

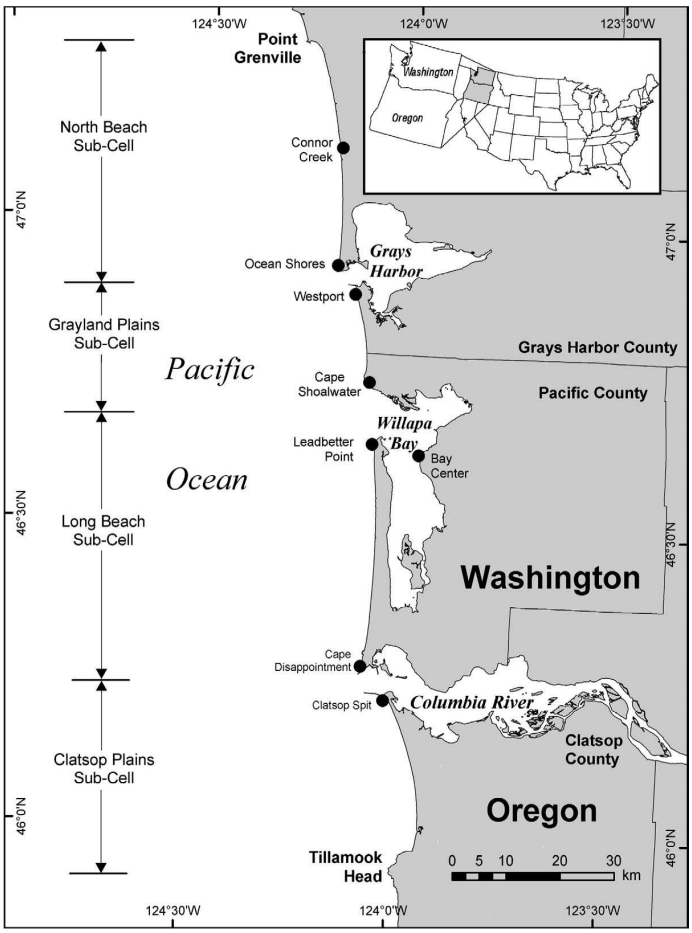

Figure 1.1 CRLC with name places and erosion hot spots (black dots) (Gelfenbaum and Kaminsky ,2010).

1.2.2 Tide

The north-eastern Pacific Ocean is characterized by a mixed semi-diurnal tide with a mean tidal range of around 2.4 m. On top of this semi-diurnal tide, a lunar cycle induces a low-frequency variation of spring and neap tides within the two to four meter range (Figure 1.2).

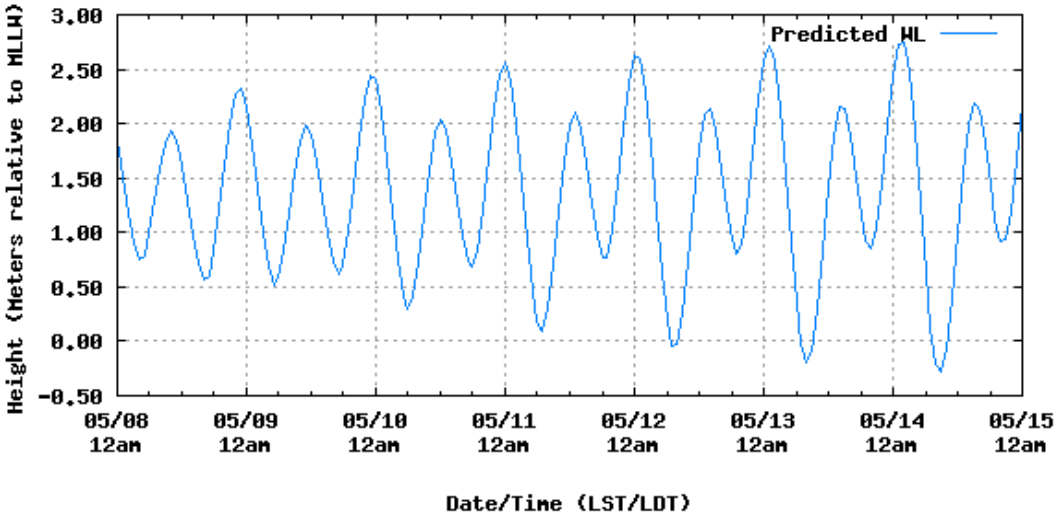

Figure 1.2 *Predicted tidal water level at Astoria station 05/08/2010 – 05/15/2010 (tidesandcurrents.noaa.gov).*

The 6 main tidal constituents in the north-eastern Pacific Ocean are, in order of their amplitude: M_2, K_1, O_1, S_2, N_2, and P_1. In its propagation onshore and into the estuary the tide is affected by processes as bed friction, density gradients, wind and wave stresses, and current interactions. The mean tidal range in its first 15 miles into the estuary first increases and then decreases. The initial increase in tidal range in the lower estuary is the result of the funnel-like shape of the channel system. The cross-sectional area decreases sharply upriver from the entrance causing an increase in tidal range. Further up river the loss of tidal energy to friction is so large that the tidal range decreases upriver despite the decreasing channel cross-section. Changes in river flow also have a strong effect on the tidal properties. Under high river flow conditions, the tidal range is much reduced and the tidal wave moves upriver much more slowly (Fox et al, 1984).

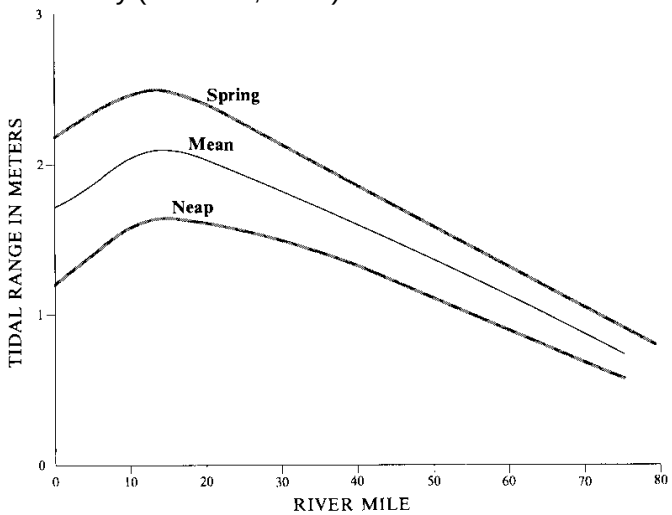

Figure 1.3 *Spring, neap and medium tidal range for the Columbia River up to river mile 80 (from Jay, 1984)*

1.2.3 River

The Columbia River is the fourth largest river in the United States, ranked in average discharge at the mouth (7,500 m^3/s) (Kammerer, 1990). The river originates in the Rocky Mountains in British Columbia, Canada and enters the United States in the state of Washington. It then forms the boundaries between the states of Oregon and Washington before it empties into the Pacific Ocean. The river has a total length of 2000 km and a drainage basin of 670,000 km^2 (Figure 1.4). The discharge of the Columbia River is strongly seasonal variable. From late fall till early spring discharges are around 2,000 to 4,000 m^3/s. Snow melt causes the average discharge to peak to around 12,000 m^3/s in the spring/summer (Bottom et al., 2005). The highest ever observed river discharge was close to 35,000 m^3/s (in 1894, before the river was dammed). The lowest ever observed river discharge was around 340 m^3/s, during the initial closure of the John Day dam (Figure 1.5).

Figure 1.4 CR drainage basin (http://www.wikipedia.org).

1.2.4 Engineering the Columbia River

From around 1920 to 1984 the Columbia River has undergone a lot of construction works beneficial for irrigation, flood control and power generation (Figure 1.5). In 1933 the first dam for hydroelectricity was built. Nowadays the Columbia River Basin is the most hydroelectrically developed river system in the world with a generating capacity of 21 million KiloWatts. The construction of fourteen dams on the main stem of the river and a total of over 400 dams within the rest of the drainage basin significantly altered the rivers hydrograph and sediment load.

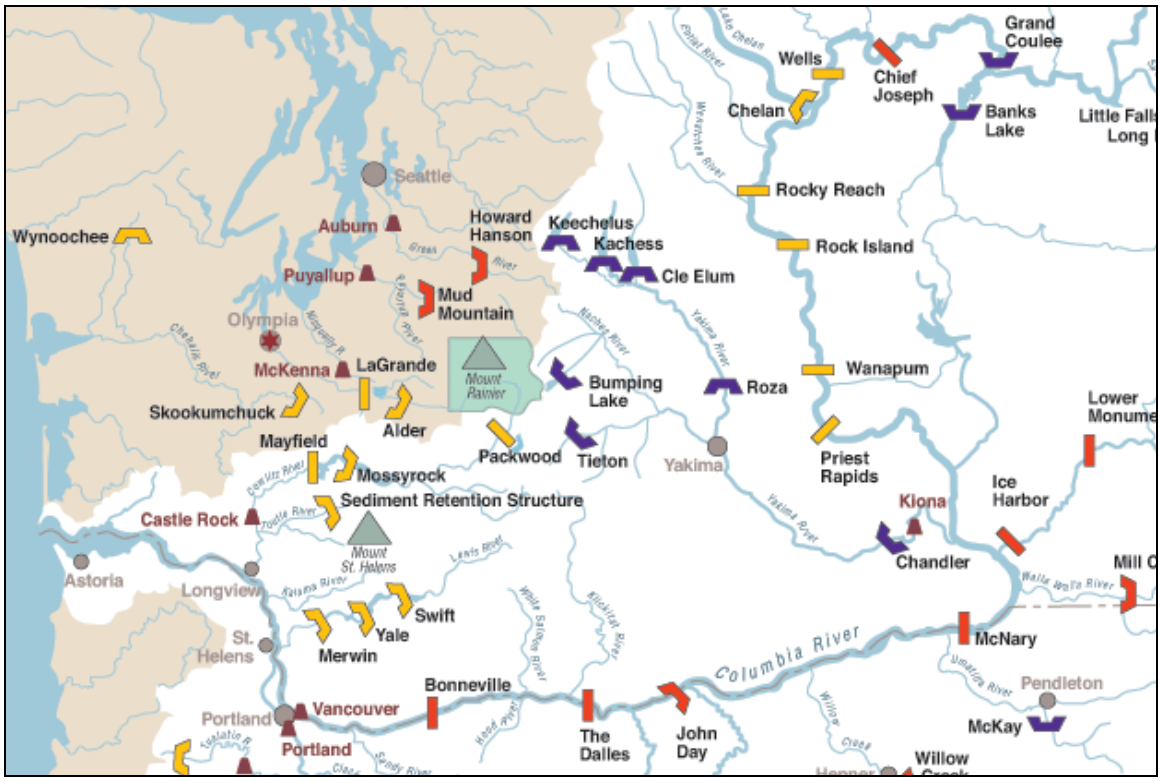

Figure 1.5 Columbia River dam construction.

Two mayor dams in the vicinity of the mouth of the Columbia River and the estuary are the Bonneville dam and the Dalles dam (Figure 1.5). Construction of the Bonneville dam happened in phases. The first powerhouse and spillway (left and middle construction of Figure 1.6) were constructed between 1933 and 1938. The second powerhouse (right structure of Figure 1.7) was constructed between 1974 and 1982. The Dalles dam has a similar phased construction, its first fourteen units completed construction by 1960 and the second eight units by 1973. The first construction phases of the two dams had a result of only moderate river control. The river flow was not yet completely controlled at these phases.

Figure 1.6 The Bonneville dam.

Figure 1.7 The Dalles Dam.

Although the total water transport remains nearly unchanged, flow regulations by dam construction has had a significant effect in reducing peak flows in the Columbia River (Sherwood et al., 1990). The bar plot of Figure 1.8. shows that dam construction led to a more controlled moderate flow. From 1881 up to present, discharge peaks were reduced, discharge lows were increased and mean discharge values stayed more or less the same.

The discharge evolution graphed in Figure 1.8 is divided into five-year periods. The first dam on the main stem of the Columbia River that was constructed was the Rock Island Dam in 1933 (see also Figure 1.5). It's influence of reduced peak flows in the downriver monthly discharge at The Dalles is visible from Figure 1.8. After 1933, dam construction on the Columbia River continued and by 1973 another ten dams upriver of The Dalles discharge point had reached their complete construction. A mayor impact that the dam construction on the Columbia River had was the alternation of seasonal flow of the river. At the beginning of the 20th century, roughly 75% of the Columbia River's flow occurred in the summer, between April and September. By 1975, the summer proportion had been lowered to about 50% in order to meet higher electricity demands during the winter. The strong seasonal pattern of the river was hereby thus eliminated. Other interesting points from the figure are the flood flows of especially 1894, 1948 and 1996.

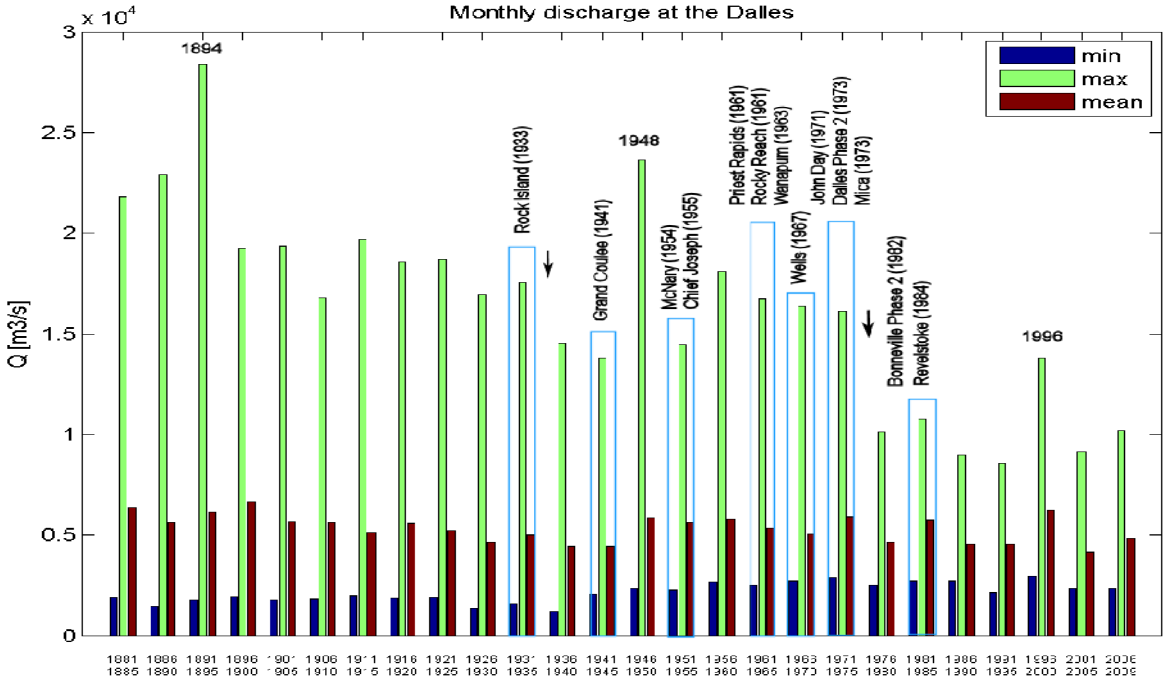

Figure 1.8 *Monthly historic discharge at the Dalles station.*

1.2.5 Waves

The wave climate in the north-eastern Pacific Ocean is characterized by a seasonal variation of summer conditions with smaller waves (average significant wave height of around 1.75 meter and periods of around 8 seconds) and winter conditions with larger waves (average significant wave height of around 3 meters and periods of around 10 seconds). Storm waves in the winter can peak significant wave heights of over 10 meter, up to values of even 14 meter. Wave period can reach values up to 20 seconds. A rose of the wave climate is given in Figure 1.9.

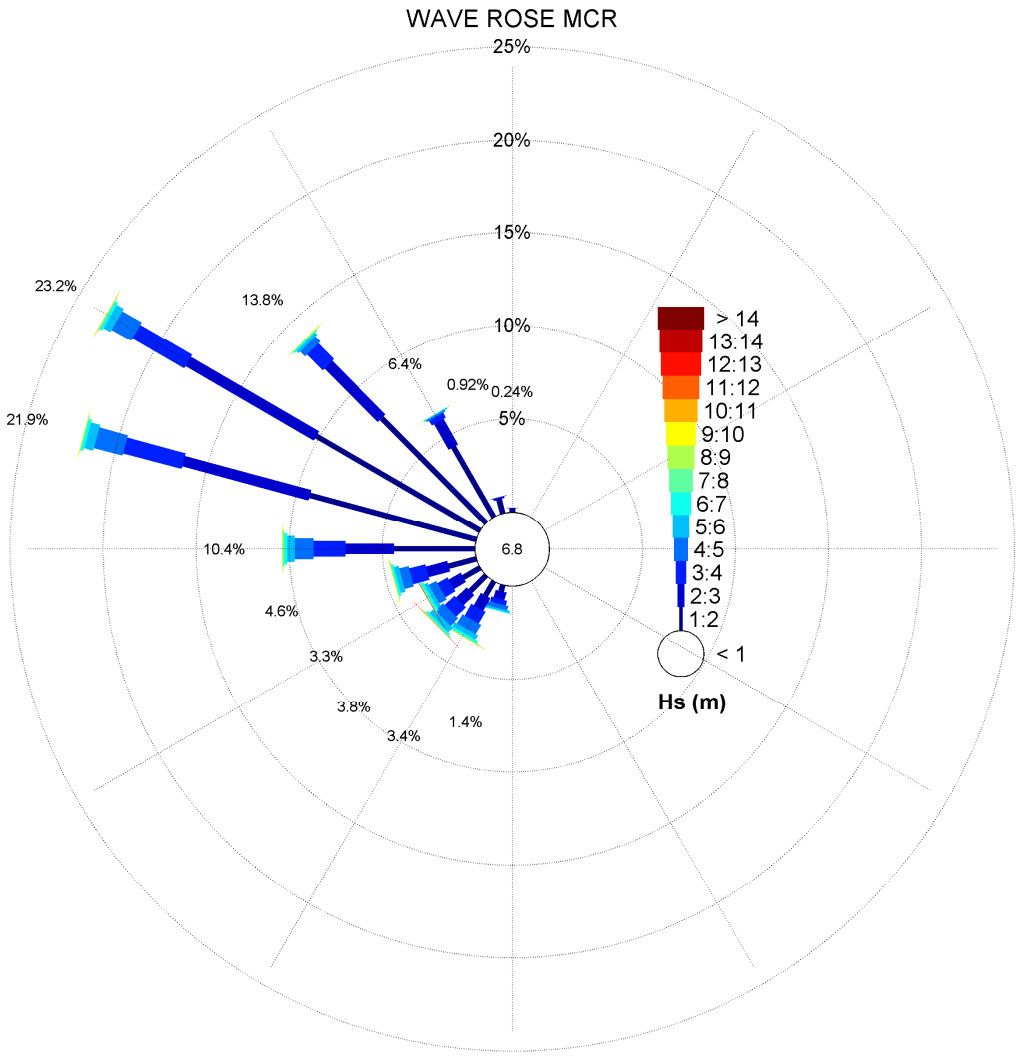

Figure 1.9 Wave rose MCR.

1.2.6 Sediment

Sediment distribution

The beaches of the CRLC are primarily comprised of well-sorted medium to fine sand with a time- and alongshore-averaged median mid beach grain-size of approximately 0.20 mm (Figure 1.10). The general trend suggests that grain sizes decrease with increasing distance from the Columbia River (Ruggiero et al., 2005). Coarse to medium sized sand (D_{50} > 0.21 mm) dominates the inlet and the estuary. (Fox et al, 1984). See Appendix B.

Sediment supply

The fluvial sand supply approximately decreased from 4.3 million cubic meters per year (Mm^3/year) in the interval 1878-1935, to 2.6 Mm^3/year during 1935-1958, and further down to 1.4 Mm^3/year in 1958-1997. This three-fold decrease in fluvial sand transport down the river to the estuary is having uncertain impact on the sand supply to the coast (Gelfenbaum et al. 1999). Though it is likely that sand supply from the river to the coast has decreased, the natural trapping tendency of the estuary may be minimizing the potential total sediment loss to the littoral system (Jay et al., 1990).

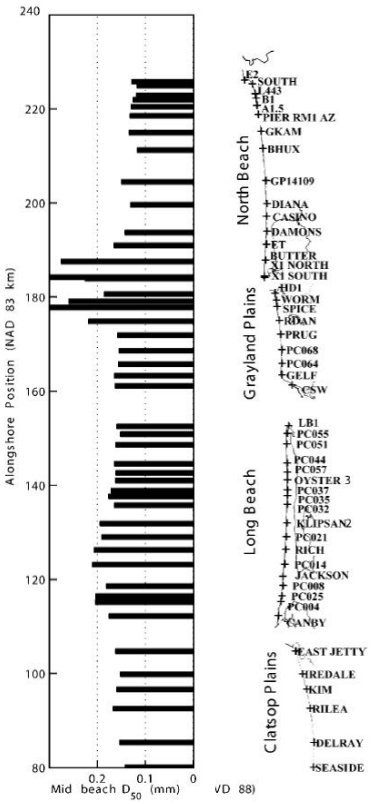

Figure 1.10 Average median grain size distribution beaches CRLC (adjusted from Ruggiero, 2005).

1.3 Problem description

The dynamic behaviour of the CRLC called for a better understanding of the hydrodynamic and morphodynamic behaviour of the system. The detailed interaction and quantitative influence of the processes responsible for the morphological change within the CRLC are however not fully understood nor proven. The complex interaction of the constant changing hydrodynamic and morphological processes of amongst others: tides, currents, waves, river discharge, density gradients, and sediment transports that arise in a complex coastal area such as the CRLC are difficult to describe and investigate. Process-based numerical models however are more and more used as a valuable tool to simulate and help describe and understand the complex behaviour of coastal systems. United States Geological Survey (USGS) and Deltares therefore collaborated on the development of process-based numerical models to be able to better understand the morphodynamics and hydrodynamics within the CRLC. This study focuses on the morphology at the Mouth of the Columbia River (MCR). The morphological development at the mouth of the Columbia River as a result of the anthropogenic influence of river entrance jetty construction has been the dominant driver of coastal change of the entire CRLC. Evaluation of long-term morphological change at MCR using process-based modelling could provide a valuable insight in processes driving morphological change of a complex coastal area as the CRLC. Understanding the morphodynamic behaviour can ultimately support management decisions and refine scientific

questions. Examples are the application of the model to help inform dredge material placement, aid in coastal infrastructural spatial planning and for example help channel maintenance dredging decisions amongst many others.

1.4 Previous studies

The Columbia River Littoral Cell is a well investigated area in which a lot of research was carried out in a numerous amount of studies. From 1996 to 2002, USGS and the Washington Department of Ecology (DOE) performed a study to examine the coastal evolution, processes, geology, and hazards of the Columbia River Littoral Cell (CRLC), called the Southwest Washington Coastal Erosion Study (SWCES). The initiator of the study was the inexplicable erosion trend that arose in the former mainly accreting littoral cell, threatening coastal communities that had developed on the accreted land over the years. The SWCES was aimed at developing a regional-scale understanding of coastal processes and the morphodynamics within the littoral cell to facilitate land-use planning and resource-management decisions in the future. Gelfenbaum and Kaminsky (2010) grouped the large amount of studies that directly or indirectly followed from the SWCES into the following five categories:

1 Coastal Change: These studies involved the analyses of the past and present geomorphic changes of the littoral cell. In which the influence of various forcing conditions on the observed coastal changes were addressed Examples are: Sherwood et al.(1990), Kaminsky et al. (1997), Kaminsky et al. (2010).
2 Sediment Budget: These studies characterized and quantified the sediment sources, pathways and sinks within the littoral cell. Examples are: Buijsman et al. (2003), Gelfenbaum et al. (1999)
3 Coastal Processes: These studies included measuring, monitoring and modelling currents, waves, sea level, sediment transport, and other processes that drive coastal responses over a wide range of spatial and temporal scales.
4 Management Support: These tasks developed information and products valuable for local, state, and federal coastal management and land-use planning efforts.
5 Predictive Modelling: These efforts were based on integrated data sets derived from the analysis of coastal change, sediment budgets, coastal processes, and other environmental forcing conditions and geological constraints. These data helped clarify important geologic and oceanographic processes that governed the coastal changes and refined the conceptual and mathematical models used to make quantitative predictions. The collaboration between USGS and Deltares specifically helped in the development of various location-specific process-based numerical models of the CRLC. Process-based numerical modelling so far to a certain degree helped in getting a better regional-scale understanding of coastal processes and morphodynamics of the littoral cell. Case specific process-based numerical modelling studies that have been performed in the CRLC are addressed in the following paragraph:

For a more detailed overview of the SWCES and its products reference is made to the website: http://www.ecy.wa.gov/programs/sea/swces/index.htm.

1.4.1 Process-based numerical modelling in the CRLC

In all three of the estuaries of the CRLC process-based numerical models have been applied. At first a process-based morphological model was used to examine flow, wave and sediment transport processes around the inlet and ebb-tidal delta of the Grays Harbor estuary, as described by Gelfenbaum et al. (2003). This study was a first attempt in constructing a

process-based model capable of modelling observed morphological changes (one year morphological simulations) of a coastal area within the CRLC. Input reduction techniques and forcing conditions schematizations in the application of the former Delft3D-MOR module were tested. Limited hydrodynamic verification and calibration of the model had a limited result in simulating the observed morphological changes. However, to a certain degree resemblance of morphological changes were modelled.

An approach to medium-term coastal morphological modelling has been done for the southerly located Willapa Bay estuary performed and described by Lesser (2009). A new generally applicable morphological model that was assigned to the existing Delft3D-FLOW module has been tested in this study. A main objective was to validate the application of the model in simulating resulting morphological change over a period of several years in a complex coastal environment such as the Willapa Bay. Furthermore, morphological acceleration techniques were tested in this study and the errors introduced by the use of these acceleration techniques were isolated and quantified. The model predictions of morphological behaviour on the time-scale of years showed some qualitative skill. Most of the general patterns were reproduced, but the magnitude and/or the precise location of the changes were not predicted well by the model. Input reduction and morphological acceleration techniques applied in this study led to practical and satisfactory results, but could doubtless be improved.

Also for the most complex estuary of the CRLC, the Columbia River estuary process-based numerical modelling studies have been performed. A quasi real-time hydrodynamic and sediment transport model was constructed as described by Elias and Gelfenbaum (2009). This model was constructed to examine and isolate the physical processes responsible for sediment transport and morphological change at the Mouth of the Columbia River. The model was able to simulate the dominant features in the tidal flow, salinity and wave fields observed in field measurements. By varying the number of forcing conditions in the model, the dominant sediment transport processes and mechanisms were also identified. The time-scales of the simulated morphological change of this quasi real-time model however were still small compared to the morphologic development scale of the ebb-tidal delta. The obvious next step was to take this model towards the application of *long-term* morphological modelling. Verification of the long-term morphological performance of the Delft3D module in a complex river influenced delta area is an important goal. An important step that needs to be taken in the long-term morphological simulation is the proper schematization of representative forcing conditions. Ultimate goal in this is to realistically simulate the observed long-term morphological changes. And thereby take an important first step in understanding the dominant processes affecting sediment transport and morphological change in an energetic coastal environment as the MCR.

1.5 Objectives

The overall goal of this thesis is to develop a long-term morphological model and investigate methods and modelling approaches in simulating the complex estuarine area of the MCR. Calibration and validation of long-term morphological modelling of the MCR is necessary to make long-term simulations possible and identify the influences of the different processes on the morphological development. Specific objectives are:

1 Verification of appropriate schematizations of forcing processes responsible for long-term morphological change within the complex estuarine area of the MCR.

2 Model (hind cast) the long-term morphological changes at MCR with Delft3D and compare the observed and computed bathymetric changes for the interval of 1926-1958.

3 Analyse the impact of different levels of detail in schematization of forcing processes on the long-term morphological development.

4 Analysis of processes responsible for long-term morphological change at MCR. Give a detailed description of the system's behaviour.

5 Describe methods used for long-term morphological modelling in this estuarine area

6 Perform morphodynamic simulations for the interval of 1958-1999 and describe the overall performance of the model in the application of simulating the observed long-term morphological changes.

1.6 Thesis Structure

Chapter 2 discusses the available bathymetric data and observed morphological changes from pre-jetty conditions to present. In Chapter 3, the applied model, it boundary and forcing conditions and schematizations are presented. Chapter 4 continues with an analysis of the general process responsible for the morphological change at the MCR by looking at the influence of individual parameters. Chapter 5 forms the calibration phase of the model towards long-term morphological modelling, several morphology related settings are tested and explored. Chapter 6 presents the set-up and results of the final long-term morphological simulations. Chapter 7 discusses the conclusions of the study. A general conclusion and the specific objectives are presented. The chapter is concluded by given the model limitation, deficiencies and improvements and recommendations for continuing research.

2 Morphological change of the MCR

2.1 Jetty construction

Over the last two centuries, navigability of the Columbia River entrance has been high. The entrance however always had a dynamic morphological behaviour. In 1882, as a result of this dynamic morphological behaviour of the entrance, the Board of Engineers made plans to improve the navigational safety at the Columbia River entrance. In 1885, construction of the southern entrance jetty started as a result of this (Figure 2.1). The jetty was constructed to narrow, deepen and stabilize the channel and thereby improve navigation. Long-term morphological impacts of the jetty construction however were not really thought off let alone taken into account. At the beginning, there was little change in the entrance region resulting from the southern jetty construction but by 1895 the main channel began to swing north and deepen to ultimately reach a depth of 10.6 meters. After that the channel continued to migrate north and began to shoal again. By 1902, the channel had broadened and bifurcated to form two channels. Because the best channel was again only 6.7 meters deep, plans for the extension of the South Jetty and construction of the North Jetty were made. Construction of the South Jetty extension began in 1903 and was completed in 1914. Construction of the North Jetty began in 1913 and was completed in 1917. Parallel to jetty construction, maintenance dredging of the entrance channels began in 1903. Subsequently, construction of Jetty A and the Sand Island dikes followed in 1939 to further stabilize the entrance channel (Sherwood et al.,1990). The construction of these and other jetties in the littoral cell later showed to have a huge impact on the overall morphological behaviour of the system over the last century.

Figure 2.1 Jetty construction MCR.

2.2 Observed morphological changes

As part of the Southwest Washington Coastal Erosion Study (SWECS) a historical regional sediment budget study of the Columbia River Littoral Cell (CRLC) has been performed by Buijsman et. al. (2003) to describe and quantify the morphological changes that occurred at the entrances of the different estuaries of the CRLC from around 1860 up to present. The basis for this study were various bathymetric and topographic data from a numerous amount of surveys from 1860 up to present. Data from surveys within a similar time span were combined to be able to form full bathymetric coverage (Figure 2.2) of in total four historic times. For the Mouth of the Columbia River this division is as follows:

- 1868 (pre-jetty condition)
- 1926 (post-jetty condition)
- 1958
- 1999

The periods between the successive historic bathymetric maps are from now on addressed to as Period A, B, and C, respectively. The results of the sediment budget study by Buijsman et al. (2003) are used to calibrate and validate the long-term model applied in this study. From the analysis of the bathymetric changes in the different periods the influence of the jetty construction and the general historic morphological behaviour can be addressed.

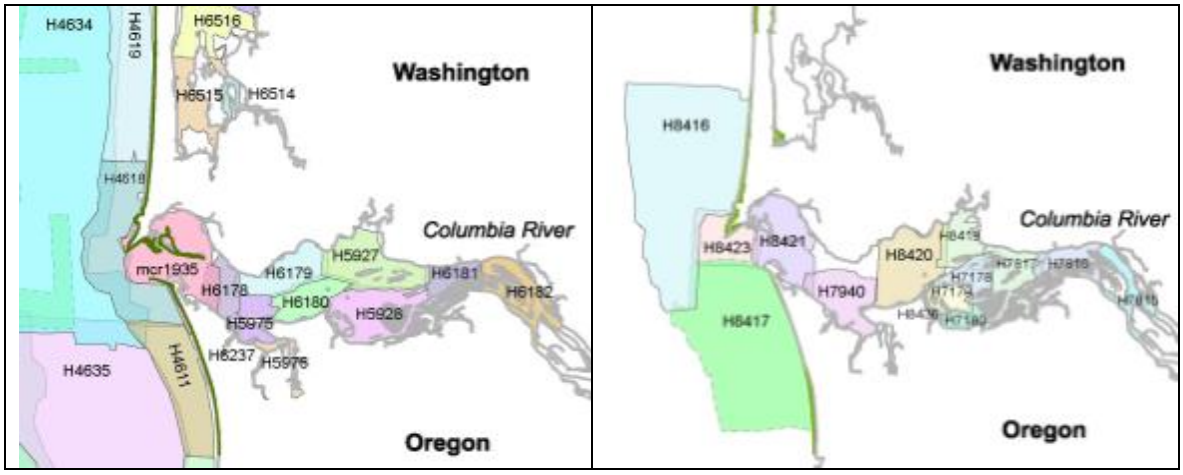

Figure 2.2 Example overview available bathymetric surveys for the years 1926 (left) and 1958 (right) (source http://walrus.wr.usgs.gov/swces).

The main focus of this study is on the morphological change between the years 1926 and 1958 (Period B). This period is thought to be best suited to test the long-term morphological performance of the model. Uncertainties in the pre-jetty condition such as the dynamic behaviour of certain areas such as for instance Clatsop Spit but also the gradual jetty construction in Period A are hereby taken out. Furthermore, the initial uncertain morphological response to the jetty construction already took place. There is still however sufficient time left for the rest of the morphological adjustment of the system to the jetty construction. The modelling of the more residual long-term response is thus focused on. This study specifically focuses on the morphological behaviour at the Mouth of the Columbia River. Special focus is therefore on the compartment of the inlet, the inner delta and the outer delta. Ultimately, the performance of the model is also verified for Period C (1958-2000) to be further quantify the long-term performance of the model.

Buijsman et al. (2003) showed that the morphology of the entrance and adjacent shores changed significantly as a consequence of jetty construction, pile dike construction

and river damming. In general, it can be stated that the ebb-tidal delta moved offshore, the inlets and inner delta eroded and the adjacent shores at first accumulated sand and finally turned towards an erosive behaviour. A more detailed description of the morphological change for the various periods as found by Buijsman et. al. (2003) is given below. The initial morphological change from pre-jetty to post jetty condition between 1868 and 1926 is also given for the sake of completeness and understanding.

2.2.1 Period A, 1868, (pre-jetty) – 1926, (post-jetty)

Period A describes the short-term morphological changes that have occurred as a result of the construction of the jetties (see Figure 2.3). Despite the dynamic behaviour of the entrance channels, the mouth of the Columbia River is believed to have been more or less morphologically stable before jetty construction had started. Smaller scale disturbances as the seasonally varying wave and river climate are not believed to affect the long-term morphological development and the area is therefore believed to be in a more or less morphological equilibrium before the beginning of jetty construction. Jetty construction from 1903 and onward however significantly distorted this equilibrium.

Buijsman et. al. (2003) divided the area into different compartments to be able to quantify the absolute volume change of the period per particular compartment. These compartments are amongst others the outer delta, the inner delta, the inlet, the south flank, and the spits of Peacock Spit and Clatsop Spit.

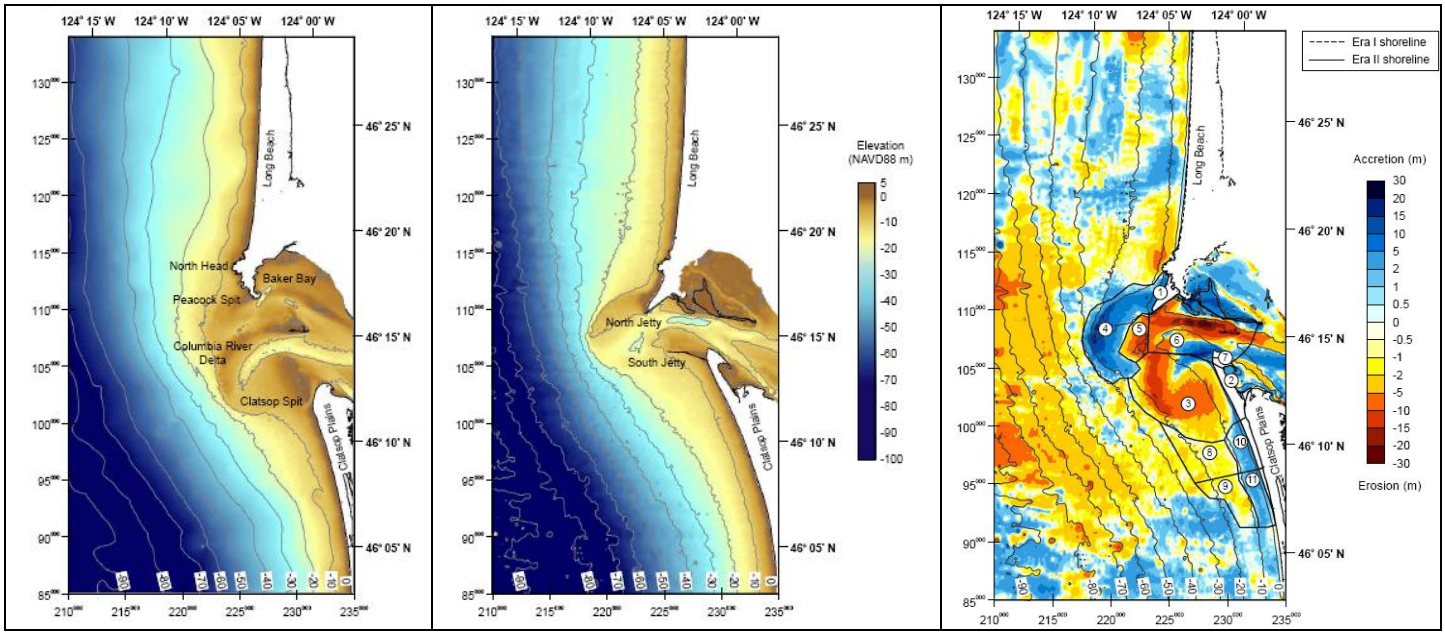

Figure 2.3 Bathymetric surfaces for the years 1868 (left), 1926 (middle) and bathymetric changes for Period A(right)(following from Buijsman et. al. (2003)).

In the pre-jetty condition, the Columbia River entrance was characterized by a broad and shallow ebb-tidal delta complex with a varying number of inlet channels, the entrance was flanked by the shallow shoals of Peacock Spit and Clatsop Spit (Figure 2.3 (left)). To improve navigation, the South Jetty was constructed between 1885 and 1889 across the Clatsop Shoal. Deterioration of the jetty due to waves and currents and the northward migration and shoaling of the channel led to an extension of the South Jetty and the construction of the North Jetty in respectively 1903 and 1913. Overall, the jetty constructions reduced the width

of the river mouth from approximately 9.6 km to 3.2 km. The entrance channel as well as the ebb-tidal delta eroded by the increased tidal currents as a result of the confinement. Part of this sand was transported seaward and deposited in a new ebb-tidal delta further offshore. The South Flank, South of the South Jetty eroded because it was no longer influenced by the ebb-jet, this sand was partly transported to the northwest to accrete in the outer lobe of the ebb-tidal delta and partly transported onshore to accrete Clatsop Plains. Clatsop Plains accreted over seven squared kilometres [km^2] of land within five kilometres of the South Jetty. Offshore Clatsop Plains however eroded, which possibly also contributed to the accretion of Clatsop Plains. Peacock Spit accreted nearly four km^2. Also the coast of Long Beach accreted a little. Sand from the entrance may also have moved into the Columbia River estuary, contributing to the accretion of the flood-tidal delta.

The amount of sand dredged out of the area is small compared to the morphological changes and therefore Buijsman et. al. (2003) neglects the effects of dredging and disposal on the sediment budget. The net change for the delta, inner delta, inlet, Clatsop Spit inlet and the adjacent coasts of Long Beach and Clatsop Plains combined is 112 million cubic meters [Mm^3] erosion. The net change for the flood-tidal delta and the upper estuary is 164 Mm^3 accretion (Table 2.1). The net accretion of all the compartments is thus 52 Mm^3.This net accretion is accounted for by the net influx of sediment from the Columbia River to the estuary of 4.3 Mm^3/year, in total 168 Mm^3 for Period A. This net influx of sediment increases the export of sediment out of the Columbia River entrance by 116 Mm^3.

In general it can be stated that the construction of the jetties at the Columbia River entrance caused the inlet to erode, sand from the ebb-tidal delta to indirectly move onshore, resulting in shoreline advance along Clatsop Spit of up to seventeen meters/year and Peacock Spit of up to thirteen meters/year, whereas the remainder of Clatsop Plains and Long Beach hardly accreted. Furthermore, the flood-tidal delta and the upper estuary overall imported sediment.

Table 2.1 Bathymetric changes for Period A, 1868-1926 (following from Buijsman et. al. (2003)).

Period A	
Compartment	**Volume change [Mm3]**
Peacock Spit (1)	21.68
Clatsop Spit (2)	25.99
South Flank (3)	-217.48
Outer Delta (4)	171.53
Inner Delta (5)	-47.49
Inlet (7)	-116.41
Clatsop Spit Inlet (7)	5.18
Long Beach	26.56
Clatsop Plains	48.04
• Inner shoreface (8)	-10.44
• Inner shoreface (9)	-19.30
• Near shore (10)	14.68
• Near shore (11)	14.50
Flood-tidal delta	91.74
Upper estuary	72.31

2.2.2 Period B, 1926 (post-jetty) – 1958

Morphologic equilibrium was not yet reached at the end of Period A so the readjustment of the morphology at the mouth of the Columbia River to the jetty construction continued in Period B (Figure 2.4).

The inlet and the inner delta continued to erode (104 Mm^3) and this sediment may have contributed to the further development of the outer delta (101 Mm^3) (Table 2.2). The regions of greatest accumulation along the coast shifted away from the Columbia River entrance. Clatsop Spit started to erode and the central part of the Clatsop Plains sub-cell prograded significantly with shoreline change rates of 7-8 meter/year. The inner shoreface along Clatsop Plains and Clatsop Spit eroded (86 Mm^3) and this sand may have moved southward and onshore, contributing to the further accretion of Clatsop Plains (61 Mm^3). North of the Columbia River entrance Peacock Spit continued to accumulate sand (6 Mm^3) but at a slower rate than in Period A. North of North Head, the southern 20 km of Long Beach prograded (76 Mm^3), whereas the northern 20 km of Long beach eroded (24 Mm^3) of which the last is thought to be related to processes at the Willapa Bay entrance. The flood-tidal delta and the upper estuary continued to accumulate sand (34 and 41 Mm^3 respectively). The off-shore compartment northwest of the outer ebb-delta (23) may represent a deposition from a plume of fine sediments released by the Columbia River, as a result of a peak river flow in 1948. Again the volumes of dredging and disposal are small compared to the total volume changes. The net change over the inlet, ebb-tidal delta, and adjacent coasts is 46 Mm^3 accretion. The net change for the estuary is 111 Mm^3 more accretion than erosion. The net accretion of all the compartments is thus 157 Mm^3. The supply of sand from the Columbia River to the estuary might account for 83 Mm^3 of the observed accretion. If the estimates of the northward sediment flux at the northern tip of Long Beach (45 Mm^3) and dredging (70 Mm^3) in the Columbia River estuary are accounted for, then the net accretion is increased by 115 Mm^3 to a total of 190 Mm^3. Some uncertainties in the bathymetric volume-change calculations, sediment fluxes, and the lack of bathymetric coverage along northern Long Beach might have contributed to this net accretion value.

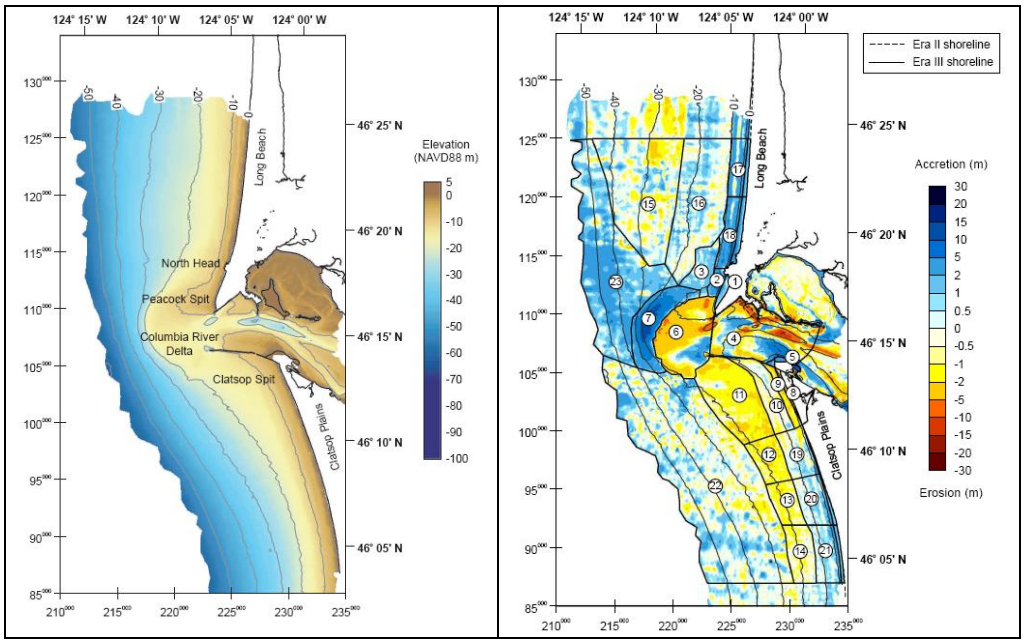

Figure 2.4 *Bathymetric surfaces for the year 1958 (left) and bathymetric changes for Period B (right) (following from Buijsman et. al. (2003)).*

In general it can be stated that the estuary, the outer ebb-tidal delta, and the beach dune complexes of Long Beach and Clatsop Plains accreted and that the inlet and the inner-delta continued to erode. It can also be concluded that the areas of greatest accumulation moved further away from the entrance.

Table 2.2 Bathymetric changes for Period B (following from Buijsman et. al. (2003)).

Period B	
Compartment	**Volume change [Mm3]**
Peacock Spit (1)	5.58
• Near shore (2)	8.77
• Offshore (3)	8.26
Inlet (4)	-53.77
Clatsop Spit Inlet (5)	3.74
Inner Delta (6)	-54.19
Outer Delta (7)	101.30
Clatsop Plains	61.17
Clatsop Spit (8)	-4.64
• near shore (9)	-6.14
• near shore (10)	-3.20
South Flank (11)	-42.76
Clatsop Plains	-13.18
• Outer shoreface (12)	-9.05
• Outer shoreface (13)	-7.30
• Outer shoreface (14)	
Long Beach	51.70
• North	-24.31
• South	76.01
• Outer shoreface (15)	-5.37
• Inner shoreface (16)	12.79
• Near shore (17)	15.55
• Near shore (18)	25.19
Flood-tidal delta	33.54
Upper estuary	41.27
Clasop Plains	
• Near shore (19)	1.01
• Near shore (20)	6.20
• Near shore (21)	7.72
Clatsop Plains offshore (22)	32.04
Off-shore compartment northwest of the outer ebb-delta (23)	113.45

Special focus in this study is on the morphological change at the Mouth of the Columbia River. Focus is therefore especially on the morphological change in the compartments of the Inlet, the Inner Delta, and the Outer Delta (Table 2.2, blue).

2.2.3 Period C, 1958 – 1999

Limited data is available for the year 1999, the inlet only has a partial coverage and also for the estuary there is no recent complete coverage available. It can however be stated that the adjustment of the morphology at the Columbia River entrance due to jetty construction still continued in Period C. The inner delta, the inlet and the south flank continued to erode, whereas Long Beach and Clatsop Plains continued to accrete (see Figure 2.5).

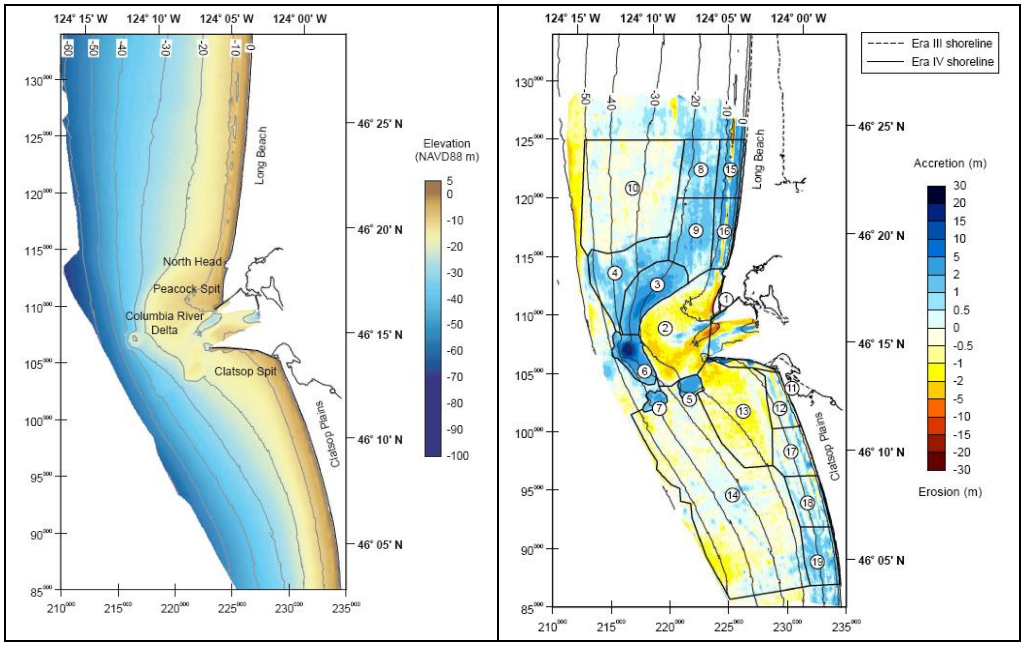

Figure 2.5 Bathymetric surfaces for the year 1999 (left) and bathymetric changes for Period C (right) (following from Buijsman et. al. (2003)).

The outer delta continued growing westward, accumulating 45 Mm^3. Dredge disposal sites accumulated an additional 56 Mm^3 of sand. During this period, approximately 3.4 Mm^3/year of mostly sand was removed from the entrance channel by dredging. The inner-delta and Peacock Spit continued to erode, loosing approximately 55 Mm^3. The beach-dune complex of Long-Beach accreted 127 Mm^3. The shoreline at Clatsop Spit stabilized and accreted only 0.3 Mm^3. The beach-dune complex of Clatsop Plains accreted 50 Mm^3. The south flank lost 30 Mm^3 and this sand may have moved southward and onshore to contribute to the accretion of Clatsop Plains. The net change along Clatsop Plains is 21 Mm^3 more accretion than erosion. The inner shoreface erosion of Clatsop Plains (26 Mm^3) may also have contributed to this accretion. The net change over the study area is 221 Mm^3 accretion. This imbalance might be due to the incomplete bathymetric coverage of the inlet, the estuary and the shelf along Long Beach and southern Clatsop Plains. The northward littoral drift at northern Long Beach (57 Mm^3) and gains to the estuary of 1.4 Mm^3/year supplied by the river are not accounted for in this sediment balance. The shoreline progradation rates of Period C are in general smaller than in Period B.

Table 2.3 Bathymetric changes for Period C (following from Buijsman et al. (2003)).

Period C	
Compartment	**Volume change [Mm3]**
Peacock Spit (1)	-7.48
Inner Delta (2)	-47.07
Outer Delta (3)	45.13
North Delta (4)	22.02
Disposal site A (5)	6.57
Disposal site B (6)	45.79
Disposal site C (7)	3.85
Long Beach	127.05
• Inner shore face north (8)	13.38
• inner shore face south (9)	22.64
• Offshore (10)	-5.13
• Near shore north (15)	17.71
• Near shore south (16)	14.10
Clatsop Spit (11)	0.03
• Near shore (12)	0.34
Clatsop Plains	50.48
• South Flank (13)	-30.27
• Offshore (14)	-25.84
• Near shore (17)	2.52
• Near shore (18)	5.18
• Near shore (19)	13.55

3 Model schematization of the MCR

3.1 Delft3D

In the simulation of the hydrodynamic and morphodynamic processes of the MCR the process-based numerical model Delft3D is used. Delft3D is a modelling system developed by Deltares in close cooperation with the Delft University of Technology. It allows for hydrodynamic computations in coastal, river and estuarine areas. The Delft3D software package consists of several modules. Each module focuses on specific processes such as hydrodynamic flow, sediment transport, morphodynamics, water quality, ecology and waves. The modules can be coupled for process interaction. In this study the Delft3D-FLOW module and the Delft3D-WAVE module are used. Delft3D-FLOW simulates the non-steady flow, transport phenomena (such as sediment transport, density gradients and heat), and morphology (Deltares, 2010a, Lesser et al.,2004). Delft3D-WAVE is applied to simulate the evolution of short waves using the 3rd generation SWAN-model (Booij et al., 1999).

The general modelling approach in Delft3D is that hydrodynamic flow is calculated on a boundary fitted grid to which bathymetry, initial conditions and boundary conditions are applied. Sediment transports are calculated following the flow and wave field, according to the applied sediment transport formula. Variations in sediment transports in their turn determine the morphological development of the model. The processes of flow, waves, sediment transport and morphological updating are all executed at each time step according to the 'online' approach (Roelvink, 2006, see Figure 3.1).

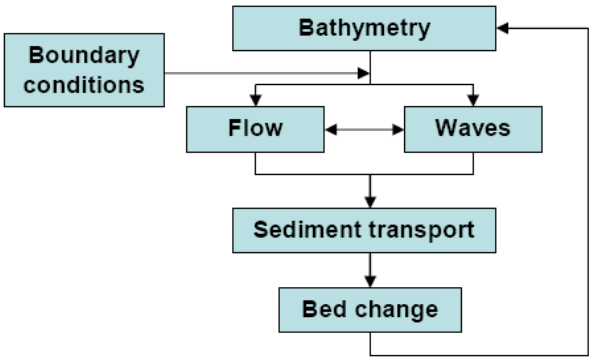

Figure 3.1 Schematic overview Delft3D calculation steps (Roelvink, 2006).

For a more detailed description and for practical use reference is made to the user manuals of Delft3D-FLOW and Delft3D-WAVE. (Deltares, 2010)

3.2 Background

The hydrodynamic and sediment transport model of the MCR described by Elias and Gelfenbaum (2009) forms the basis for this study. This MCR model application was constructed to examine and isolate the physical processes responsible for sediment transport and morphological change at the MCR. The MCR model is capable of simulating the dominant features in the tidal flow, salinity, wave fields and sediment transports. The next step and main objective of this study was to take the quasi real-time model towards the application of long-term morphological modelling. An important goal in this is to verify appropriate long-term schematizations of forcing conditions such as tides, river discharge and

waves in which the seasonal variation of these conditions is accounted for. The majority of the input and hydrodynamic settings that are used in the long-term morphological model of the MCR emanate from the calibrated and validated quasi real-time hydrodynamic and sediment transport MCR model and are directly adopted in this study. Examples of which are the validated bottom roughness coefficients, horizontal and vertical eddy viscosity and diffusivity parameters, wind drag coefficients but also wave energy related parameters such as wave growth by wind, depth-induced wave breaking parameters, white-capping, bottom friction and non-linear wave-wave interactions.

3.3 Long-term morphological modelling

In order to reach the objective of the development of a long-term morphological model of the MCR, both input reduction and morphological acceleration techniques need to be applied. Input reduction is reached by the development of appropriate schematizations of boundary forcing conditions as tidal flow, waves, wind and river discharges. The schematizations of the forcing conditions should account for seasonal variations of the wave, wind and river discharge climate and fortnightly variations of the tide. An important aspects is to also account for the joint-probability of waves and discharges as a result of the strong seasonal variation of both these forcing conditions. Secondly, acceleration techniques need to be applied in the long-term morphological model to bridge the gap between hydrodynamic and morphological timescales and benefit computational times.

3.3.1 Grid and boundaries

In order to properly model the hydrodynamic processes at the MCR such as tidal oscillations, waves, density-driven circulations, river flow, and wind, the model grid needs to extend well beyond the MCR area. On the seaward side, the grid extents 20 nautical miles in westward direction up to the offshore wave buoy 46029 (deployed and operated by the National Oceanic and Atmospheric Administration's (NOAA) National Data Buoy Center (NDBC) (http://www.ndbc.noaa.gov)). From which quality controlled wind and wave data are available from 1984 up to present. Extension of the seaward domain boundary up to this point allows for direct wind and wave implementation to the model. The grid extends about 30 kilometres in both northward and southward direction from the MCR to allow for proper development of currents, tides, wind, waves, density-driven circulations and river run-off. The western open-sea boundary (Figure 3.2) is a water-level boundary, forced with a representative morphological tide (§ 3.2.3). The north and the south boundaries are prescribed as so called Neumann boundaries. Neumann boundaries impose the alongshore water level gradient and velocity distribution that develop under a tidal wave travelling along the coast (Roelvink and Walstra, 2004). Neumann boundaries allow for the undisturbed propagation of currents out of the model that are impossible to predict and impose as a boundary condition without running the model. Wind is implemented as a time-varying, spatially uniform shear-stress on the free-surface. Waves are forced as time-varying conditions on the open sea boundaries of the wave grid. On the landward side the model extends into the lower estuary and up to the USGS river gauging station 14246900 (http://waterdata.usgs.gov/nwis/) at the Beaver Army Terminal (BAT) for which measured water levels and river discharge data is available. These data provide an accurate upstream boundary description The extension of the model over the lower estuary also allows for accurate infiltration of the salt wedge, wetting and drying of the tidal flats and wetlands and hereby accurate reproduction of the tidal prism, the tidal currents, and the tidal propagation (Elias and Gelfenbaum, 2009).

Grid schematizations are in general a trade-off between the processes to be modelled and computational time. Grid cells should accurately represent the local hydrodynamic

processes and provide a sufficient description of the bed characteristics. As a result of this, the offshore grid cell sizes in this model study reach values up to 3 kilometres while grid sizes at the mouth and in the estuary are about 250 meters. In total, the grid consists of about 9000 active cells. To speed up computations, domain decomposition was applied by specifying three sub-domains (Figure 3.2). Domain decomposition allows for parallel computation of each sub-domain. The domain decomposition divides the total domain in three sub domains, the sea-domain (blue), the estuary domain (green), and the river domain (red). Both the sea domain and the estuary domain are resolved with nine vertical layers. The river domain consists out of a single vertical layer.

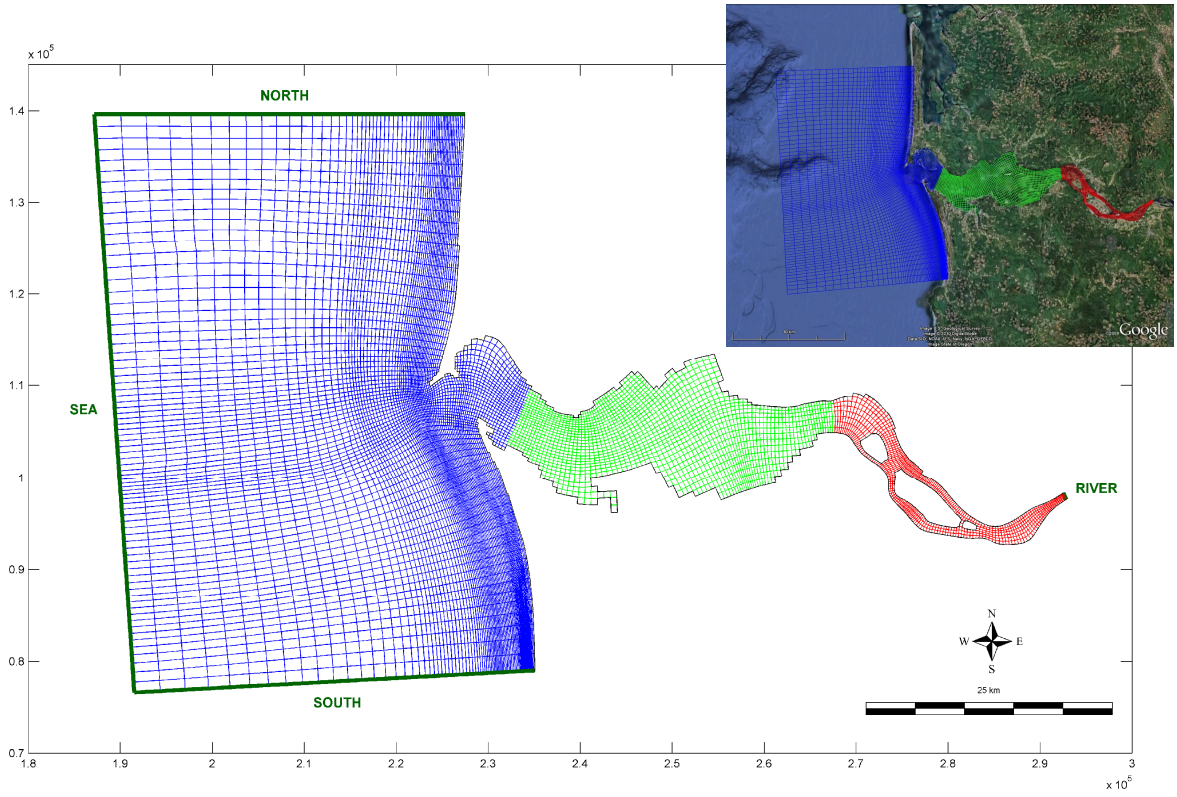

Figure 3.2 *Total MCR model domain, consisiting of the decomposed domains: sea(blue), estuary(green) and river(red).*

3.3.2 Bathymetry

Bathymetries for the years 1926 and 1958 (Figure 3.3) are made applicable for the analysis with Delft3D from the derivation of post-processed measured data as described by Buijsman (2003).

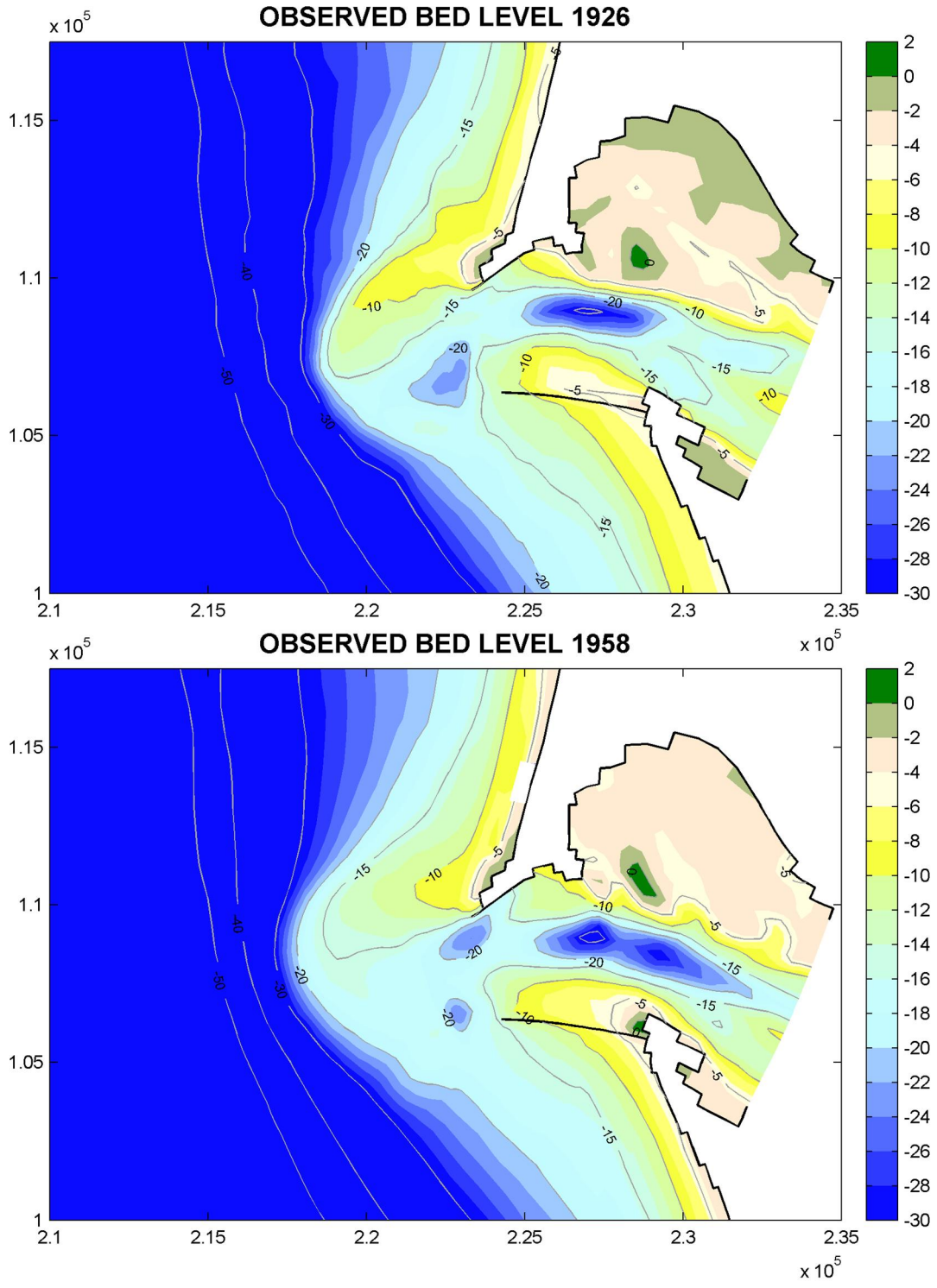

Figure 3.3 Observed bed level 1926 (top) and 1958 (bottom).

3.3.3 Morphological tide

The main idea of tidal input reduction is to reduce computation times. Tidal input reduction replaces the complex time series of tidal water levels and current fluctuations with a simplified tide (Gelfenbaum et al 2002, Grunnet, 2004, Lesser 2004, and Lesser, 2009) and is based on the principle of Latteux (1995). Latteux states that a morphological tide can be chosen wherein residual sediment transports (or morphological change) most closely match the residual sediment transports for the entire spring-neap tidal cycle. This allows to reduce the spring neap cycle to a single daily signal. Lesser (2009) states that during a morphological simulation, each of the selected wave conditions should be simulated for the duration of full morphological tides in order to account for the random phasing between waves and tides that occurs in nature. Random phasing should especially be accounted for in the application of a morphological tide with a morphological acceleration factor (Lesser, 2004). The application of a morphological tide and the simulation of wave conditions over one full morphological tide in combination with morphological acceleration factors strongly benefits the total computation time of long-term morphological simulation. In the process of doing so, long-term morphological simulations can be achieved using hydrodynamic simulations of only a fraction of the simulated duration. For an explanation of the morphological scale factor reference is made to § 3.2.8.

The set-up of the morphological tide follows from the tidal constituents applied to the quasi real-time model of the MCR. The western open-sea boundary in this model is forced by the 6 main tidal constituents for water levels of the north-eastern Pacific Ocean to generate the tidal modulation. The tidal amplitudes and phases of the different tidal constituents are given in the following table.

Table 3.1 Tidal boundary constituents MCR.

Tidal constituent	Amplitude SW [m]	Phase SW [°]	Amplitude NW [m]	Phase NW [°]
M_2	0.957	225	0.939	224
K_1	0.442	233	0.443	233
O_1	0.286	216	0.282	217
S_2	0.275	249	0.268	247
N_2	0.195	202	0.192	201
P_1	0.134	229	0.134	229

Tidal reduction in the present study is based on Lesser (2009), that is based on the work of Hoitink et al. (2003). Lesser reduces the total set of tidal components to a combination of just two: M_2 and C_1 (in which the amplitude of $C_1 = \sqrt{2O_1K_1}$ and the phase is $\phi_{C1} = \frac{\phi_{O1} + \phi_{K1}}{2}$. The interaction of the M_2, O_1, and K_1 in the area seems crucial in the residual transport patterns. Hoitink et al. (2003) point out that the residual sediment transport caused by the interaction of the three constituents can be expected to be more important than the well known residual transport due to the non-linear interaction of the M_2 tide with the M_4 over-tide if the formulation: $2O_1K_1 > M_2M_4$ holds. This will be the case in most locations on the west coast of the United States, as well as in many other locations around the world where the diurnal tidal constituents O_1 and K_1 are significant. The tidal constituents that represent this case-specific morphological tide thus follow from the M_2 and the C_1 components. Where the diurnal constituent C_1 with a tidal period of 2 x M_2 will interact with M_2 to produce the same third order velocity moment, and therefore residual sediment transport, as the O_1 and K_1 tidal constituents would. A representative tide which accounts for the interaction and residual third

order moment of the O_1, and K_1 constituents can thus be achieved by applying a simple repeating double tide consisting of only M_2 and C_1. This tide will have a period of 24 hours 50 minutes and 28 seconds (1490.47 minutes, frequency of 14,492°/hour) and will display a daily inequality, the magnitude of which will depend on the relative phasing of the M_2, O_1, and K_1 tidal constituents.

Lesser (2009) also addresses that a scaling factor should be applied to the tidal constituents of the morphological tide to preserve total tidal energy. The optimum scaling factor can be determined by trial and error of residual sediment transport between a morphological tide simulation and a full spring-neap astronomic simulation. In order for the morphological tide to produce the same residual sediment transport and morphological change patterns as the full-astronomic tide, the selected morphological tide is generally 7-20% larger than the full-astronomic tide (Lesser, 2009). Lesser determined this scaling factor to be 1.08 for the neighbouring Willapa Bay inlet. Given the similar tidal climate this 1.08 factor is also used in the present study. The morphological tidal amplitudes will then follow from 1,08*(M_2+C_1):

The frequencies of the M_2 and the C_1 components were adjusted slightly to make the period of the morphological tide exactly 1490 minutes, with the adjusted M_2 component having a period of exactly 745 minutes. The new tidal boundary conditions that follow from this are given in the table below.

Table 3.2 Harmonic water level boundary conditions morphological tide.

Tidal constituent	Frequency [°/hour]	Amplitude SW [m]	Phase SW [°]	Amplitude NW [m]	Phase NW [°]
C_1	14.496644	0.543	224	0.540	225
M_2	28.993288	1.033	225	1.014	224

The following figure shows the offshore water level for a full-astronomic tide and a representative morphological tide for the duration of a full spring-neap cycle.

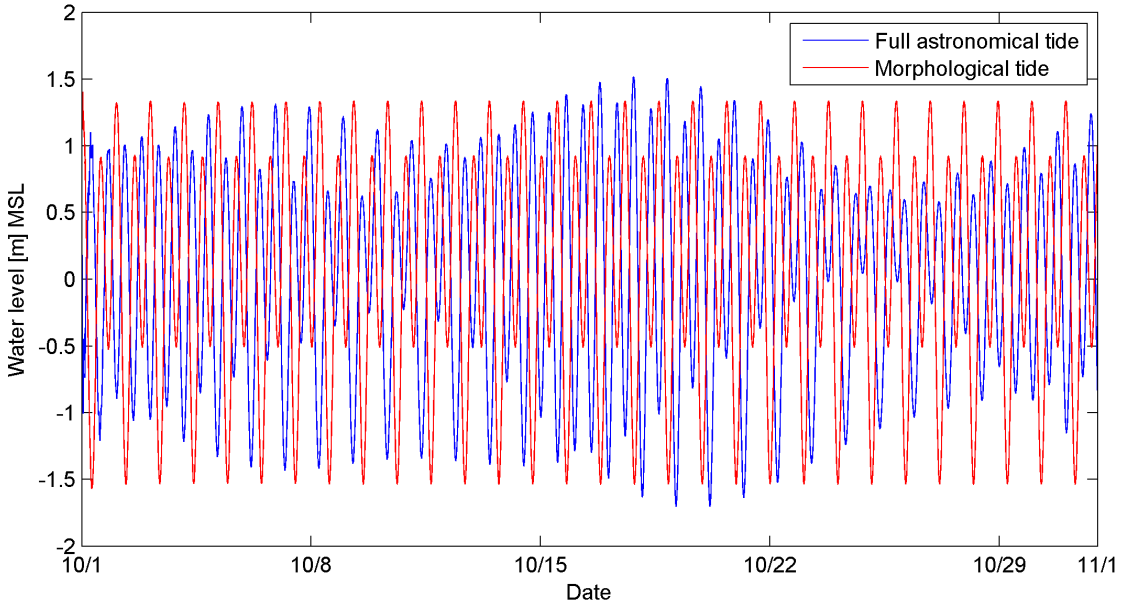

Figure 3.4 Tidal water levels, full-astronomic tide (blue) and morphologic tide (red)

Neumann boundaries

The relation between the tidal forcing at the offshore boundary (water level type) and the forcing at the cross shore boundaries (Neumann type) follow from Roelvink and Walstra (2004) and Deltares (2010a).The amplitude of the Neumann boundary follows from:

$$\frac{2\pi}{L} * \zeta \tag{3.1}$$

In which ζ is the amplitude in meters of the tidal constituent of the water level boundary and L is the tidal wave length [m] that may be estimated from the phase difference between the two boundary points according to:

$$\varphi_{AB} = \frac{2\pi}{L} d_{AB} \tag{3.2}$$

In which d_{AB} is 63000 meters and represents the distance between the two boundary points. Given the orientation of the cross-shore and alongshore boundaries a phase difference of 90° is present between the water level boundary and the Neumann boundary. This leads to the following Neumann boundary conditions:

Table 3.3 Harmonic Neumann boundaries conditions morphological tide.

Tidal constituent	Frequency [°/hour]	Amplitude SW [m]	Phase SW [°]	Amplitude NW [m]	Phase NW [°]
C_1	14.4966443	3.2159e-6	314.4635	3.1970e-6	314.8365
M_2	28.9932886	1.7467e-5	315.4925	1.7138e-5	314.4275

Harmonic analysis river discharge

Jay (1984) states that tidal propagation in the Columbia River at least reaches all the way up to Columbia City at river mile 83. This means that tidal effects are still strong at the Beaver boundary, and should therefore be accounted for in the morphodynamic boundary representation.

With the implementation of a morphological tide at the sea boundaries, a schematized set of tidal constituents is created. The tidal flow out of the model induced by these constituents needs to be accurately balanced by the boundary tidal inflow. The tidal flow at the boundary assigned by a harmonic total discharge consisting out of the contribution of the M_2 and C_1 components only. A river discharge can be assigned on top of this. In order to get to know the individual amplitudes of the discharges of the M_2 and C_1 components a harmonic analysis has been carried out on available measured discharge data at the Beaver Army Terminal using the Matlab based analysis *t_tide* (Pawlowicz et al., 2002). Measured quarter of an hour interval discharges for a period of 3 months have been analyzed (see Figure 3.5).

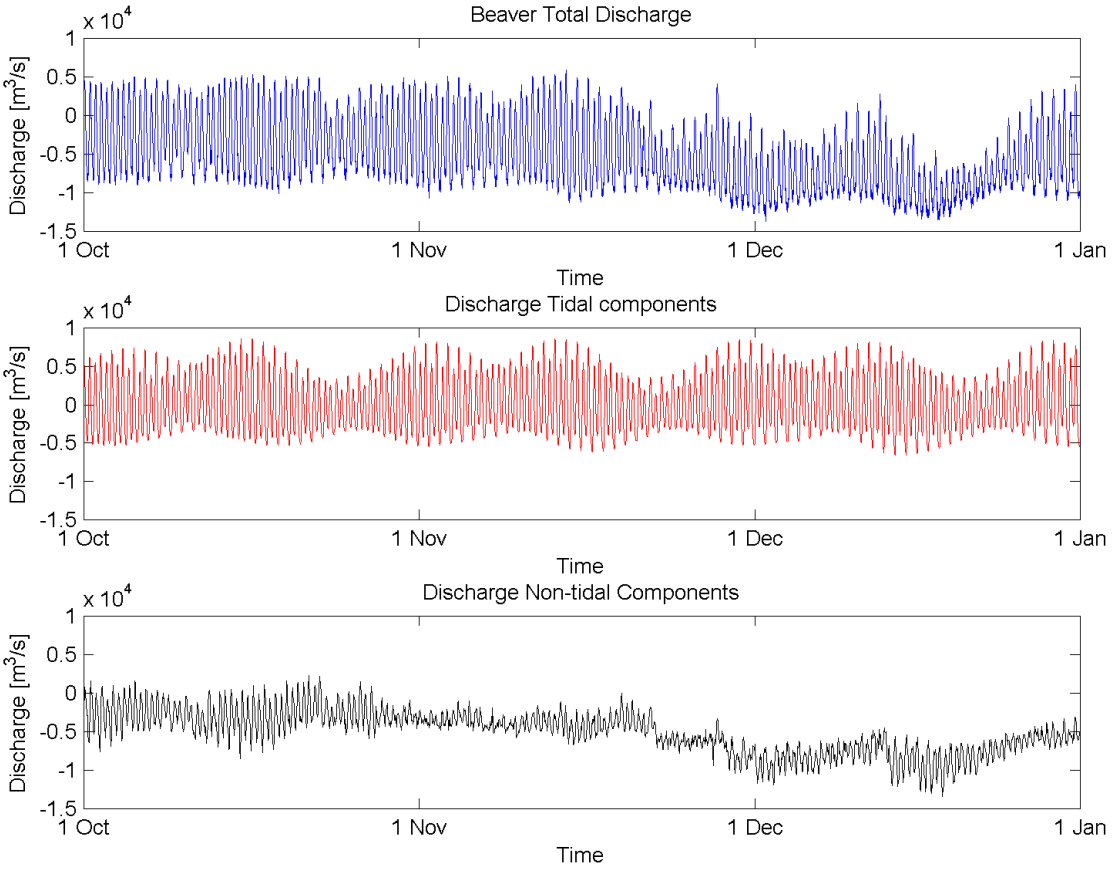

Figure 3.5 Harmonic analysis measured discharge.

The top plot of Figure 3.5 shows the time-series of the measured total discharge for the analyzed 3-month period. The middle plot shows the time-series of the contribution of the harmonic tidal components to the total discharge, resulting from the harmonic analysis. The bottom plot finally shows the time-series of the contribution of the non-tidal components to the total discharge, i.e. the river discharge.

The harmonic signal of the tidal components has further been divided (see Figure 3.6) to show the individual contribution of the ten most important tidal components using the Matlab based analysis of *t_predic (*Pawlowicz et al., 2002).

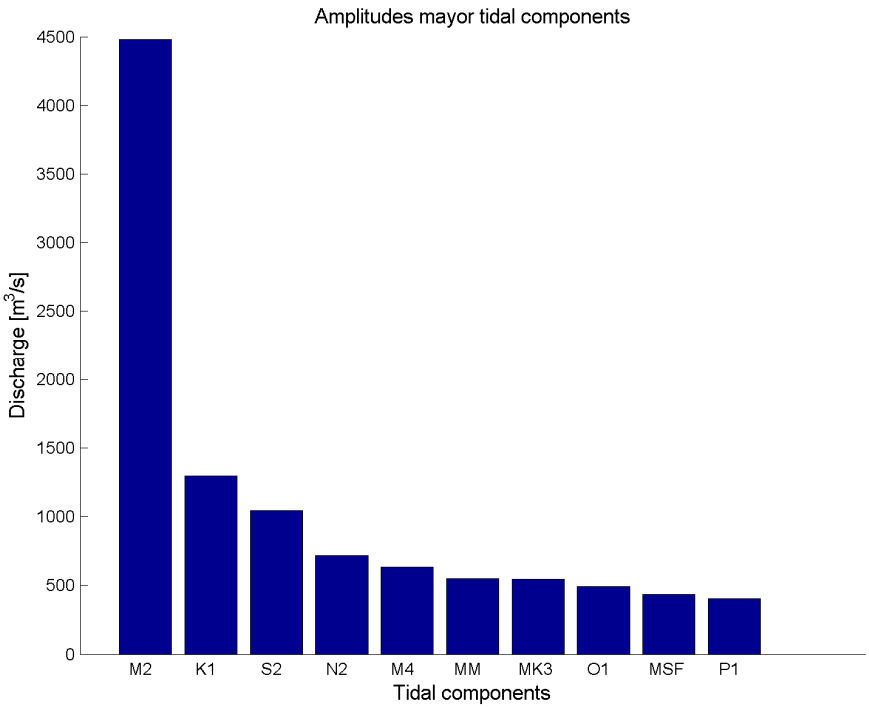

Figure 3.6 Amplitudes ten mayor tidal components at the Beaver Army Terminal.

Figure 3.6 shows that the six major offshore tidal components are still active at the Beaver Army Terminal. In addition to this, shallow water over tides such as the M_4, the M_M and the MK_3 have developed as a result of bottom friction that the tide experiences in its propagation through the estuary and further upriver. Only the derived M_2, K_1 and O_1 components are taken form the harmonic analysis and implemented in the harmonic boundary conditions at the river domain to balance the morphological tide at the sea domain, where also the same scaling factor of 1,08*(M_2+C_1) is applied. In which again: $C_1 = \sqrt{2O_1K_1}$. This leads to the following harmonic boundary conditions at the Beaver Army Terminal:

Table 3.4 Harmonic river boundary conditions.

Tidal constituent	Frequency [°/hour]	Amplitude [m^3/s]	Phase [°]
C_1	14.4966443	1129	157.36
M_2	28.9932886	4840	71.73

The application of a morphological tide at the river boundary section using a harmonic analysis on a measured discharge is a result of the fact that no measured historic discharge is available at the Beaver Army Terminal. It is also not possible to purely implement a river discharge at the Beaver Army Terminal boundary since according to Jay (1984) the tide propagates through the assigned river boundary. Since at the sea boundary a morphological tide is implemented consisting out of only two tidal components, the assumption is made that the river boundary should follow this set of components in order to balance the tidal flow. The effect of the generation of second order shallow water over tides at the river boundary is not taken into account by only applying the M_2 and C_1 component. The application of a pure two constituent morphological tide at the river boundary mathematically not founded. It is a first attempt in the process of modeling the long-term morphological behavior of a high energetic estuarine system. The fact that the focus of the study is on morphological processes at the mouth of the Columbia River and that the tidal prism through the mouth strongly dominates

the tidal signal at the river boundary implies that the effect of a possible underestimation of the tidal signal at the river boundary will not affect the morphological behavior at the mouth much. Additional sediment transports induced by the shallow water over tides at the river boundary are not taken into account. It is assumed that these transports do not affect the general morphology at the mouth much considering the distance from the river boundary to the mouth and their order of magnitude.

To be able to quantify the effect of the application of a schematization of boundary forcing conditions at both the seaward boundary and the river boundary on the sediment transport, a comparison of cumulative total transports through the mouth is given (Figure 3.7) for a tide consisting out of six tidal components with a measured river discharge signal and a reduced harmonic tidal and river discharge signal.

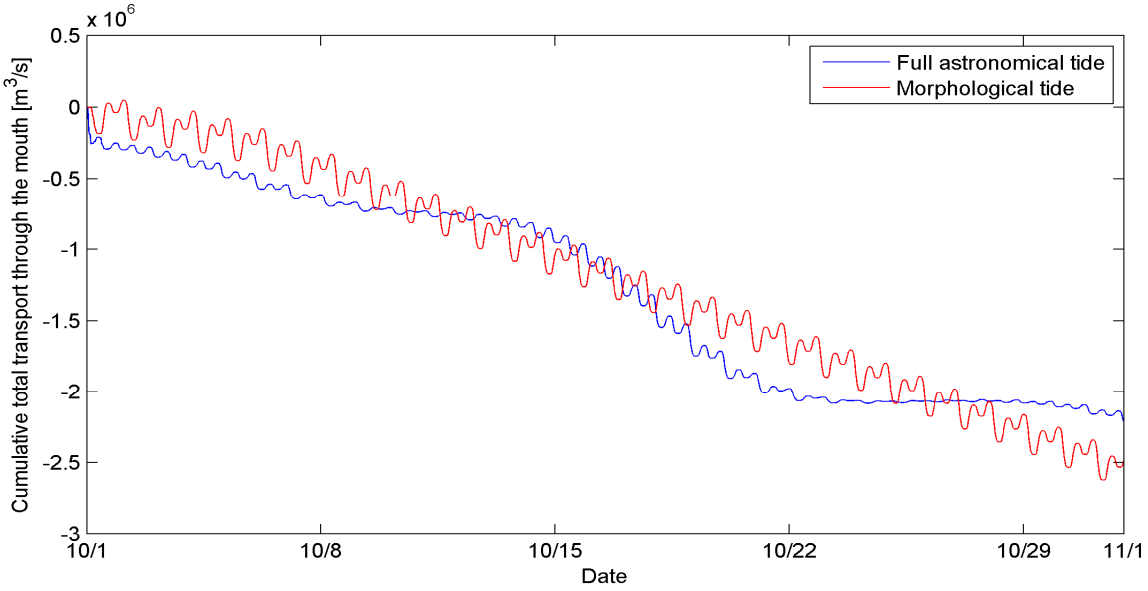

Figure 3.7 Cumulative total transports through the mouth.

Figure 3.7 shows that the total transports through the mouth are overestimated by about 12 % in a schematization of both the tidal and the discharge signal. For the remainder of the study this deviation is however accepted, with it being a first attempt in schematizing the complex system of the MCR. It is however appoint of attention and discussion.
A possible solution to avoid the uncertainties implied by a morphodynamic boundary representation would be to extent the model up to the Bonneville dam and create a boundary here. An accurate upstream river boundary description is maintained while the tidal signal through the boundary will be completely taken out. Full hydrodynamic calibration and validation of this extended model will however be time-consuming. Preliminary unpublished attempts have so far not given correct results.

3.3.4 Joint probability of discharge and waves

Both wave-and density-driven flows govern the sediment transport at MCR. Analysis of both the wave and discharge data (Figure 3.10 and Figure 3.13) shows that both forcing conditions are highly seasonal variable. With the higher wave heights having the potential for importing sediment transport through the mouth and the higher river discharges having the potential for exporting sediment transports through the mouth. For correct long-term morphodynamic simulation the joint probability of discharges and waves should be accounted for. The joint probability of discharges and waves is taken into account by creating seasonal river discharge climates and seasonal wave climates.

3.3.5 River discharge schematization

River discharges at the model boundary of Beaver Army Terminal (BAT) for the 1926-1958 time-frame (Period B) need to be schematized. Historic daily and monthly river discharge for this period is however solely available for the USGS river gauging station, The Dalles, 14105700 (http://waterdata.usgs.gov/nwis/) at river mile 191.5. Tributaries downriver from the Dalles station increase the total river discharge at BAT. To account for this increase a determination of the river discharge ration between the Dalles and BAT is done on present daily discharges between 1992 and 2010. Daily discharge signals are used to sufficiently take into account peak flows and still take out the majority of the tidal components that disturb the net river discharge signal. In Figure 3.8 measured daily discharge signals for 1992-2010 are compared between the Dalles station and BAT.

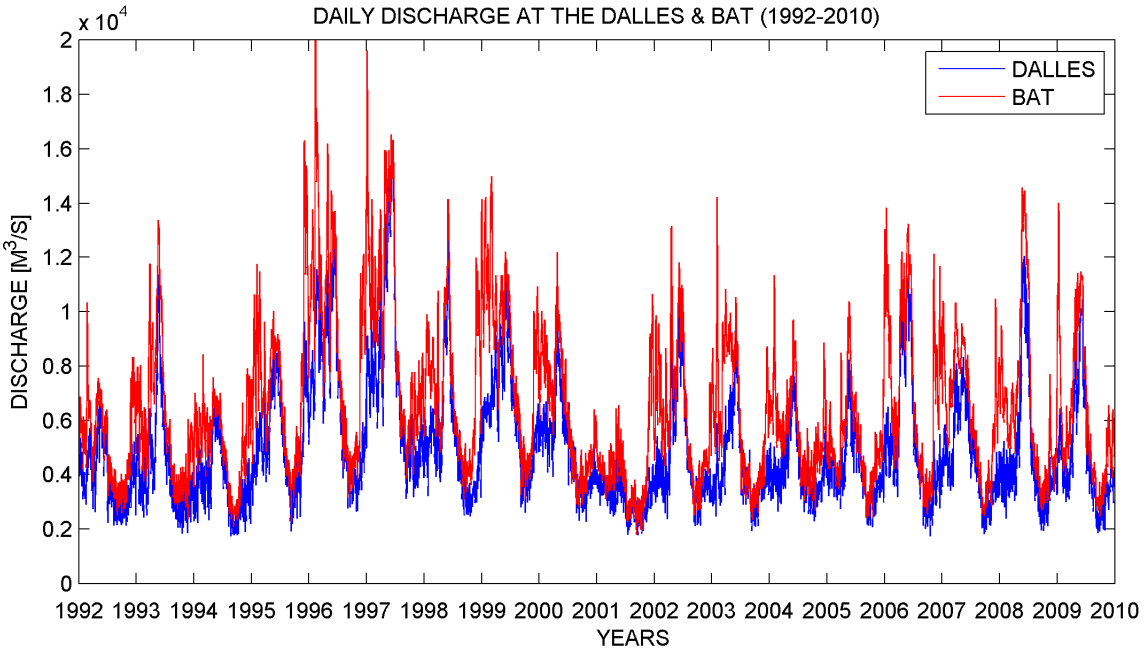

Figure 3.8 Daily discharge analysis The Dalles and Beaver Army Terminal 1992-2010.

Figure 3.8 shows that the general daily discharge signal of peaks and lows for the two stations is the same. The amplitudes of the discharge signal at BAT are however higher as a result of the contribution of the downriver tributaries. With an assumed more or less linear difference between the discharges at the Dalles and at BAT a simple factorisation of the available historic discharge data at the Dalles is performed to create a historic discharge signal for BAT. The discharge ratio follows from the comparison of the mean daily discharge of the two stations and is 1.31.

In Figure 3.9 the created factorised discharge at the BAT station from the measured Dalles station discharge is shown in comparison to the measured discharge at BAT and the root-mean-squared error.

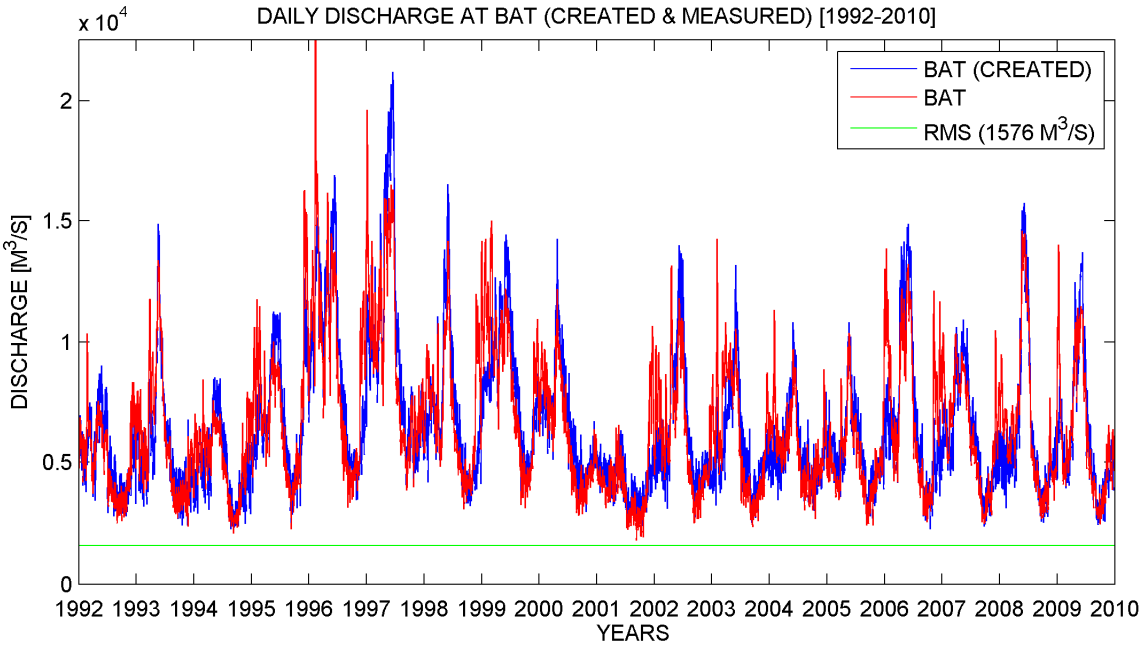

Figure 3.9 *Discharge comparison the Dalles and Beaver Army Terminal created.*

Without complete river blockage as a result of downriver dam construction before 1982, there was no completely controlled discharge and therefore no severe alternation of the river discharge below Bonneville in comparison to the historic measured discharge at the Dalles.
It is however noted that the Bonneville Dam downriver of the Dalles station has influenced the river discharge signal at BAT from the moment it finished its construction in 1982. This effect could however not be taken out of the comparison of present day discharges between the Dalles station and BAT.

The same factor is now used to create a historic discharge for the BAT station for period B from the historic Dalles station data. Measured historic daily discharge at the Dalles station is multiplied by the factor of 1.31 and the new created daily historic discharge for the Beaver Army Terminal station is plotted according to its occurrence in days of the year in Figure 3.10.

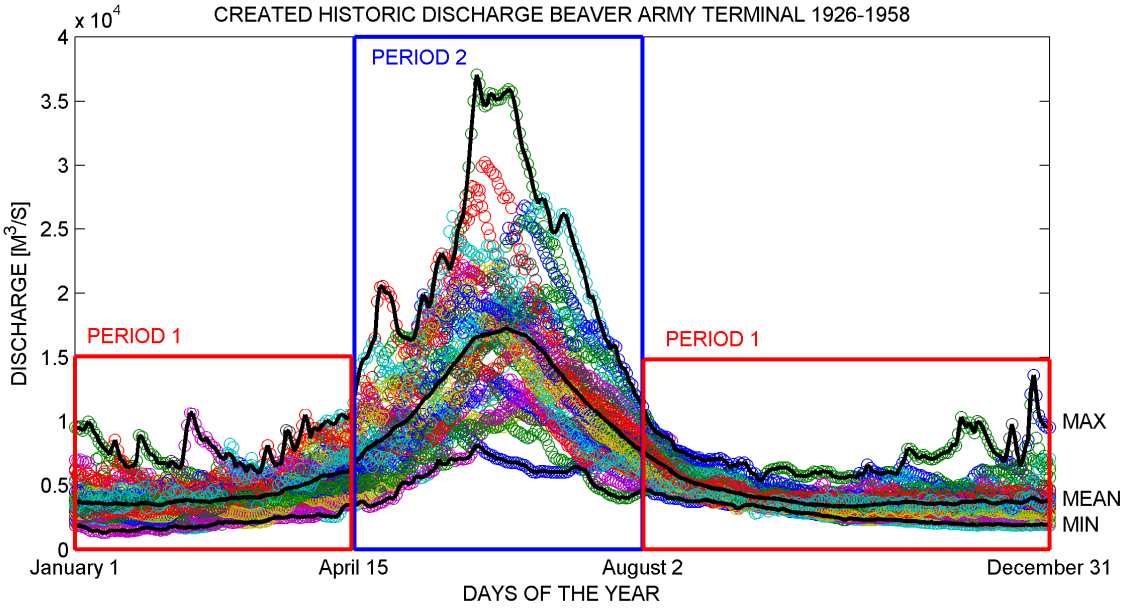

Figure 3.10 Historic created discharge distribution Beaver Army Terminal per day of the year.

The plot shows a strong seasonal distribution of the historic discharge. The overall mean discharge is around 6400 m^3/s. River discharges peak from mid April until the beginning of August as a result of snowmelt. For further schematization, the river discharge is separated into two periods. Period 1 ranges from the 2nd of August till the 14th of April, where the maximum discharge always stays below 11000 m^3/s. Period 2 ranges from April 15th till August 1st. Peak snowmelt flows arise in this period up to values of even 37059 m^3/s (1948 flood discharge). Both periods are now distributed in several discharge classes according to their probability of occurrence. Each period at least holds a bin below the mean discharge, around the mean discharge, and an upper peak value discharge.

Table 3.5 Discharges period 1 and period 2.

Period	1	2
Minimum	1335 m^3/s	3361 m^3/s
Max	10646 m^3/s	37059 m^3/s
Mean	4145 m^3/s	12508 m^3/s

This leads to the following historic discharge schematization, separated in the two river seasonal periods.

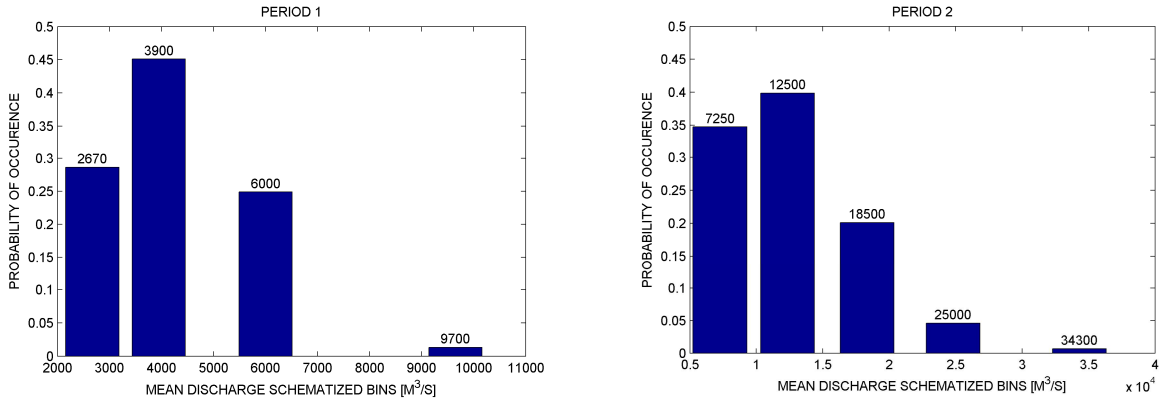

Figure 3.11 Discharge classes and their probability of occurrence for period 1(left) and period 2(right).

3.3.6 Wave climate schematization

Directional hourly wave data is available from offshore wave buoy 46029 for 1995-present. Years that hold less than two third of the total year-round data are considered to provide insufficient data for this analysis (see the table in Figure 3.12). This leads to 10 years of usable wave data. Historic wave data is unavailable in the area and therefore recent wave data is used to schematize the historic wave climate. The overall change in wave climate over the last 50 to 75 years is thereby considered not to have changed. The objective of the wave climate schematization is to define a wave climate consisting of a limited number of offshore wave classes which produce the same residual sediment transport patterns and rates as the full set of offshore wave conditions.

YEAR	DATA %
1995	28.7
1996	40.0
1997	86.5
1998	59.0
1999	92.3
2000	41.1
2001	97.8
2002	97.8
2003	97.8
2004	94.1
2005	70.0
2006	95.5
2007	55.8
2008	79.3
2009	69.3

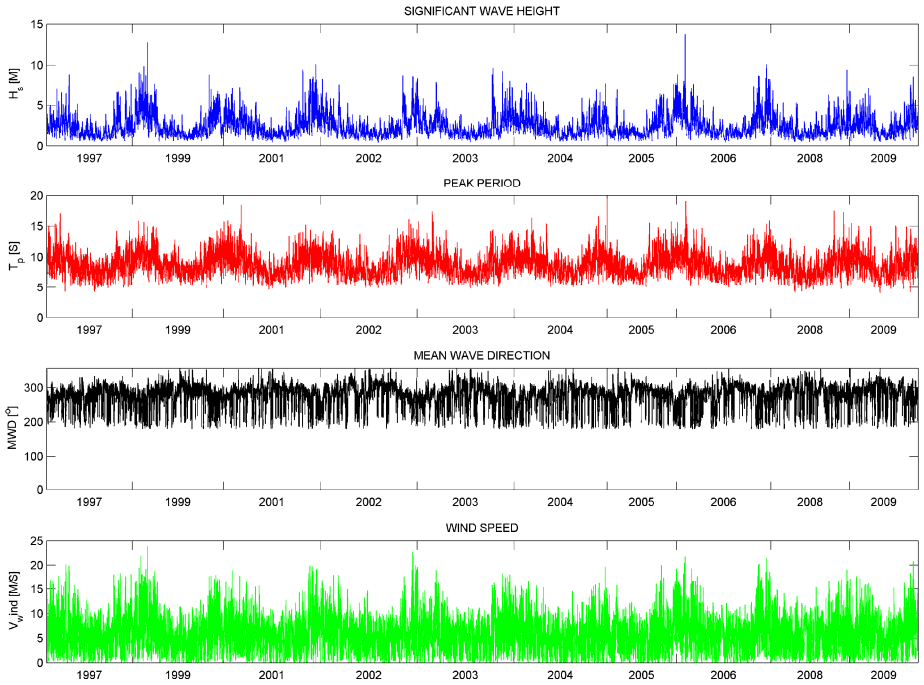

Figure 3.12 Wave date from station 46029.

Analysis of the wave data shows that a strong seasonality exists in the wave data (Figure 3.13). To account for the joint-probability of occurrence of the river discharge and the wave conditions, the same seasonal distribution in periods is applied in the wave climate schematization as in the river discharge schematization.

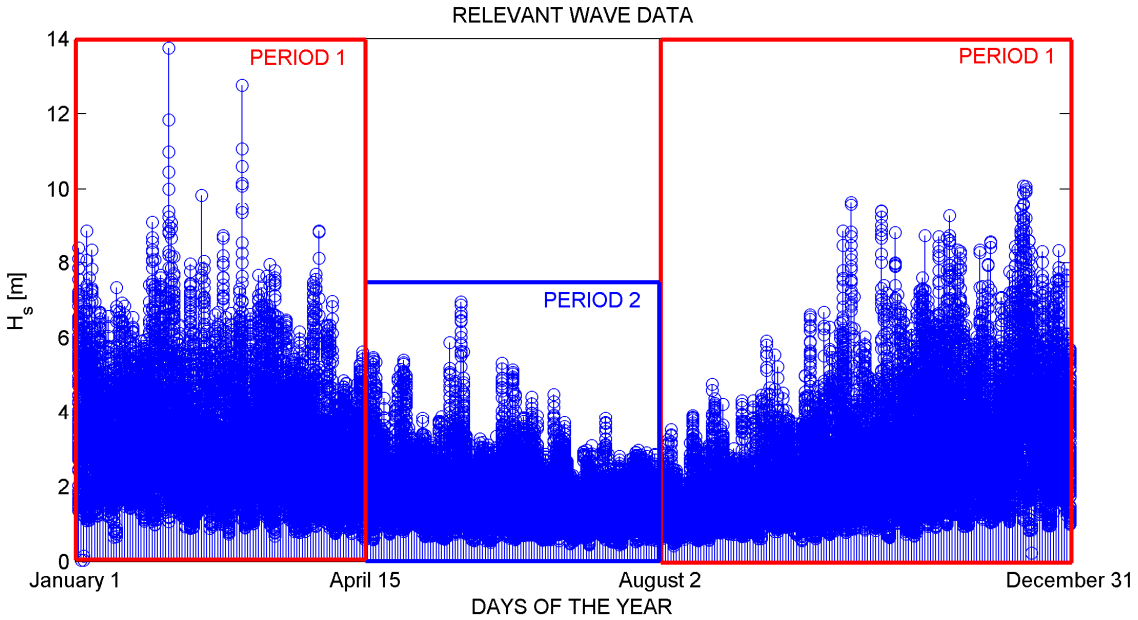

Figure 3.13 *Wave data from station 46029 distributed per day of the year.*

Waves in Period 1 reach significant higher values than in the calmer spring/summer Period 2. Wave heights in Period 1 can reach values of up to 14 meters. While the average significant wave height for this period is about 3 meters. The waves in Period 1 predominantly come from the west-north-west with the higher waves predominantly coming from the south-west (see Figure 3.14 left). Period 2 on the other hand has maximum wave height values of less than 7 meters and an average significant wave height value of 1.75 meters. For period 2 the waves also predominantly come from the west-north-west with the higher values predominantly from the west and west-south-west (see Figure 3.14 right).

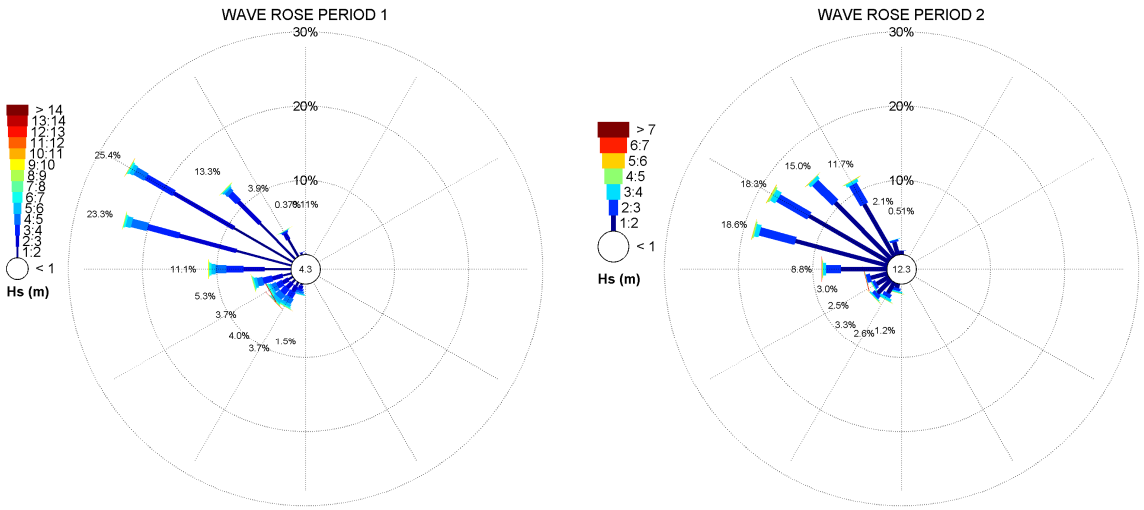

Figure 3.14 *Wave roses for Period 1 (left) and Period 2 (right).*

Two different wave climate schematizations are used in the process of getting to the final long-term morphological model. In the calibration phase a first insight basic wave climate schematization is used as described in §3.2.6.1. This basic wave climate schematization is applied in combination with a mean river discharge. The calibration phase is considered to

provide space to test the overall morphological behaviour of the model. Individual effects of certain combinations of forcing conditions are not yet considered to be important in this phase. The stability and the overall morphological behaviour of the model are more important. A basically schematized wave climate will thus suffice. In the final runs however a more detailed wave climate schematizations, using the Energy Flux method as described in §3.2.6.2 and by Dobrochinski (2009) is used in combination with the Opti-routine (Mol, 2007, and §4.1). A seasonally varying river discharge schematizations as described in §3.2.4 is used in combination with this detailed wave climate. The joint occurrence of waves and discharges and the influence of peak values are taken into account by the application of these schematizations.

3.3.6.1 Basic wind and wave climate

In the basic wind and wave climate schematization a total number of eight wave conditions are withdrawn from the total wave data. The eight wave conditions are separated in four wave height classes and two directional classes. In which the distribution of the wave height represent small waves ($H_s \leq 1.2$m), average waves ($1.2\text{m} < H_s \leq 3\text{m}$), above average waves ($3\text{m} < H_s \leq 5\text{m}$), and high waves ($5\text{m} < H_s \leq 9\text{m}$). Wave heights greater than 9m are not taken into account in this basic wave climate schematization. The distribution into directional classes is simply taken to represent waves coming from a more southern direction ($180° < \varphi \leq 270°$) and waves coming from a more northern direction ($270° < \varphi \leq 360°$). The parameters per wave condition represent mean values of all the data within each particular bin. The following table gives the total distribution of the basic wave climate schematization.

Table 3.6 Basic wave climate schematization.

Wave condition	H_s [m]	T_p [s]	Dir [°]	V_{wind} [m/s]	Probability [-]	Duration [days/yr]
$H_s \leq 1.2$ m						
wc1	0.96	7.44	233	3.78	0.053	19
wc2	1.03	7.20	297	4.13	0.090	33
1.2 m$< H_s \leq$ 3 m						
wc3	2.10	8.32	242	6.10	0.135	49
wc4	2.03	8.49	295	5.44	0.482	176
3 m$< H_s \leq$ 5 m						
wc5	3.92	9.63	235	9.13	0.083	30
wc6	3.75	10.58	289	6.62	0.112	41
5 m$< H_s \leq$ 9 m						
wc7	6.10	11.14	231	11.29	0.027	10
wc8	5.94	12.11	289	8.37	0.018	7

3.3.6.2 Energy Flux method

In the energy flux method (Dobrochinski, 2009), representative wave conditions are separated according to the concept of equal energy. In the energy flux method, each derived wave conditions holds about an equal amount of energy. Especially for morphological simulations this equal energy concept benefits the wave climate schematization. The influence of each wave conditions on the morphology is hereby considered to be more evenly distributed in comparison to the traditionally schematized wave climate. An assigned number of directional (n) and wave height (m) bins determines the equal energy distribution. At first, a distribution in wave direction is done. In which each directional classes is filled with individual waves that in total hold $1/n^{th}$ of the total energy of the wave set according to:

$$E_{tot} = \sum_{i=1}^{j} E_{f_i} = \sum_{i=1}^{j} (\frac{1}{8} \rho g H_{s_i}{}^2 * C_g) \quad (3.3)$$

In which ρ is the water density (kg/m3), g is the gravitational acceleration (m/s^2), $H_{s,i}$ the significant wave height of each wave and C_g the deep water wave group celerity (m/s), following C_g=1.56T. In which, T is the wave period.

Secondly a distribution in significant wave height is done. Each significant wave height class is built out to hold 1/mth of the total energy that the particular directional bins now holds. The total energy per completed bin, in both directional and wave height thus holds 1/n*mth of the total energy of the wave set. A representative wave height for each bin is than re-derived from the mean energy flux of the bin together with a mean energy flux direction. The wave period for each bin follows from the mean period of the bin. The wind speed has been added to the method in this study and also represents the mean wind speed. With this equal energy distribution of the wave conditions the less important lower wave heights are combined more to increase their effect on the total morphology. The higher wave heights on the other hand are separated more to let their relatively high effect on the morphology come out more. With the energy flux-method, the resolution of the morphologic more effective wave conditions is thus increased while the resolution of the morphologic less effective wave conditions is decreased. In this study, following the river discharge schematization, the wave climate schematization is separated into two seasonal periods. For the high energy period 1, a wave climate consisting out of in total 107 wave conditions is determined. Ten directional wave classes versus ten wave height classes (Hs≤10.5 m) are separated. Together with seven individual peak conditions (Hs>10.5 m). For the lower energetic period 2, a wave climate consisting out of in total 72 wave conditions is determined. Eight directional wave classes versus eight wave height classes (Hs≤6 m) are separated. Eight individual peak conditions (Hs>6 m) complete the schematization. The following figures represent the wave climate schematization according tot the Energy Flux method. Individual peak conditions are given separately and so are the standard deviation of the taken mean period and wind speed for both period 1 and period 2.

Period 1

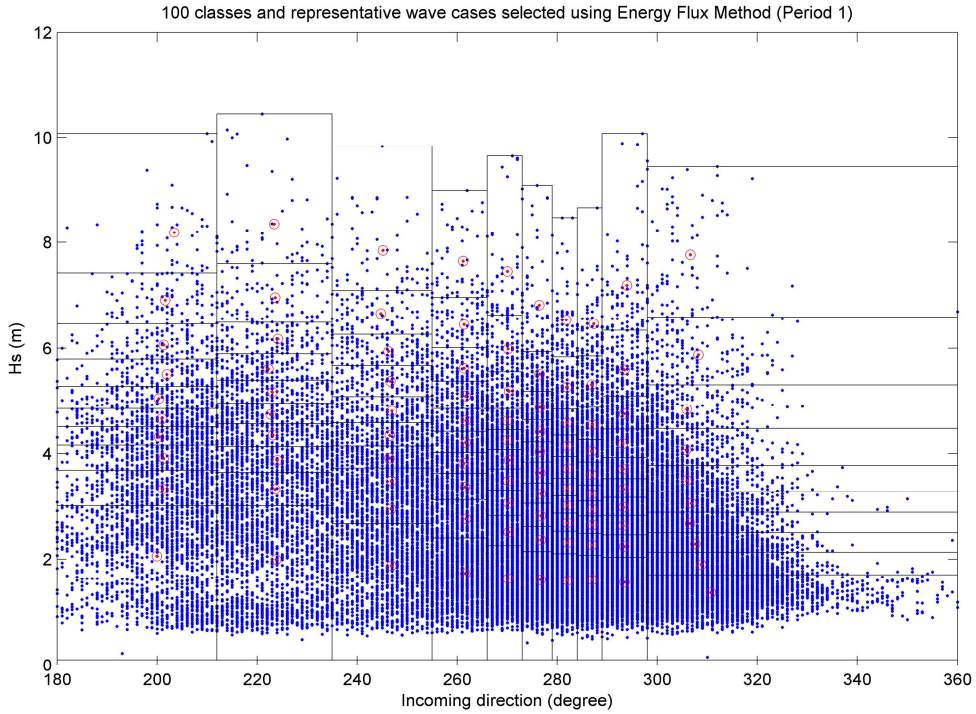

Figure 3.15 Energy Flux method wave climate schematization for Period 1.

Following the wave height plot rose of Figure 3.14, from Figure 3.15 it shows that the majority of the waves in Period 1 centre around the wave direction of 270°. For the energy flux wave climate schematization leading to smaller directional and wave height bins around this wave direction. The high resolution of wave classes in this particular section thus gives a high resolution schematization for dominant wave conditions. Less important wave conditions are given a lower resolution in schematization. Figure 3.15 also shows that the higher waves more dominantly come from a more southern direction (<270°).

Table 3.7 Remaining individual peak conditions, Period 1.

Wave condition	H_s [m]	T_p [s]	Dir [°]	V_{wind} [m/s]
101	12.76	14.95	222	20.00
102	11.07	13.95	226	20.90
103	10.60	13.04	209	18.90
104	13.75	14,45	230	20.10
105	13.74	14,60	233	19.00
106	10.98	13,65	228	17.50
107	11.84	14.25	237	18.30

Individual peak values are taken out of the total schematization since their individual importance was thought to influence the morphology more than when they would be implemented in the general schematization. There effect would then be nullified by the other, generally much lower waves within the bin.

Both the period and the wind speed for each created wave conditions are obtained by taking the mean value of all of the individual wave data within each bin. To show whether it is correct to apply this mean value in the further analysis, the standard deviation of both the period and the wind speed for each conditions is given in the following figures.

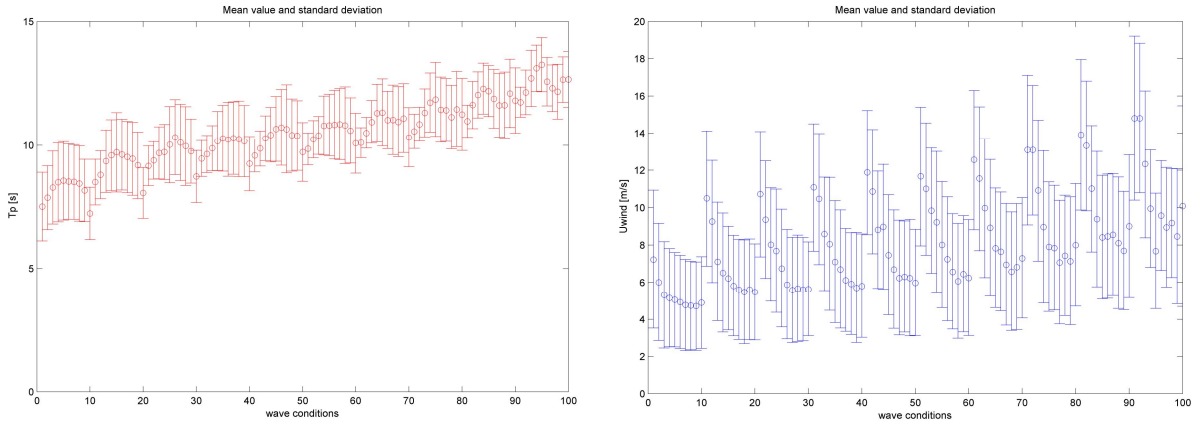

Figure 3.16 Mean value and standard deviation for peak period (left) and wind speed (right), Period 1.

The mean standard deviation of the wave period in Period 1 is 1.19 seconds with a mean relative standard deviation of 11.66%. The mean standard deviation of the wind speed in Period 1 is 3.24 meters per second with a mean relative standard deviation of 42.11%. From this analysis it is concluded that applying the mean value of all the wave periods in the bin in the wave climate schematization is justified. Applying the mean value of the wind speed however is due to its great divergence not justified. A limited available correlation between the wave height and the wind speed however still led to the application of this mean value in this study.

Period 2

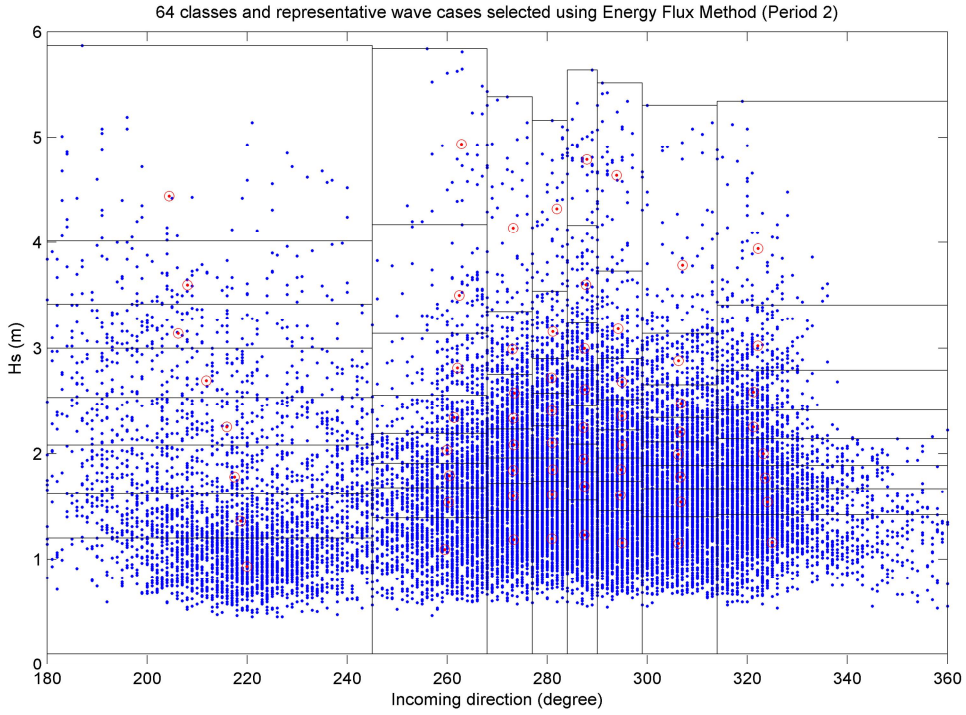

Figure 3.17 Energy Flux method wave climate schematization for Period 2.

Figure 3.17 shows the schematization of wave conditions for Period 2. The majority of the waves centre around a direction of about 290 degrees and wave heights of about 2 meters. Maximum wave height are smaller than 6 meters. While some individual peak values succeed this 6 meters. Wave heights however still stay below the 7 meters in Period 2.

Table 3.8 Remaining individual peak conditions, Period 2.

Wave condition	H_s [m]	T_p [s]	Dir [°]	V_{wind} [m/s]
65	6.67	12.21	258	10.50
66	6.87	12.40	252	10.80
67	6.47	12.13	251	11.40
68	6.58	12.28	257	9.00
69	6.96	12.86	253	8.10
70	6.44	12.31	253	8.10
71	6.16	12.19	255	8.00
72	6.01	12.28	249	8.10

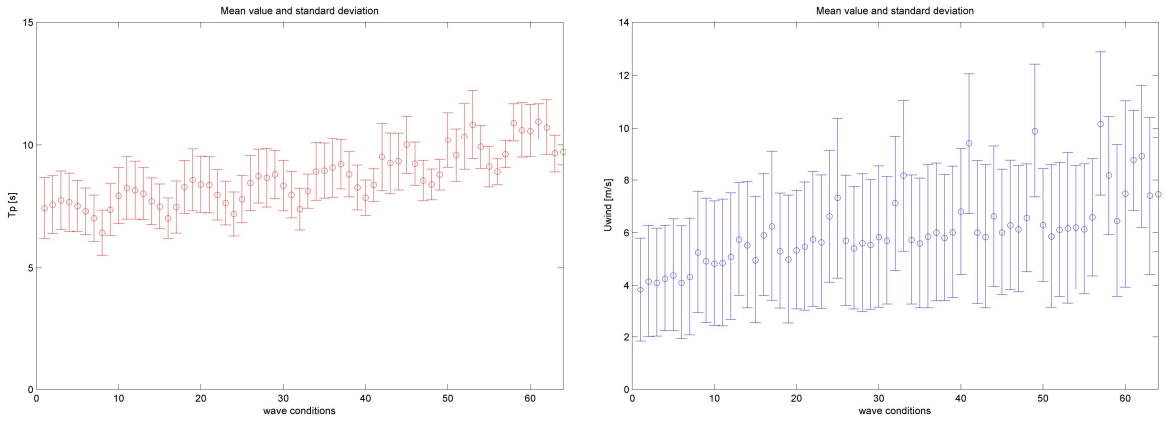

Figure 3.18 *Mean value and standard deviation for peak period (left) and wind speed (right), Period 2.*

The mean standard deviation of the wave period in Period 2 is 1.00 second with a mean relative standard deviation of 11.71%. The mean standard deviation of the wind speed in Period 2 is 2.47 meters per second with a mean relative standard deviation of 41.88%. Again, application of the mean period per wave bin in the wave climate schematization is considered to be justified, while the application of the mean value per wave bin in the schematization of the wind speed is not justified however still applied.

3.3.7 Opti-routine

With the energy flux method a high resolution wave climate has been created that for Period 1 and Period 2 in total consists out of 179 wave conditions. In combination with the river discharge schematization, the total amount of possible occurring combination of waves and discharges is 778 conditions (Period 1;107*4=428 conditions, Period 2;72*5=360 conditions). Obviously this vast amount of conditions is still too big to be accounted for in the simulations. The opti-routine (Mol, 2007) as described in §4.2 is used to reduce this set of conditions for the final long-term simulations to a practical amount.

3.3.8 Morphological acceleration factor

Morphological changes take place over a much longer time periods than hydrodynamic changes. To overcome the problem of having to perform a simulation over morphological time scales of years to decades, a morphological acceleration factor (Lesser, 2004) is implemented in the Delft3D model. The morphological acceleration factor (MorFac) multiplies the sediment fluxes to and from the bed by a constant factor (Figure 3.19). thereby effectively extending the morphological development.

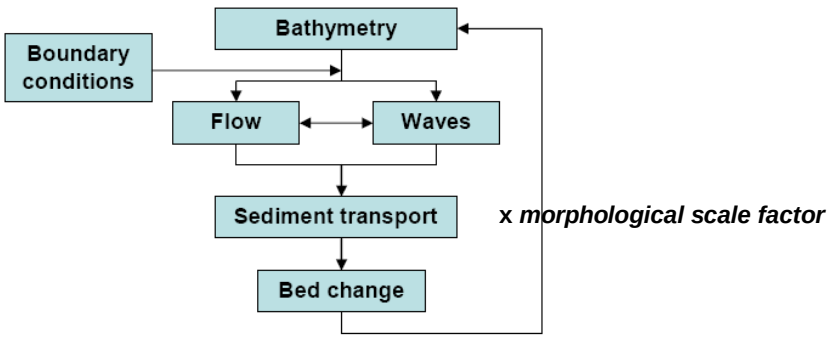

Figure 3.19 Schematic *overview Delft3D-Online with morphological acceleration factor (Roelvink, 2006).*

The morphological scale factor implies that long term morphological simulations can be achieved using hydrodynamic simulations of only a fraction of the required duration. There are however limits to the MorFac that can be applied, depending on the characteristics of the location under consideration. The selection of a suitable morphological acceleration factor remains a matter of judgement and sensitivity testing for the modeller. Some limitations hold however when the morphological scale factor is applied to coastal situations subjected to oscillating tidal currents and other time-varying forcing conditions. (Lesser, 2004). Generally, it requires that bed elevation changes and the changes to the associated sediment transport patterns must be able to be assumed to be approximately linear for changing MorFac over the full sequence of MorFac times tides. The validity of the assumption of linearity can easily be tested, by conducting repeated simulations with different morphological scale factors and appropriately adjusted hydrodynamic simulations. As an indication, however, previous studies (Lesser et al, 2003, Grunnet et a., 2004,and Reniers et al., 2004) have indicated that MorFac in the range of 10 to 100 can usually be safely applied in coastal zones where waves are significant.

3.3.8.1 *Validity linear assumption MorFac*

A variable morphological scale factor per wave conditions is applied in the simulations. This has the desirable effect that higher acceleration factors are applied to the more common, and generally smaller, wave height conditions, during which the morphology is less active. Smaller acceleration factors are applied to the larger and less common wave conditions where the morphology is more active and large acceleration factors might cause problems. In order to reduce computation times as much as possible an optimal value for the morphological scale factor needs to be found. Three simulations form the calibration of the applicable morphological scale factor. Initially a as high as possible variable morphological scale factor is applied under which a maximum morphological scale factor of 100 is allowed. Subsequently the factors are halved and divided by four to see the effect of the increased morphological scale factor on the morphological behaviour and to check whether the increase in morphological scale factor has a linear morphological development. The number of morphological tides over which a certain wave condition is simulated is thereby respectively doubled and quadrupled.

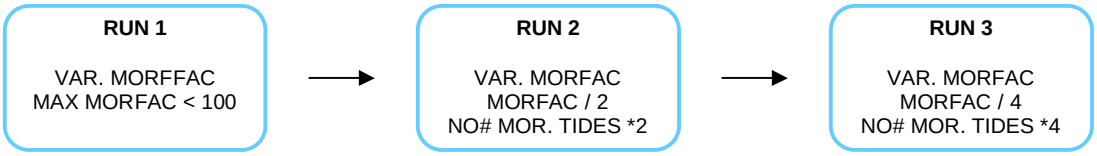

Figure 3.20 Schematic overview calibration runs variable morphological scale factor.

For each wave conditions the morphological scale factor will depend on the probability of occurrence of that particular wave conditions in a schematized five year climate. The number of full morphological tides over which a wave condition is simulated depends on its probability of occurrence together with the assumed maximum allowed morphological scale factor. A five-year climate is schematized instead of a one year climate to limit computation time. In the following table, the basic wave climate schematization (§3.3.5.1) with the applied morphological scale factor and number of morphological tides is given for the calibration simulation with the highest applied morphological scale factor, Run1. Morphological scale factors for Run 2 and Run 3 follow from a division by 2 and 4 respectively. The number of morphological tides per condition need be multiplied by 2 and 4 respectively for the justified comparison between the simulations to hold.

Table 3.9 Basic wave climate schematization with applied morphological scale factors.

Wave condition	H_s [m]	T_p [s]	Dir [°]	V_{wind} [m/s]	Probability [-]	Duration [days/5yr]	# mor. tides	Mor. Fac.
$H_s \leq 1.2$ m								
wc1	0.96	7.44	233	3.78	0.053	97	1	93.48
wc2	1.03	7.20	297	4.13	0.090	164	2	79.37
1.2 m<$H_s \leq 3$ m								
wc3	2.10	8.32	242	6.10	0.135	246	3	79.37
wc4	2.03	8.49	295	5.44	0.482	880	9	94.46
3 m<$H_s \leq 5$ m								
wc5	3.92	9.63	235	9.13	0.083	152	2	73.20
wc6	3.75	10.58	289	6.62	0.112	204	3	65.85
5 m<$H_s \leq 9$ m								
wc7	6.10	11.14	231	11.29	0.027	49	2	23.81
wc8	5.94	12.11	289	8.37	0.018	33	1	31.75

Determination of the allowed optimal morphological scale factor comes from the comparison of morphological behaviour of the three simulations. A as high as possible MorFac is wanted to limited computation times as much as possible. An increase in morphological scale factor should lead to identical morphological changes if the assumption of linearity is valid. At first, the total cumulative erosion sedimentation patterns of the three five-year simulations are visually compared (see Figure 3.21).

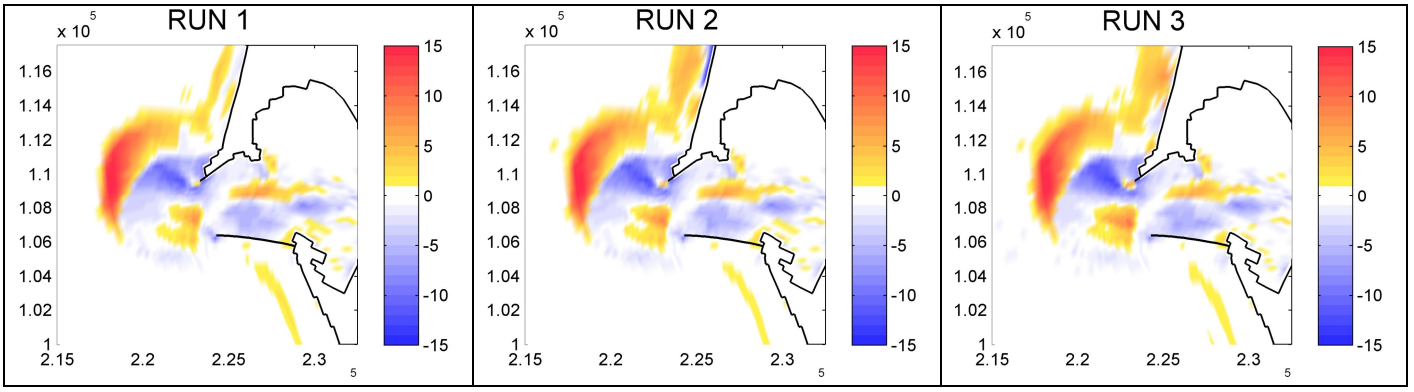

Figure 3.21 Bathymetric change, calibration optimal morphological scale factor.

A quick visual comparison shows that the three runs have similar morphological change patterns in the areas of interest, the outer ebb tidal delta, the inner ebb tidal delta and the inlet. However, further away from the mouth of the Columbia River, along the beaches, differences start to show. Since this study mainly focuses on the morphology directly at the mouth of the Columbia River, these changes are accepted as long as the stability of the model is not affected by them.

A more detailed analysis of the applicable MorFac is however required to rightfully justify the application of a certain morphological scale factor. Therefore, the volumetric changes over time of each compartment of the outer delta, inner delta and inlet are compared. From this quantitative analysis, it is possible to also weight the quantitative behaviour of the simulations in a later stadium. The cumulative volumetric change per compartment of the three calibration runs are plotted in the following three figures.

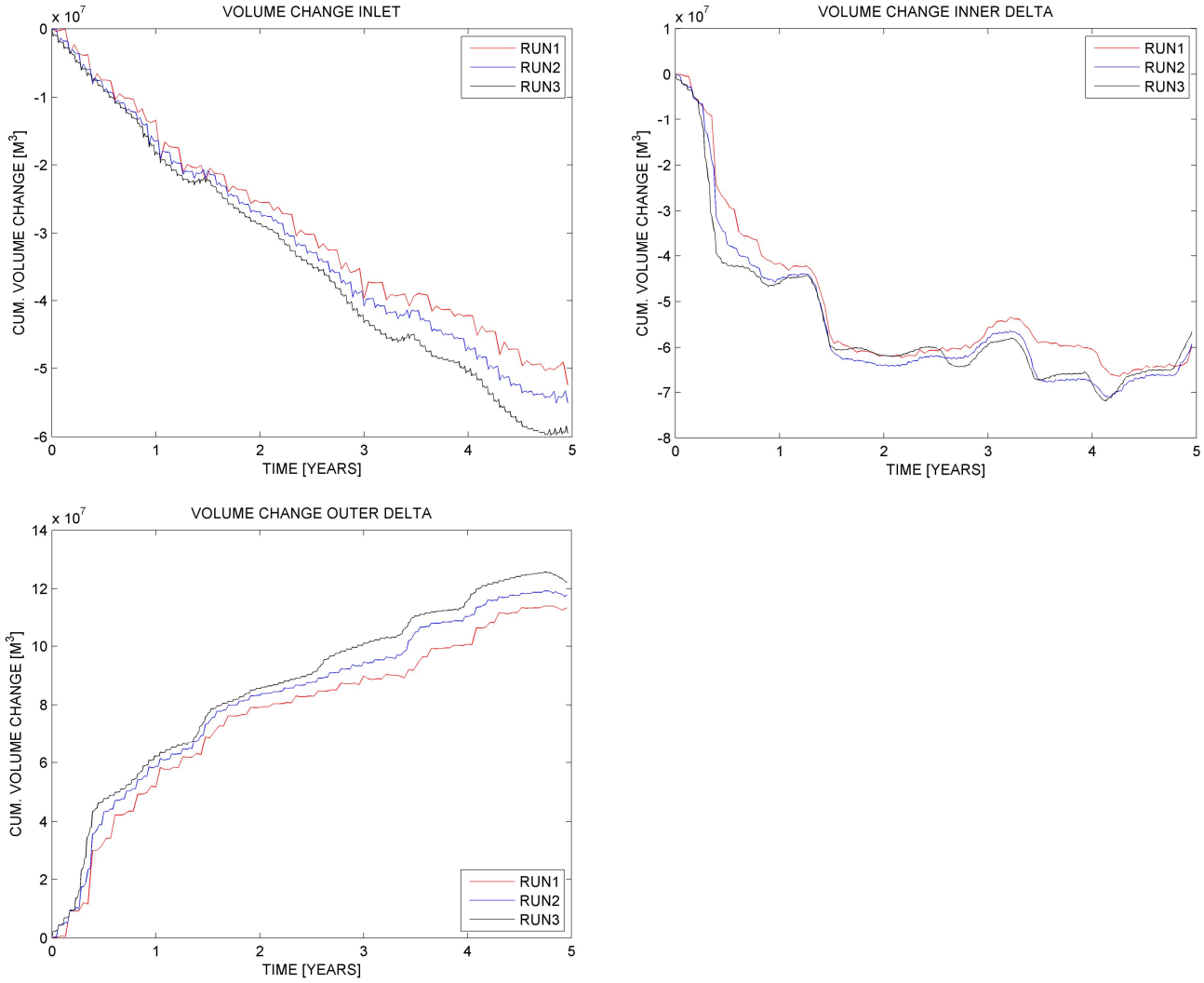

Figure 3.22 Volumetric change Outer Delta.

From Figure 3.22 it shows that in the optimization process of the morphological scale factor, general patterns of morphological change in the areas of interest are reproduced by applying the highest MorFac distribution with a maximum variable morphological scale factor of 100 in respect to the wave height. Quantitatively, there are some divergences as a result of underestimation of the simulations of higher applied morphological scale factors. The overall morphological development between the three simulation however shows a more or less linear.behaviour. The simulation of the same general pattern of the morphological change over time is considered to outweigh the quantitative change. Underestimation of morphological change could partly be a result of limited conservation of sediment mass. It is known that the differences in bed level change are not solely a result of the differences in morphological scale factors. The complex interaction of processes might also play its part in this.

Limited conservation of sediment mass is a result of the transition period between subsequent wave conditions in the application of a variable MorFac. Suspended sediment fluxes to and from the bed are multiplied by MorFac. If the morphological scale factor changes while sediment is in suspension a sediment mass error could be introduced as soon as the sediment settles again under a changed MorFac. This problem can however be minimised by carefully choosing the start and end times of a morphological scale factor value

so that suspended sediment concentrations are relatively low (i.e. around slack water) and/or approximately equal. This has however not been done in these runs, the underestimation is therefore accepted. §5.5 discusses the handling of the transition period between consecutive wave conditions in the application of a variable MorFac.

The corresponding patterns of morphological change in the area of interest between three simulations of increasing morphological scale factors allows for the application of the highest tested morphological scale factors in the further simulations. A high reduction in computational time is hereby reached. This will especially benefit the long-term morphological simulations to stay within acceptable run times. A relatively small underestimation of morphological change can however be present with the application of the highest MorFac as showed. Optimization of the start and end times of a MorFac value could solve this problem. Chapter 5 continues addressing the effect of this optimization.

3.3.9 Bed schematization

The morphology module of Delft3D currently implements two bed composition models, a uniformly mixed bed and a stratified bed, summarized and further explained following from the User Manual of Delft3D-Flow:

Uniformly well-mixed bed (one sediment layer).
The default bed composition model is the uniformly well mixed bed composition (Figure 3.23). It simply consists of one layer of sediments. This single layer can however consist out of one or multiple sediment fractions. There is however no bookkeeping of the order in which sediments are deposited. Sediments are well-mixed according the assigned available amounts. In the uniformly well-mixed bed, all sediments are directly available for erosion.

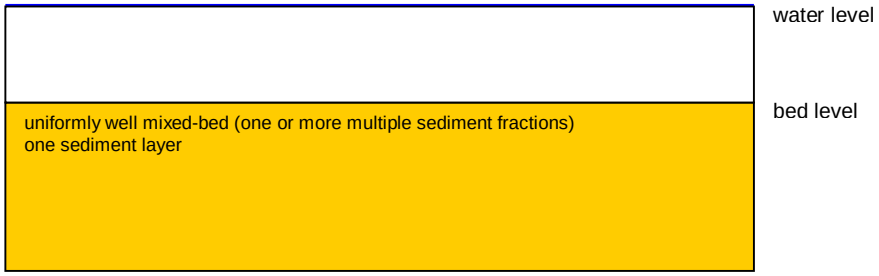

Figure 3.23 Uniformly well mixed-bed composition.

Stratified bed (multiple sediment layers).
If you have more detailed information on the bed stratification, you may use the bed stratification model and specify an initial layering of the bed composition (Figure 3.24). With the stratified bed , a user-defined number of bookkeeping under layers is included. The underlayers can be used to keep track of sediment deposits or to create a blocking effect (see section on reduced erosion). Different initial distributions of sediments can be assigned to each bookkeeping layer. Only sediments in the top-most layer are directly available for erosion.

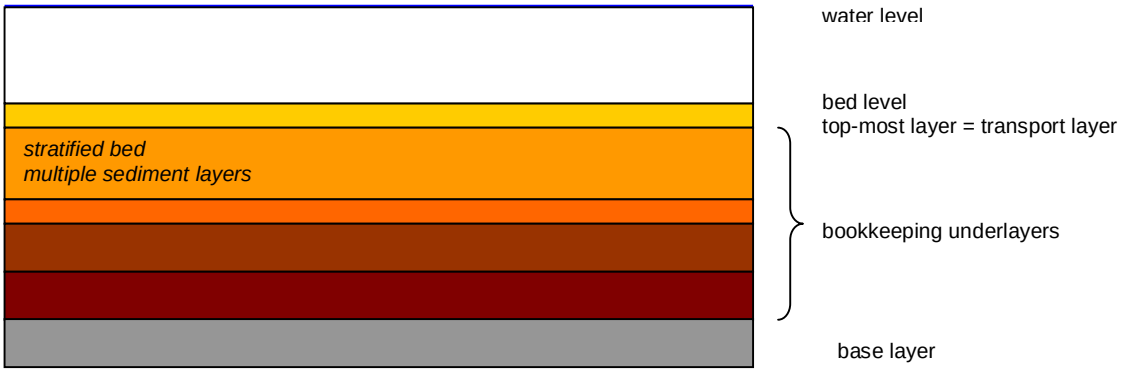

Figure 3.24 Stratified bed schematization.

The general composition of the bed for a layered bed per grid cell is divided into three main parts. The transport layer, the underlayers and the base layer (Figure 3.25). The total number of layers therefore exists out of 2+N layers, where the 2 stands for both the transport layer and the base layer and N stands for the user-defined number of underlayers in the morphological input file.

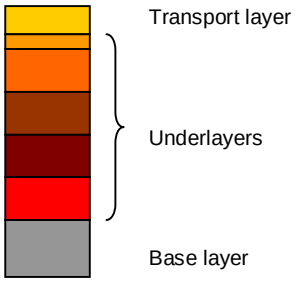

Figure 3.25 Schematic overview layers bed composition.

Transport layer

The transport layer has a distribution function. It imports sediment to the grid cell in the case of deposition and it exports sediment in the case of erosion. The thickness of the layer is user-defined and kept 'constant'. The transport layer exports sediment to the water column in the case of erosion. After the sediment has eroded, the transport layer imports sediment from the underlayer directly beneath it in the grid cell to replenish and thereby maintain the user-defined thickness. In case of deposition, sediment is imported to the transport layer from the water column, by settling. In the transport layer the sediment is mixed and it is redistributed to the underlayer, thereby maintaining its user-defined thickness again.

Underlayers

The underlayers can be seen as the buffer for the transport layer. In case of erosion it supplies sediment to the transport layer and in case of deposition it stores sediment from the transport layer.

Base layer

The base layer stores information that doesn't fit in the underlayers and is called on for in case the maximum number of assigned underlayers is reached. The two lower-most underlayers are merged to maintain the assigned maximum number of layers. The base layer is not considered as an underlayer and therefore not restricted to the assigned thickness of

the underlayers .In the following section a description is given for the process of erosion and deposition for a layered bed composition in Delft3D.

Examples of a layered bed composition subjected to deposition and erosion
Consider a stratified bed with a total thickness of 3.5 m (Figure 3.26). The bed consist of 3 different layers. The first layer is considered to be the transport layer and has an assigned thickness of 0.5 m. The second layer has a thickness of 2 m and the bottom layer has a thickness of 1 m. The maximum number of underlayers is assigned to be 3 and the thickness of the default underlayers 1 m. As said before, the initial bed composition file overrules the default thickness of the underlayer assigned in the morphological input file. However, new layers will be subjected to this maximum assigned thickness. Since the maximum number of underlayers is not reached yet, there is no base layer active. This initial condition will be modelled in Delft3D as follows:

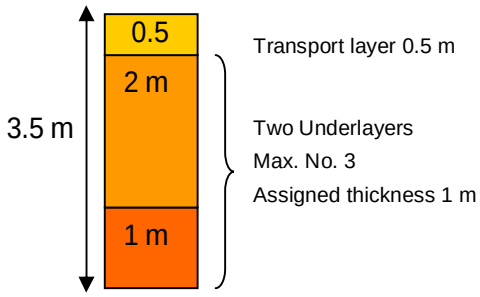

Figure 3.26 One grid cell, example condition, transport layer and two underlayers.

Deposition
When sediments are deposited (Figure 3.27) , they are initially added to the top-most layer, the transport layer (1). After mixing in the top layer, sediments are pushed towards the bookkeeping underlayers beneath it (2). With the mixing and transport the relative fraction proportions available in both the transport layer and the first underlayer change. The underlayers are filled up to a user defined maximum thickness (3). If this threshold is exceeded, a new layer is created (4). If the creation of a new layer would exceed the maximum number of layers specified by the user, layers at the bottom of the stratification stack will then form the base layer (5) and merge with the layer above if necessary to maintain the assigned maximum number of underlayers (6).

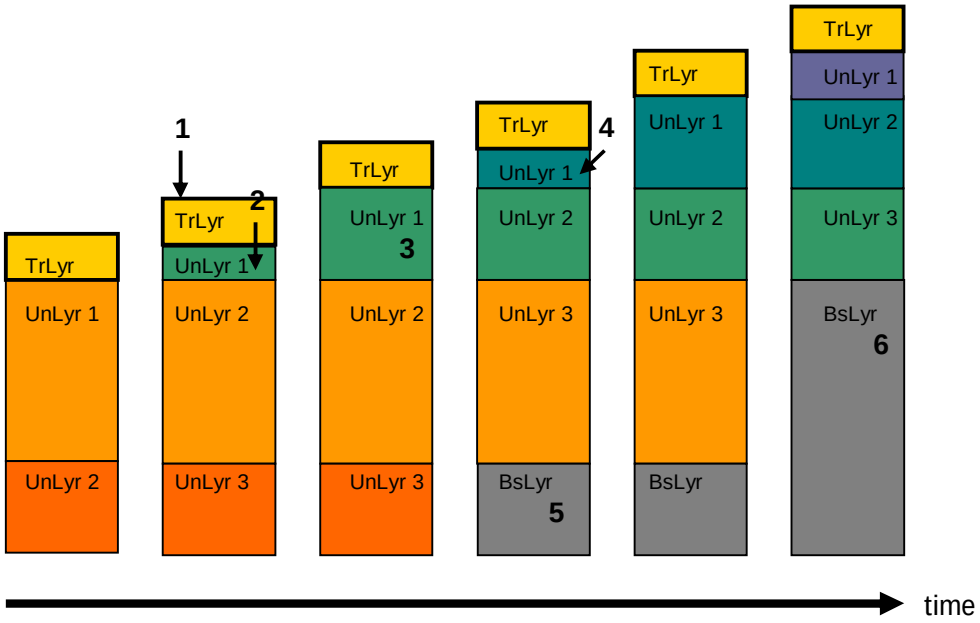

Figure 3.27 Process of deposition.

Erosion

The erosion process is almost a mirrored image of the deposition process (Figure 3.28). The transport layer exports sediment to the water column in case of erosion (1). After the sediment has eroded, the transport layer imports sediment from the underlayer directly beneath it to replenish and thereby maintain the user-defined thickness (2). The thickness of the underlayer erodes thus indirectly. After this process the sediments in the transport layer are mixed again and the proportion of available sediments in this layer thereby changes. Only sediment in the transport layer and indirectly in the first underlayer are thus available for erosion. The erosion process might carry on up to the situation where there is almost no more sediment available at the bed. A threshold thickness value is implemented that, if reached and passed, reduces the magnitude of the bed load transport with a factor: thickness of available sediment at the bed divided by the threshold value. This implementation thereby reduces the sediment transport and creates the effect of a fixed layer. Ultimately there is no more sediment available for erosion because of this effect of a fixed layer (3).

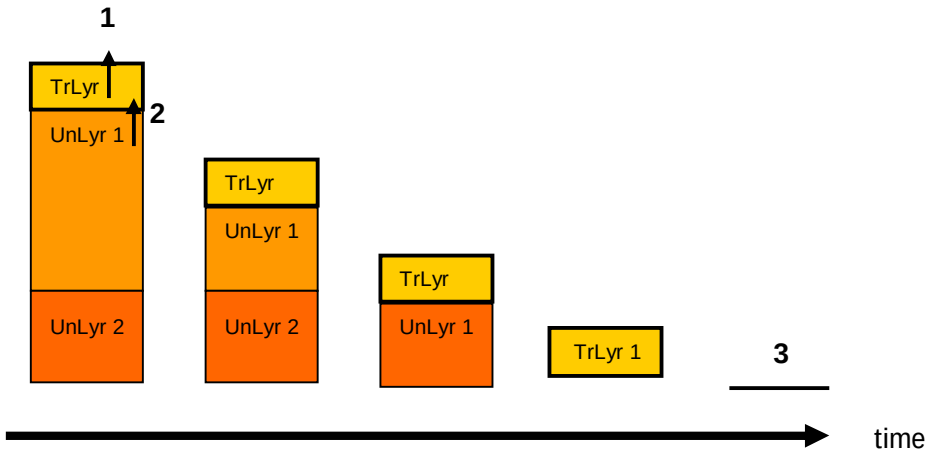

Figure 3.28 Process of erosion.

3.3.9.1 *Reduced erosive effect by applying a stratified bed schematization*

Applying stratification to a bed can positively reduce the effect of erosion.
Consider a bed consisting of several layers where each layer including the transport layer is a well-mixed mixture of a small sediment fraction and a bigger sediment fraction (Figure 3.29). Consider the situation where the critical value for erosion of the small fraction is reached and not yet the critical value for erosion of the bigger sediment. The smaller fraction erodes (1). The eroded amount of sediment from the transport layer is replenished with the well-mixed mixture from the underlying underlayer (2). The sediments in the transport layer are mixed and the ratio of the smaller fraction to the bigger fractions is decreased (3). The proportion of small fracted sediment in the transport layer has therefore decreased. Therefore less sediment is available for erosion under the same conditions. The erosion rate reduces.

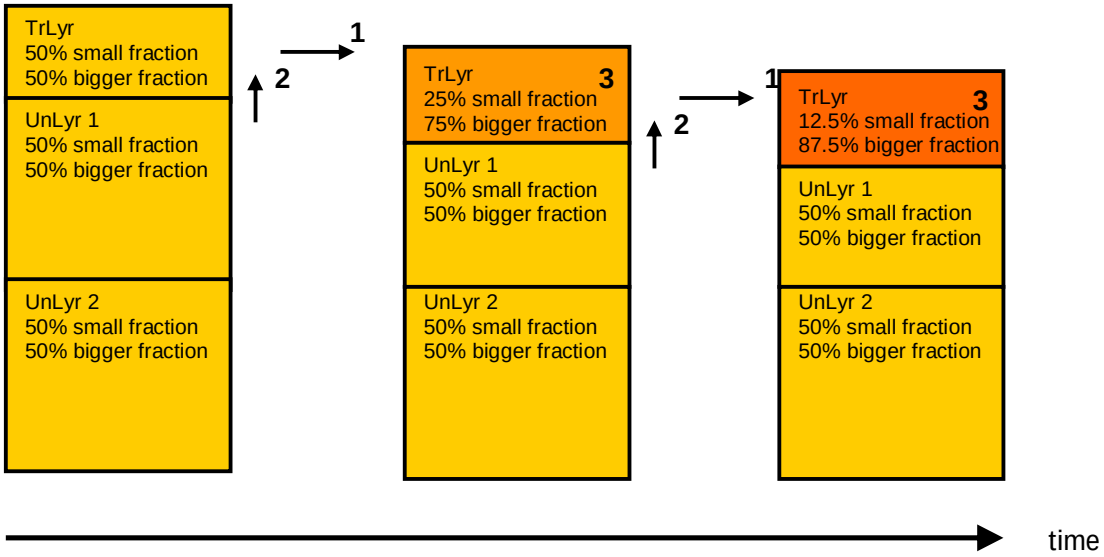

Figure 3.29 Reduced erosive effect, stratified bed.

The calibration simulations (Chapter 5) should determine the final bed schematization.

3.3.10 Sediment transport formula

The latest transport formula applicable in Delft3D, the TRANSPOR2004 by van Rijn (2004) is used in the morphological simulations of this study.

4 Analysis of processes responsible for long-term morphological change at MCR

4.1 General system behaviour

One of the main objectives of this study is to analyse the processes responsible for long-term morphological change at MCR. A general description of the system's behaviour is given in advance.

The MCR is a complex area where saline ocean tides, strong fresh river flows with high sediment carrying capacities, and a high energy wave climate meet. The system has a naturally ebb-dominant behaviour under the influence of the tide and the addition of the river flow. In which, river suspended sediment is brought to the mouth and decreased flow velocities allow sediments to settle here. An ebb-dominance of a system in combination with a high sediment supply and a high energy wave climate leads to an ebb-tidal delta formation. The ebb tidal delta plays an important role in the sediment budget of the CRLC. It forms the buffer of sediment for the adjacent shores Wave and current processes are responsible for distributing the sediment from the ebb-delta both north and southward into the littoral cell and onto the adjacent shores. As a result of which the huge spit north of the Columbia River entrance, the Long Beach peninsula for example formed. The ebb tidal delta morphology is determined by the balance between a net offshore sediment flux induced by tidal currents and river flow and a net onshore sediment flux induced by offshore waves. Wave action thus limits the area over which the ebb tidal delta can spread out. The dominant direction of the littoral drift in the CRLC distributes sediment from the Columbia River in northern direction while summer conditions may have temporarily limited southward directed transport (Figure 4.3).

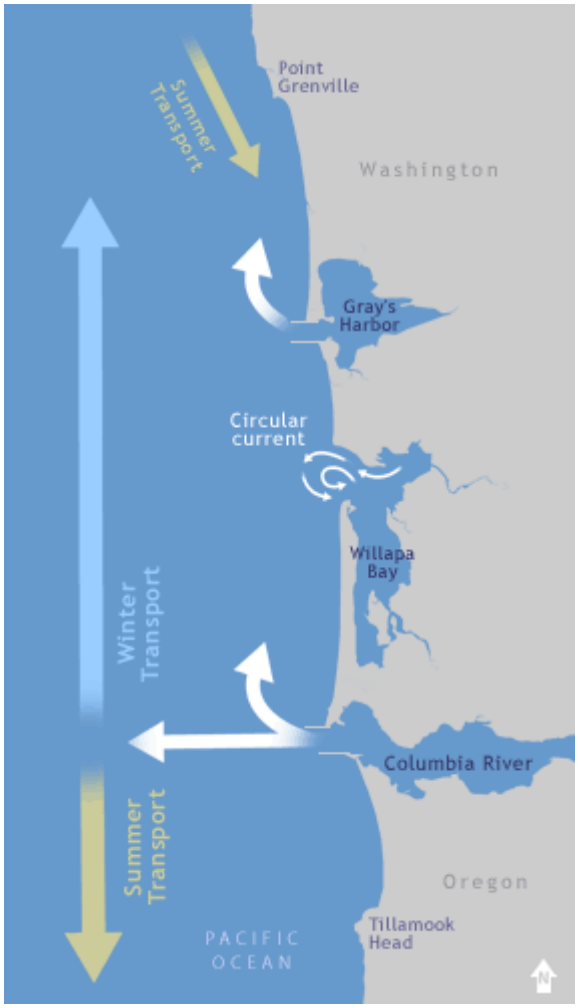

Figure 4.1 *CRLC littoral drift (http://ecy.wa.gov)*

The general system's behaviour of the pre-jetty and post-jetty condition is further analyzed by looking at bathymetric data of the various eras.

Historically, the MCR was characterized by a broad and shallow ebb-tidal delta complex consisting out of a varying number of inlet channels. The entrance was flanked by the shallow shoals of Peacock Spit (1) to the north of the entrance and Clatsop Spit (2) to the south (Figure 4.2).

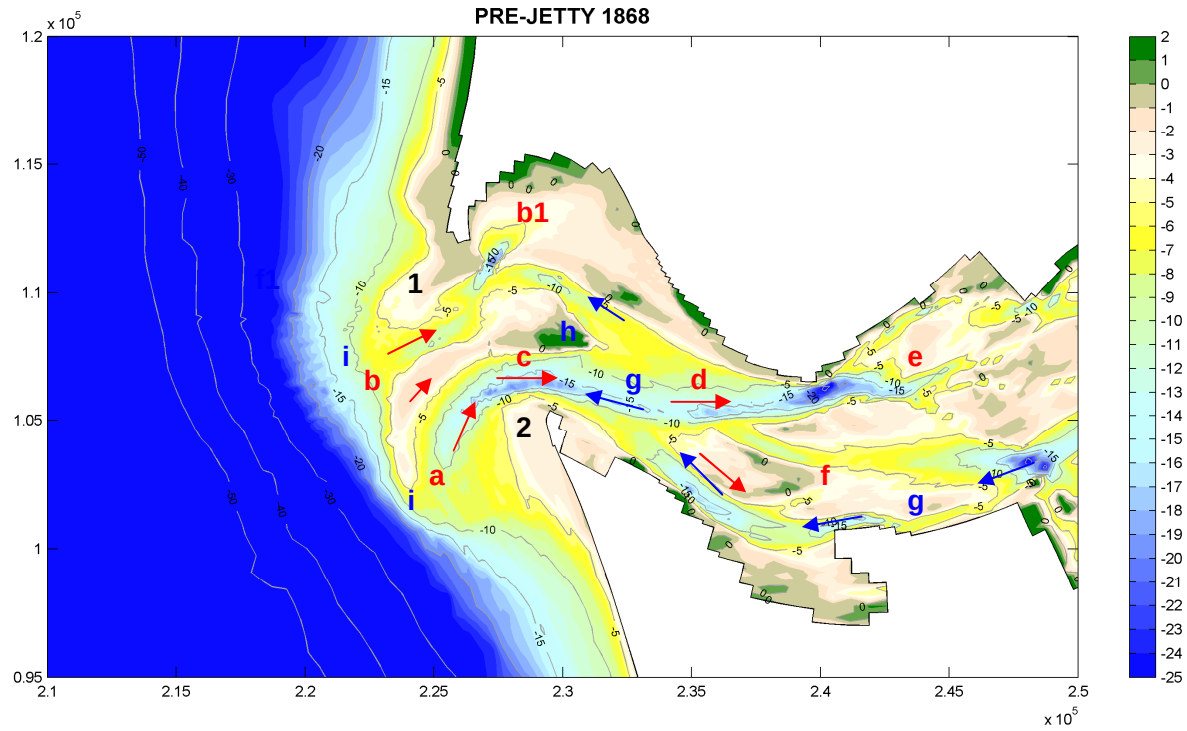

Figure 4.2 Pre-jetty bathymetry MCR 1868

A complex dynamic behaviour of bottom morphology and tidal motion governed the MCR before the construction of the entrance jetties. The interaction between bottom morphology and tidal motion is the cause of a complex three-dimensional structure of residual circulations, which are both cause and result of the morphological structure of the basin. The patterns of flood and ebb flows herein strongly determine the morphology. It is noted that, as a result of the restricted width of the river, flood and ebb currents partly follow the same pathways.

As a result of the propagation direction of the tidal wave along the coast from south to north, the incoming flood of the tide at first and predominantly enters the mouth in the southern entrance channel at (a). As the tidal wave propagates further in northward direction, the tidal flood flow also enters the mouth over the shoals and in the northern channel at (b). The flood flow in the northern entrance channel shows from the flood chute at (b1). As a result of the existing morphology, the Coriolis force and a centrifugal force the incoming flow bends to the south (c). The Coriolis force in the Northern Hemisphere, as a result of the earth's rotation forces the flood flow to concentrate more along the right bank, viewed from the flood flow direction. A secondary flow maintains the bend of the main channel and results in a gradual shift in northern direction of the channel. A centrifugal force and inertia keep the flood channel from fully developing on the right side of the entrance and therefore the flood flow extends to also develop in the northern part of the inlet (d). The northern flood channel is visible from the developed flood chute at (e). The higher water level during flood in combination with the Coriolis force allows for the flood to partly flow through the southern section of the inlet at and over the shoals (f).

During ebb, as a result of the lower water levels, the flow primarily follows the main channel (g). As a result of the earth's rotation the ebb flow will have a slight orientation

towards the right bank of the inlet viewed from the ebb flow direction. As a result of which a slight break-off from the main channel is present at (h) and an ebb flow is also present in the northern channel. Both ebb-tidal channels end in forming a shoal (i).

Descriptions of historic conditions (Sherwood, 1990) showed that prior to jetty construction the MCR had a highly dynamic morphology with a varying number of channels crossing the tidal delta over time. Figure 4.2 is therefore just a random situation of the pre-jetty morphology, in which thus two channels are present. The continuing northward migration of the southern channel however will cause the two existing channels to merge and form a single, shallower channel.

The dynamic morphological behaviour of the entrance and demand for navigational safety led to the construction of entrance jetties at the MCR. The South Jetty was constructed between 1885 and 1889 across the Clatsop Shoal to narrow, deepen and stabilize the entrance channel. Deterioration of the jetty due to waves and currents and the northward migration and shoaling of the channel led to an extension of the South Jetty and the construction of the North Jetty in respectively 1903 and 1913. In 1939 a third jetty, Jetty A was constructed to further stabilize the entrance channel. Overall, the jetty constructions reduced the width of the river mouth from approximately 9.6 km to 3.2 km. The entrance channel as well as the existing tidal delta eroded by the increased tidal currents due to the confinement. A single entrance channel formed (1, Figure 4.3) It is noted that, as a result of the reduced width of the river mouth, flood and ebb currents more and more followed the same pathways in the post-jetty condition.

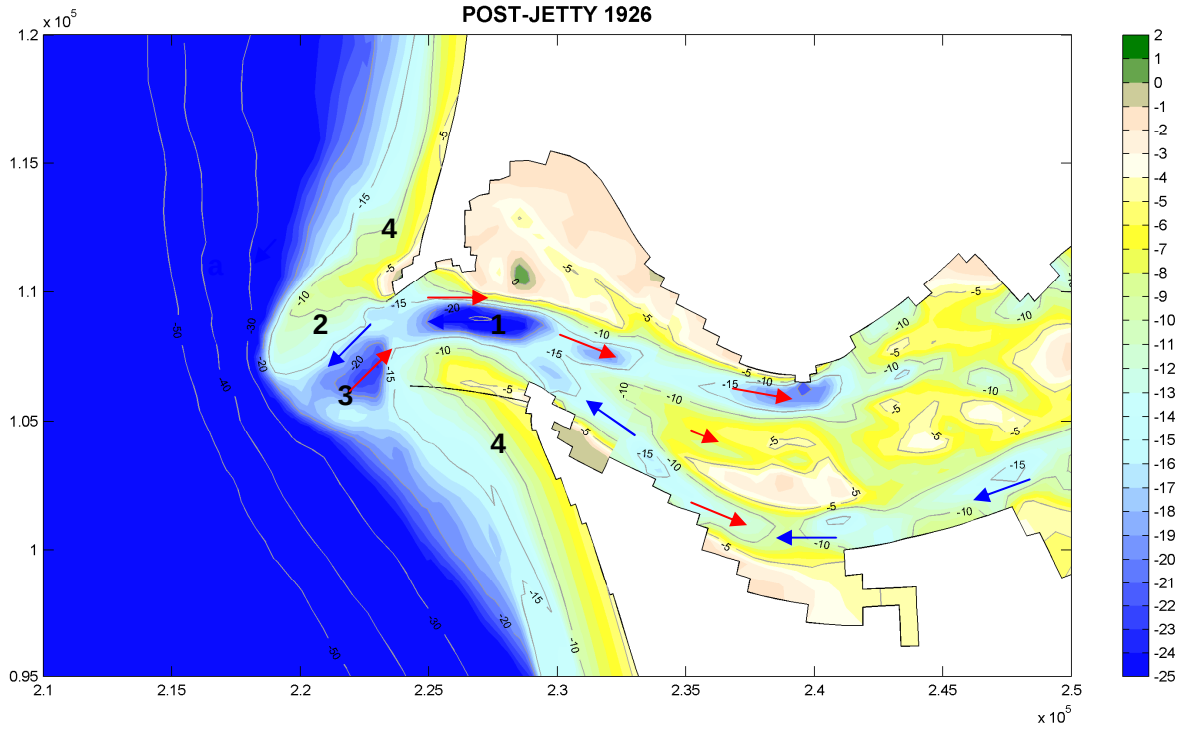

Figure 4.3 Post-jetty bathymetry MCR 1926

Elias and Gelfenbaum (2009) addressed the importance of the tidally-induced and density driven flow in the generation of residual flows and sediment transports at the MCR. The basic flow pattern at the MCR results in a surface flow of less dense fresh water towards the ocean and an opposite flow of saline seawater into the estuary along the bottom. Density differences and high stratification alter the residual flow and decrease the overall ebb-dominance (Figure 4.4). The level of stratification depends on the magnitude of the river discharge. The landward

extent of the salt wedge that arises from the interaction of the saline sea water with the fresh river discharge depends on the relative importance between the incoming tide and the river flow. Under low river flow salinity intrusion may be up to river mile 30, while under high river flow salt may be absent upriver of river mile 2 (Fox et al., 1984).

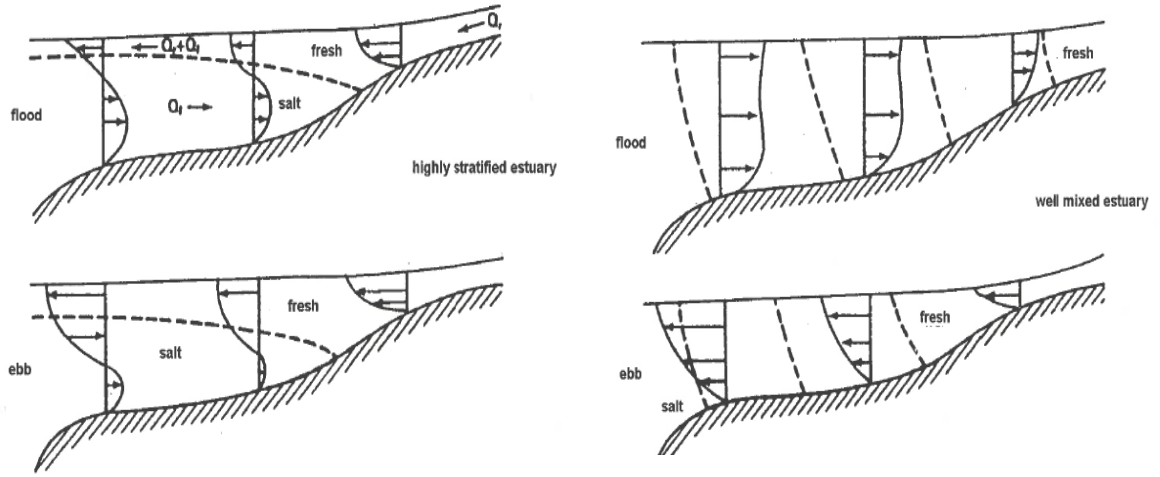

Figure 4.4 Stratification: density variations and velocity profiles (from d'Angremond, 2001)

Over decades, sand from the scoured tidal delta accumulated in a new area further offshore (Figure 4.3, 2) and the littoral drift distributed the sediment onshore causing beaches near the jetties to rapidly grow and form new land (Figure 4.3, 4). The decreasing availability of sediment from the scoured ebb-tidal delta at the mouth over time as a result of the dispersive behaviour of the waves and general littoral drift together with the reduced overall sediment supply from the river to the mouth due to severe damming of the Columbia River basin recently caused several former strongly accreting beaches in the CRLC to erode. With sand in short supply, the CRLC may be entering a long-term period of erosion.

In the remainder of this chapter, processes responsible for morphological change at the MCR, specifically for the post-jetty condition of 1926 are singled out and analyzed, using the model simulations from the *Opti-routine* as explained in the next paragraph.

4.2 Opti routine

The wave climate schematization and in this particular case, also the river discharge schematization, consist out of a large number of individual conditions. In order to reduce the run time of the morphological simulations, it is advisable to reduce these boundary-forcing schematizations to a more practical number of conditions. The morphological simulation with the limited set of conditions should however lead to a similar outcome as the morphological simulation with the full set of conditions would. A Matlab based program developed by Deltares called *Opti* (Mol, 2007) is able to handle this boundary conditions reduction. The performance of this method and the application of the representative wave climate in morphological simulations are not widely described in the literature. However, the vast amount of combinations of forcings conditions and the joint probability of occurrence of waves and river discharge in the MCR made the application of *Opti* a necessity.

Basis for the *Opti-routine* are the individual conditions that resulted from the wave climate schematization and the river discharge schematization. The wave climate schematization of the Energy Flux method (§ 3.3.5.2) for Period 1 led to 100 different wave classes and seven peak wave heights. The discharge schematization of the same period led to four discharge classes. Since every combination of these conditions is possible for Period 1, this leads to a total of $(100+7)*4=428$ different conditions, each with its own probability of occurrence. The wave climate schematization for Period 2 led to 64 different wave classes and eight peak wave heights. The discharge schematization of period 2 led to five discharge classes. A total of $(64+8)*5=360$ different conditions for period 2 are thus the result. This brings the total number of conditions for period B to $428+360=788$ conditions. This total series of conditions forms the input for the *Opti-routine*.

Each condition is run over one morphological tide. In this particular case, the mean-total transport pattern of every short-term simulation together with its probability of occurrence contributes to form a total mean transport pattern of all the conditions combined. This total set of conditions is than reduced using the *Opti-routine* by dominance and the alternation of weight factors to create a sufficiently accurate reduced set of conditions (see Mol, 2007). The reduced set of forcing conditions finally forms the basis for the final long-term morphological runs. Chapter 6 continues with the boundary forcing conditions reduction of the *Opti-routine* that than forms the basis for the final long-term simulation of Period B.

Besides the boundary condition reduction, the 788 short-term simulations that are used in the *Opti-routine* are also used in the system analysis of the MCR. The transport patterns of the various forcing conditions combinations are used to investigate and describe the morphological influence of the various processes as wave height, river discharge, and wave direction within the MCR for the post-jetty condition. In the analysis the dominance and the probability of occurrence of the various combinations is also addressed. The remainder of this chapter handles the system analysis.

4.3 Probability of occurrence of forcing conditions

The relative morphological influence of a certain combination of forcing conditions on the actual morphological behaviour of the MCR depends on the absolute morphological behaviour together with the probability of occurrence of the combination considered. In the system analysis of the MCR, the individual effects of certain combinations of forcing conditions on sediment transports at the MCR are considered taking into account their probability of occurrence. The effect on sediment transport of common occurring forcing conditions but also the transport patterns of peak conditions are analyzed. Also the effects on total sediment transports of changing wave heights, directions, and river discharges are analyzed and described.

The river and wave climate schematizations were subdivided in two seasonal climates. Period 1 covers about 70% of the year (256 days) from mid-summer to winter and Period 2 covers about 30% of the year (109 days) from spring to mid-summer. In which again, Period 1 represents a higher wave climate and a lower river discharge climate and Period 2 represents the calmer wave climate and higher river discharge climate.

Period 1

For the system analysis, the wave heights and wave directions are redistributed in coarser classes so that a more general analysis can be done. The directional classes are separated into three classes, one representing a wave coming from a more northern direction, one representing waves coming from a western direction and one representing a wave coming from a more southern direction. The wave heights are divided in four classes. River discharge classification is kept unchanged.

The following figure gives the probability of occurrence of wave heights versus direction of Period 1 in black and the yearly probabilities of occurrence in red. River discharge classes of Period 1 are given in the right figure.

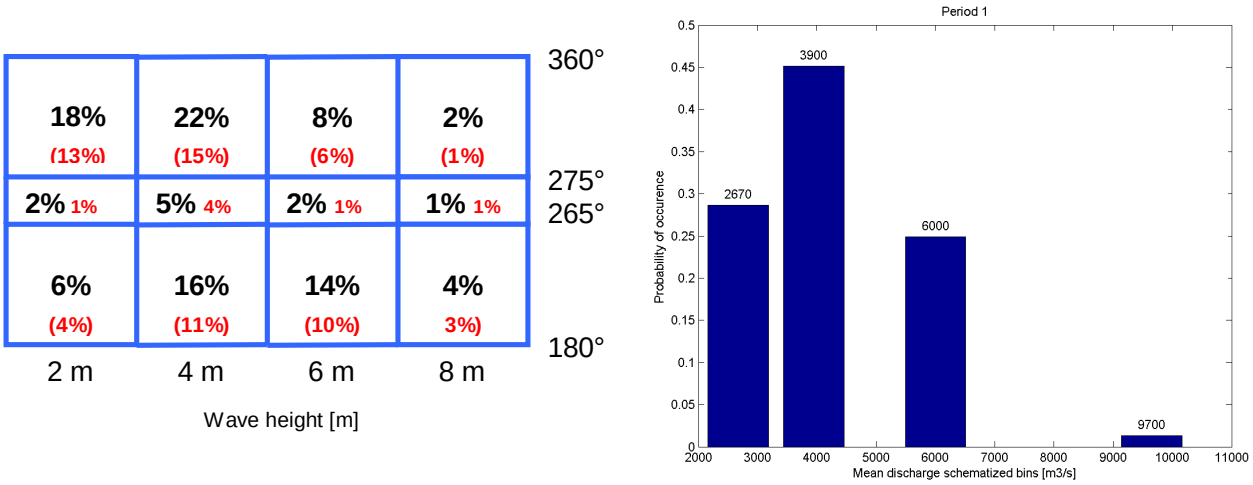

Figure 4.5 Probability of occurrence waves height versus direction(left) and river discharge(right) (Period1).

From Figure 4.5 it can be stated that in Period 1:

- 50 % of the waves come from a more northern direction.
- 10 % from a western direction.
- 40 % from a more southern direction.
- The majority of the waves coming from a more northern direction is in the 2-4 meter range.
- The majority of the wave coming from a more southern direction is in the 4-6 meter range.
- Twice as much waves with a significant wave height of around 8 m come from a more southern direction than from a more northern direction.

Period 2

The same division is done for the waves and discharge for Period 2. Again, three directional classes are separated while only 2 wave height classes are defined.

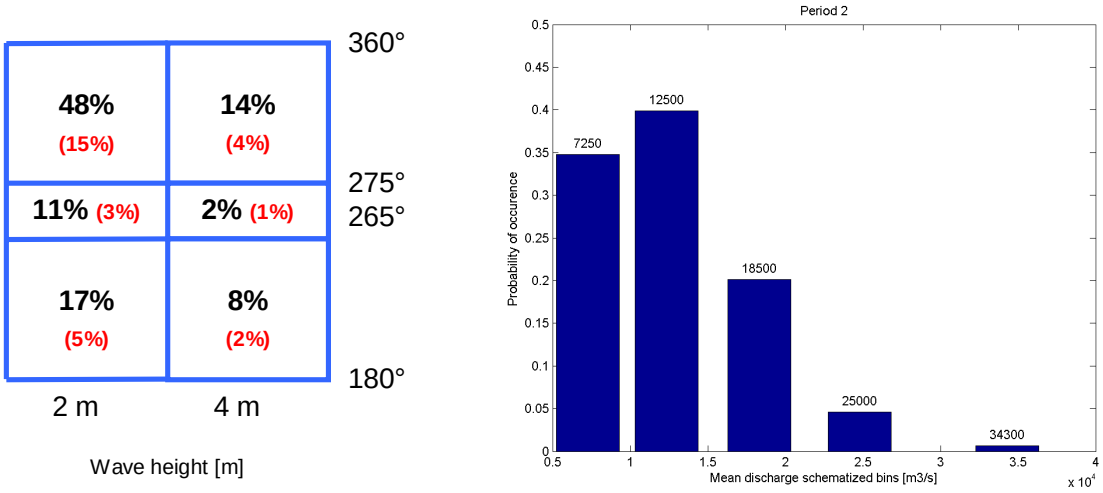

Figure 4.6 Probability of occurrence waves heights (left) and river discharge (right) (Period 2).

From Figure 4.6 it can be stated that in Period 2:

- 62 % of the waves come from a more northern direction.
- 13 % from a western direction.
- 25 % from a more southern direction.
- 48 % of the waves is in the 2 meter range and comes from a more northern direction.
- Almost three times as much waves in the 2 m range come from a more northern direction than from a more southern direction (48% versus 17%).
- The majority of the waves in the 4 meter range come from a more northern direction.

4.4 Analysis

From the previous sections it follows that the considered variables in the development of the morphological change at the MCR are:

- Wave height
- Wave direction
- River discharge

With the determined probability of occurrences of the generalized various combinations, the next step is to show the individual effects of certain combinations of variables. At first, the yearly averaged total transports through a cross-section at the mouth are plotted for changing variables. Again, a maximum of four different wave height classes (2m, 4m, 6m and 8m), three wave directions classes (220°, 270° and 307°) and nine discharge classes in the range of 2670 m^3/s to 34300 m^3/s are plotted against each other to show the general influence of the variables on the morphology at the mouth. Figure 4.7 gives an overview of the considered values of the variables.

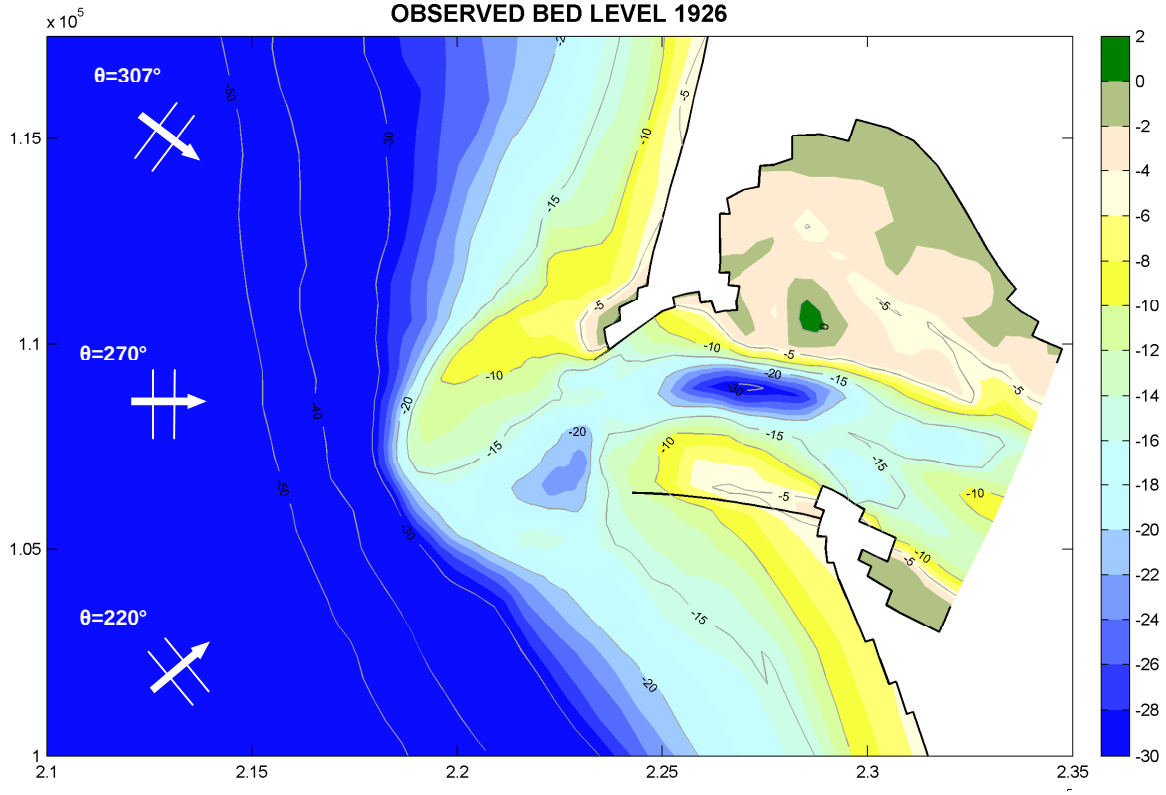

Figure 4.7 Division variables for system analysis.

4.5 Sediment transport

4.5.1 Sediment transport through the mouth

At first a variation of the significant wave height for the three directional classes is analyzed for increasing river discharges. The effect on sediment transports of increasing wave heights and increasing river discharge per uniform wave direction at the mouth can be assessed from this. Figure 4.8.gives the results for waves coming from a more southern direction.

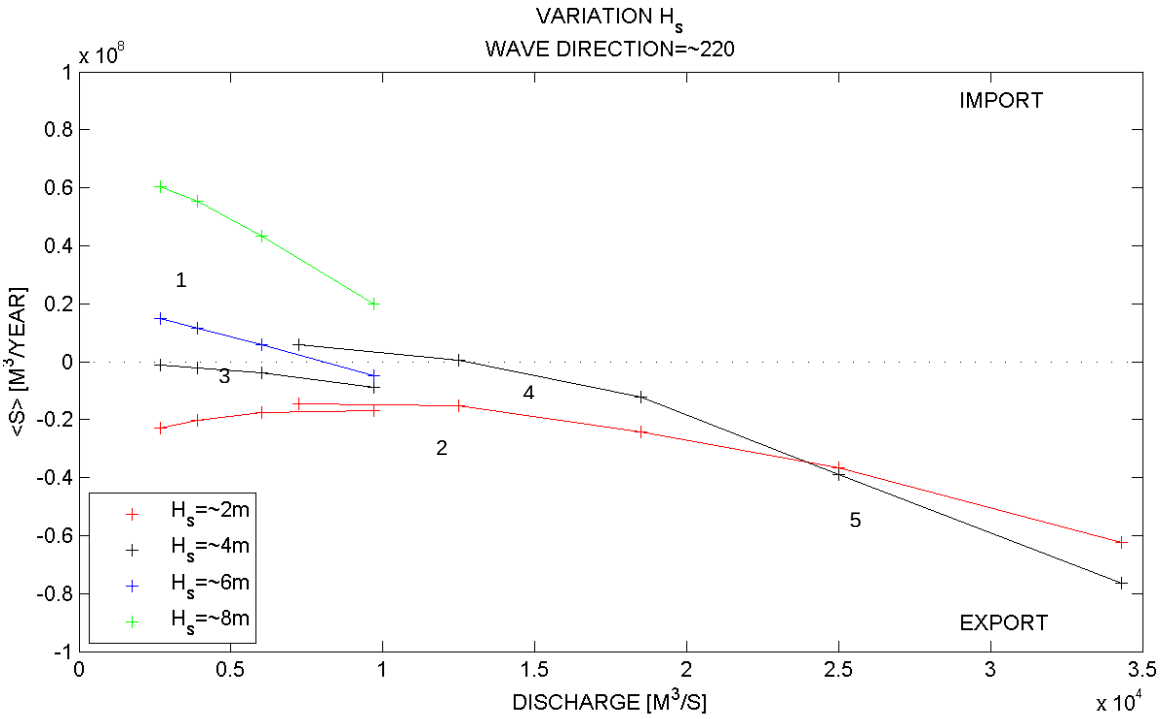

Figure 4.8 *Total sediment transport through the mouth for varying wave heights with a mean direction of 220°*

From Figure 4.8 it follows that for waves coming from a more southern direction:

- Import is possible if the waves are high enough (1). River outflow is more dominantly through the northern section of the mouth. Waves approaching the mouth from a southern direction are therefore less counteracted when they enter the mouth.
- Waves with an offshore significant wave height in the order of 2 meters will never lead to sediment import at the mouth (2).
- It seems that for a river discharge up to 12500 m^3/s and waves in the order of 4 meters, the export of sediment by the river and the tide and the import of sediment by the waves is more or less in equilibrium (3). Once the river discharge surpasses the 12500 m^3/s, the river becomes dominant with export as a result (4).
- For a discharge of 25000 m^3/s or higher, larger waves lead to larger export under as a result of larger bed disturbances (5).

Secondly, waves coming from a western direction are analyzed, which are plotted in Figure 4.9.

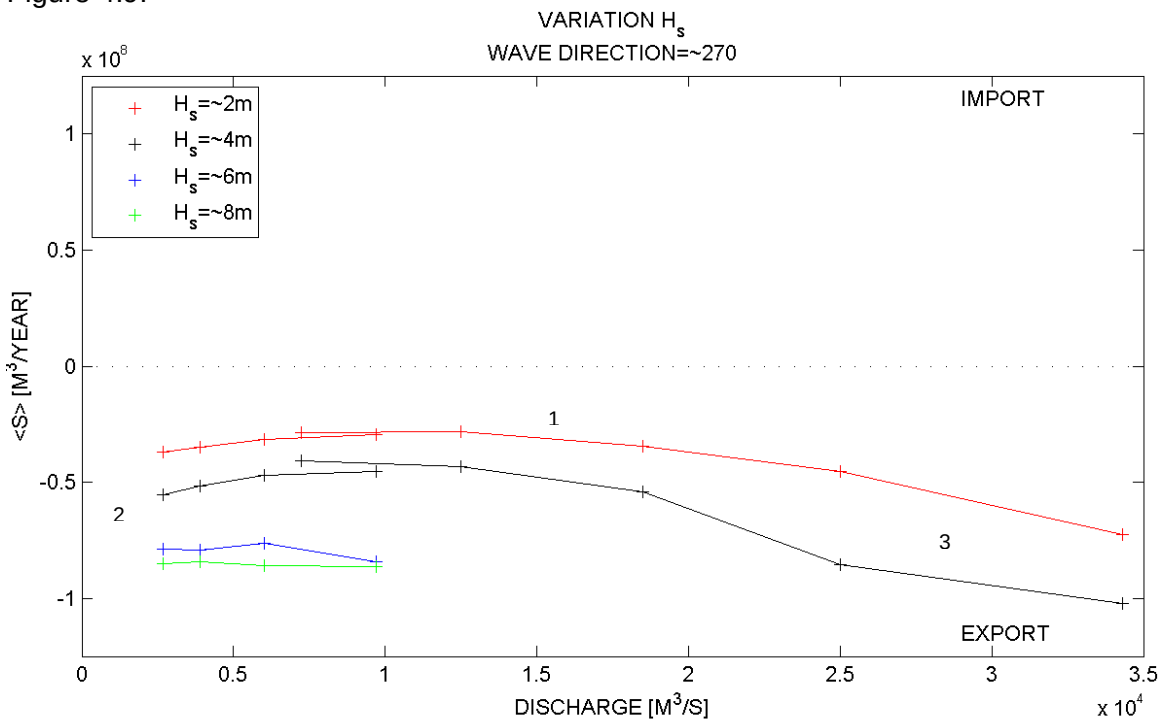

Figure 4.9 *Total sediment transport through the mouth for varying wave heights with a mean direction of 270°.*

From Figure 4.9 it follows that for waves coming from a western direction:

- Import through the mouth is never possible (1).
- Export through the mouth is larger for larger waves (2).
- Export becomes larger when the river discharge becomes larger (3)

Waves coming from a more northern direction are analyzed from Figure 4.10.

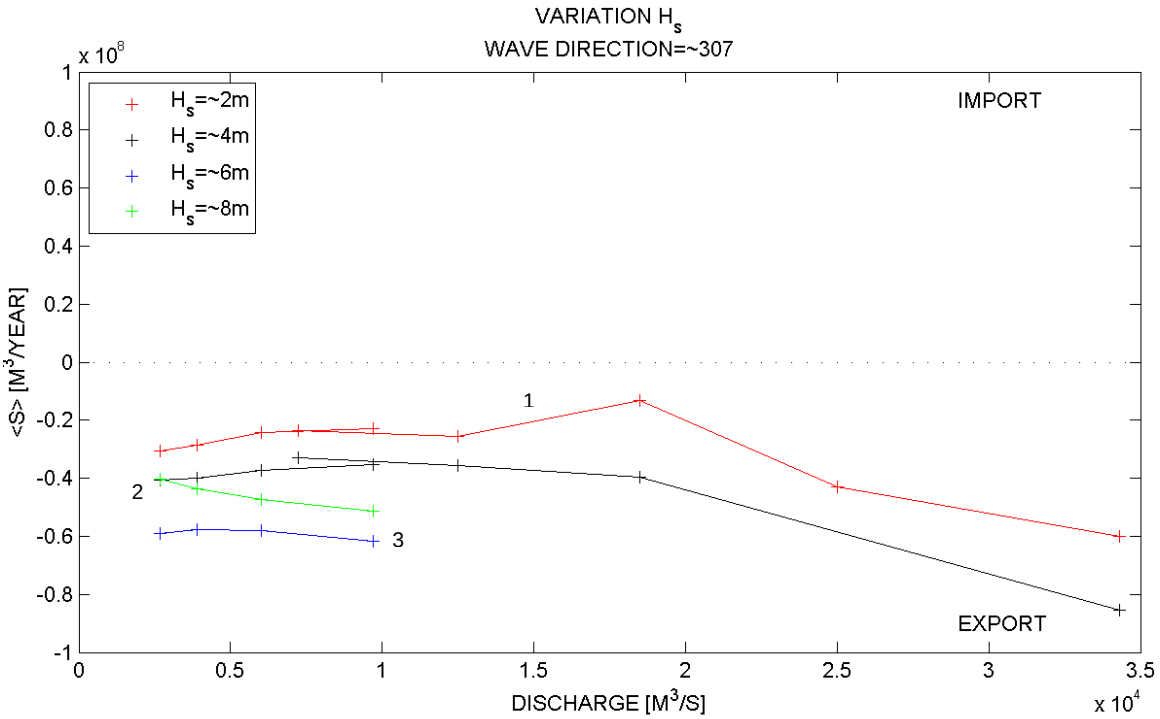

Figure 4.10 *Total sediment transport through the mouth for varying wave heights with a mean direction of 307°.*

From Figure 4.10 it follows that for waves coming from a more northern direction:

- Import through the mouth is never possible (1).
- Export through the mouth is generally larger for larger waves (2). However the export of waves with a significant wave height of 8 meters is smaller than the export of waves with a significant wave height of 6 meters (3). This could be a result of earlier breaking of the higher waves on the ebb-tidal delta and the reduced available amount of energy at the mouth through this breaking effect. A reduction in energy leads to less bottom disturbances and less available sediment in suspension for export.

A variation of the wave direction for each of the wave height classes is also given for increasing river discharges. The effect of the wave direction and increasing river discharge per uniform wave height on sediment transports at the mouth can be assessed from this. Yearly total transport through the mouth for relatively low wave heights of about 2 meters are given in Figure 4.11.

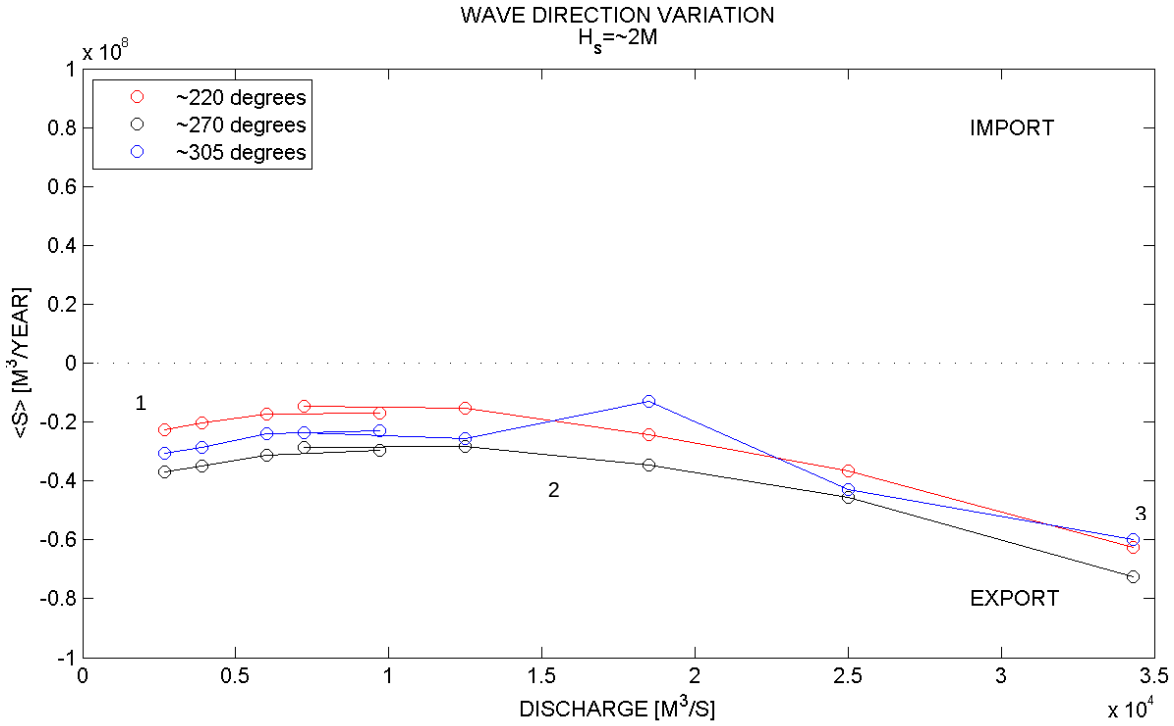

Figure 4.11 *Total sediment transport through the mouth for varying wave directions with a mean wave height of about 2m.*

From Figure 4.11 it follows that for waves with an offshore significant wave height of about 2 meters:

- Nett import is never possible.
- Generally, export for a wave coming from a more southern direction is the smallest (1). This is a result of both limited extent of the waves into the mouth due to the oblique incidence of the waves and relative high gross imports through the southern section of the mouth. Waves coming from a more southern direction experience less resistance from the more northern orientated outflow at the mouth. The Nett export is hereby thus reduced (see Figure 4.12 (1)).
- Export for a wave coming from a western direction is under any circumstance the largest (2). The relatively far reach of the waves in to the mouth as a result of the straight approach of the waves leads to high bed disturbances at the mouth and as a result of the ebb dominance of the system thus to high exports.
- Waves coming from a more northern direction hardly cause any gross import. The waves have trouble reaching beyond the mouth as a result of the northern orientated location of the ebb delta , the orientation of the jetties, and because of the northern orientated outflow at the mouth. Less sediment is brought into suspension and available for export. However export is always more than export for a southern incoming wave as a result of the limited gross import. With a high enough river discharge however the order of exports of northern and southern incident waves can change (3).

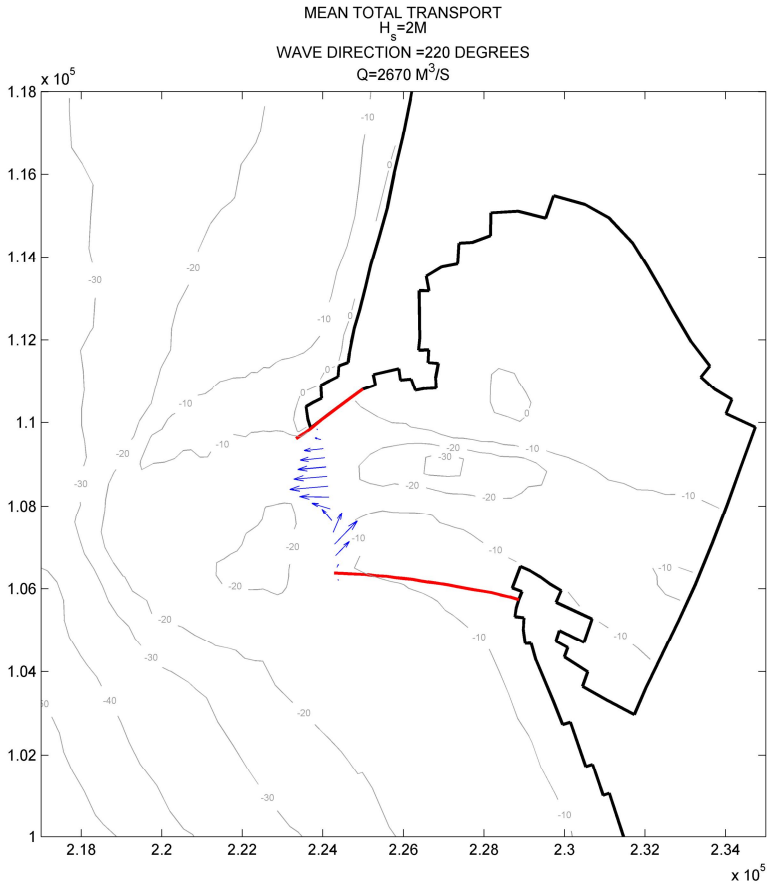

Figure 4.12 *Mean total transport through the mouth, southern wave, low discharge*

Figure 4.13 shows the yearly total transport through the mouth for above average wave heights of about 4 meters for three wave directions and nine discharge classes.

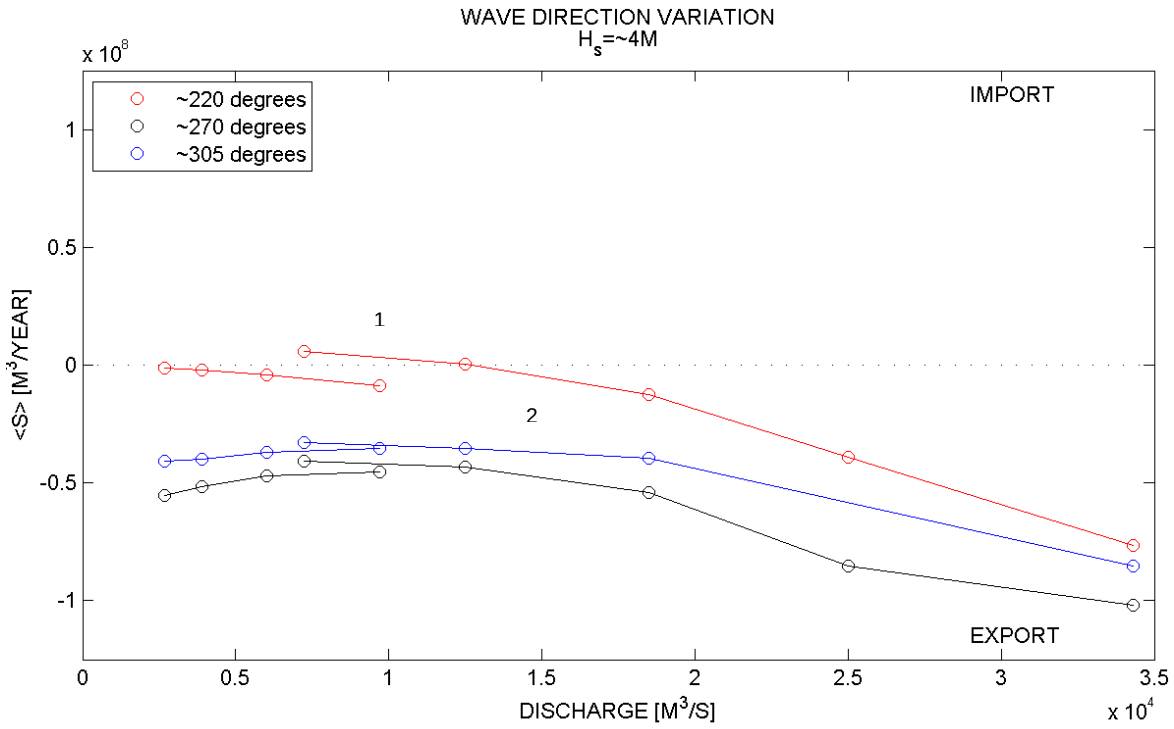

Figure 4.13 *Total sediment transport through the mouth for varying wave directions with a mean wave height of about 4 m.*

From Figure 4.13 it shows that:

- For waves coming from a more southern direction and limited river discharge, a wave height of around 4 meters is the lower limit for which import through the mouth is possible (1).
- As soon as the river discharge increases or the wave direction differs, the dominance of the river is increased and a general export pattern arises (2).
- Following the analysis of wave heights of around 2 meter, export for a wave coming from a western direction is under any circumstance the largest.
- Waves coming from a more northern direction again result into less export than waves coming from a western direction as a result of the orientation of the outer ebb delta, the outflow of the river, and of the jetties.

Figure 4.14 shows the yearly total transport through the mouth for high energy waves of about 6 and 8 meters in height for three wave directions and the four lower discharge classes of Period 1.

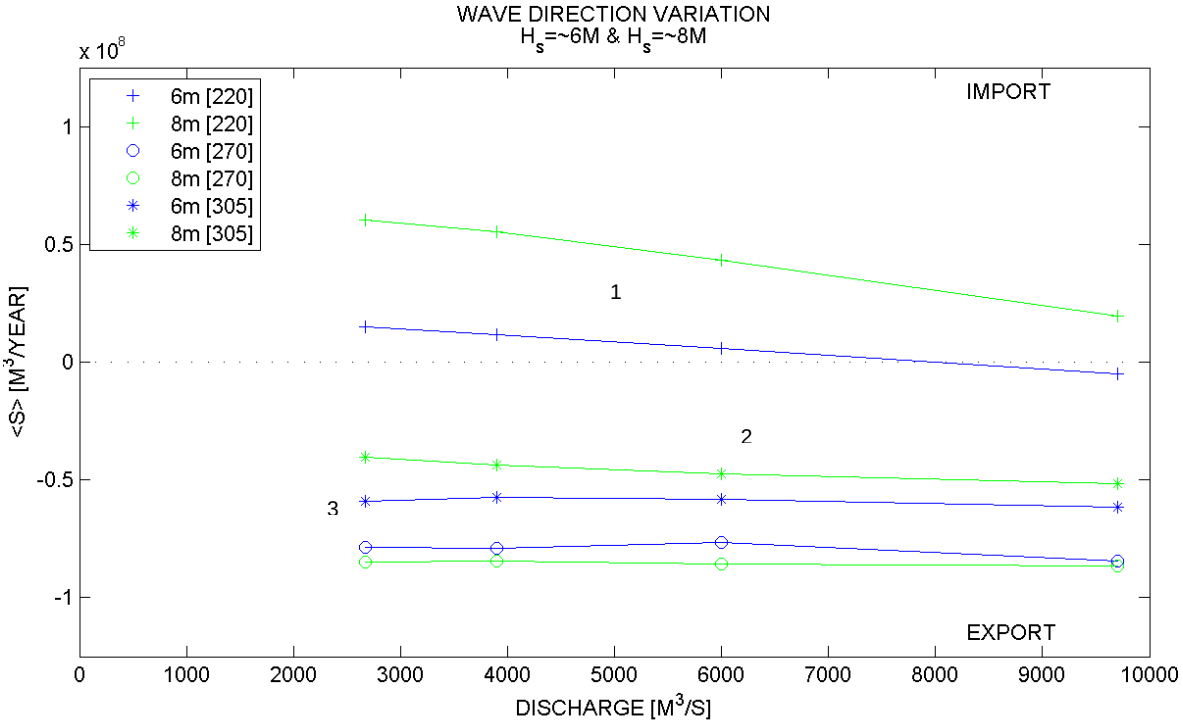

Figure 4.14 *Total sediment transport through the mouth for varying wave directions with a mean wave height of about 6 and 8 m.*

From Figure 4.14 it shows that:

- Import through the mouth is possible for high energy waves coming from a more southern direction only (1).
- A variation of the river discharge between 2600 m^3/s and 9700 m^3/s has a limited effect on import and export patterns (2).
- Export through the mouth for waves coming from a more northern direction again is lower than export through the mouth by waves coming from a western direction (3). The orientation of the outer ebb delta and the possible wave breaking effects as a result of the upper value wave heights, together with the limited reach of the waves in the inlet due to the orientation of the jetties and the river outflow are again addressed as possible causes.

4.5.1.1 General findings

- Import at the mouth is only possible for high enough waves (H_s > 4 m), coming from a more southern direction (< 270 °).
- Export through the mouth is generally larger for higher waves, however limited by wave breaking effects.
- Export becomes larger when the river discharge becomes larger.
- Export through the mouth is generally the smallest for waves coming from a more southern direction. Export through the mouth is generally the largest for waves coming from a western direction.
- Influence of the river discharge on transports through the mouth is limited for discharges smaller than 12500 m^3/s.

4.5.2 Sediment transport MCR

In order to generally quantify the effect of the variables of wave height, wave direction and river discharge at the MCR in a more spatial matter, annual transport through several transect at the mouth are given together with mean total transport patterns for the following (combinations of) variables:

- High wave versus low river discharge
- Low wave versus high river discharge
- Common wave versus a common river discharge
- Increasing river discharge
- High energy wave coming from a more northern direction
- High energy wave coming from a more southern direction

The transects focus on again transport through the mouth and transports in an out of the inner ebb delta together with long shore sediment transport in both northward and southward direction. Mean total transport patterns represent the transports over one full morphological tide. The vector scaling of the plotted mean total transports is identical for every Figure. Rough probabilities of occurrence for the various combinations are also given based on the division done in §4.3.

4.5.2.1 *High wave versus low river discharge (~3 days/year)*

Period 1 prescribes the lower river discharge classes and the higher energy wave climate. The under average discharge class of 2670 m^3/s versus a wave higher than 8 meters is analyzed. In Period 1 the higher waves predominantly come from a more southern direction (Figure 4.5).

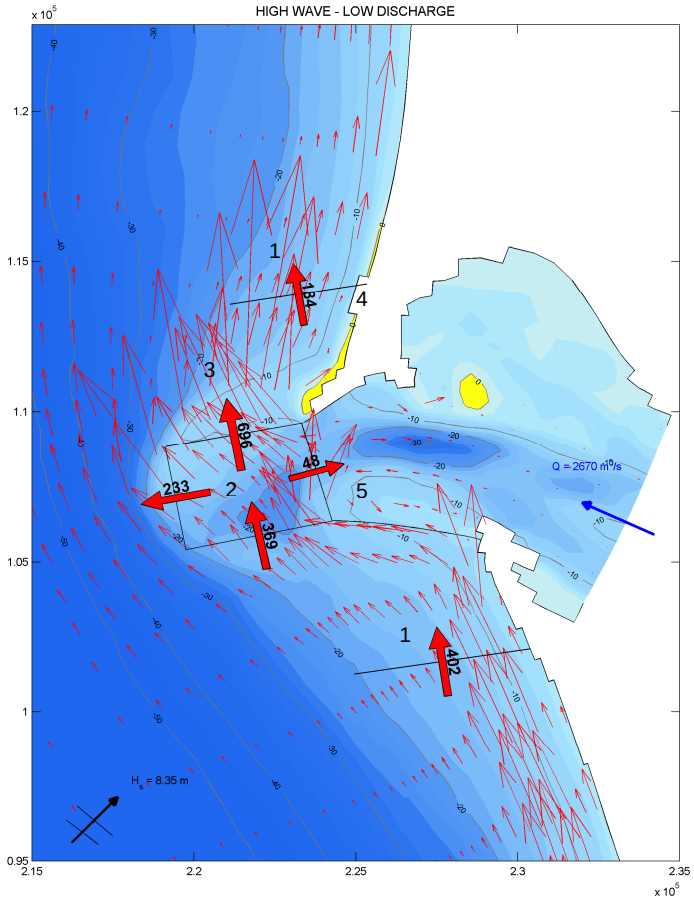

Figure 4.15 *Patterns of sediment transport and yearly transport through transects. High wave – Low discharge.*

From Figure 4.15 it shows that:

- High waves from a southern direction lead to strong northward littoral drift (1).
- The relative high waves and shallow water depth at the ebb-delta together with the induced confined flow through the mouth as a result of the jetties leads to high sediment transports at the ebb tidal delta (2). The littoral drift as a result of the oblique incidence of the waves together with the river outflow and the orientation of the tidal propagation forces these sediments northward (3).
- Annual total transports through the transect north of the mouth are lower than transports through the transect south of the mouth as a result of to the shadowing effect of the orientation of the ebb-tidal delta and the encounter of the waves with northern orientated river outflow. The gradient in sediment transport that arises in this area of lower energy could lead to erosion (4).
- At the mouth import is possible as a result of the direction and the wave height (5).

4.5.2.2 Low wave versus high river discharge (~3 days/year)

Period 2 prescribes the higher river discharge classes and the generally lower energy wave climate. The second highest river discharge class of 25000 m^3/s versus a low wave of 1.15 meters is analyzed. In Period 2 the lower waves predominantly come from a more northern direction (Figure 4.6).

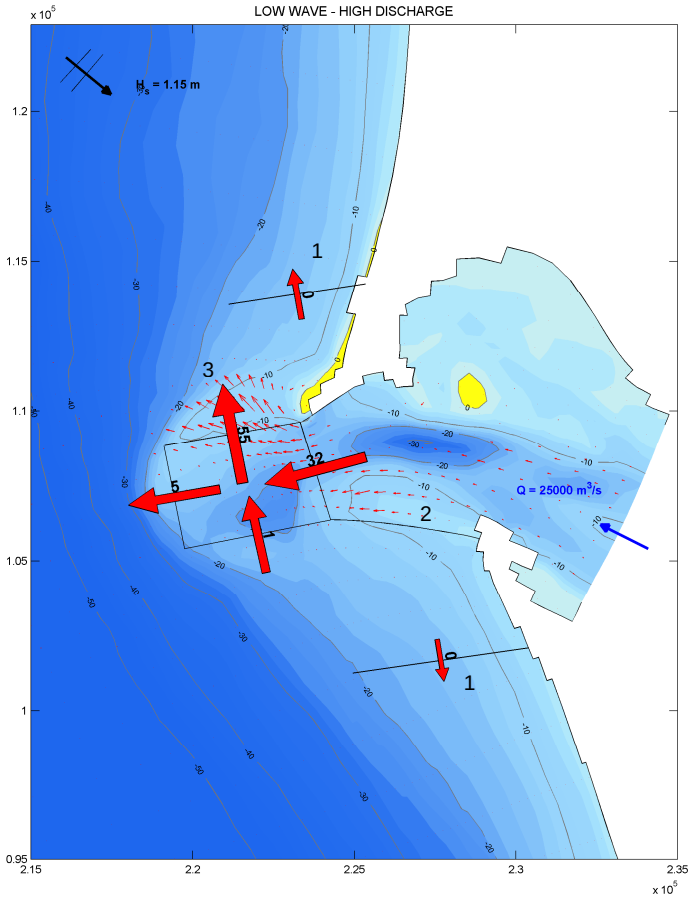

Figure 4.16 *Patterns of sediment transport and yearly transport through transects. Low wave – High discharge.*

From Figure 4.16 it shows that:

- Sediment transports in this case are predominantly influenced by the river discharge. The influence of the waves on the sediment transports is limited as a result of their limited height. This shows from the negligible overall littoral drift north and south of the mouth (1).
- Even though river outflow at the mouth generally has an orientation more at surface and at the northern section of the inlet, for this particular case, the river discharge is high enough to cause sediment transports at the shallow southern section of the inlet aswell (2). Stratification during the ebb phase over the inlet and at the mouth is limited due to dominance of the river discharge, leading to exporting transport over the entire inlet.
- Transports through the mouth turn in a more northern direction. Possibly partly due to the Coriolis force and mainly as a result of the propagating direction of the tide (3).

4.5.2.3 *Common wave versus a common river discharge (~25 days/year)*

In order to address the effect of more common conditions (according to Figure 4.5), the transports as a result of a wave height of 3 meter, coming from a more northern direction in combination with an about mean discharge of 3900 m^3/s are analyzed.

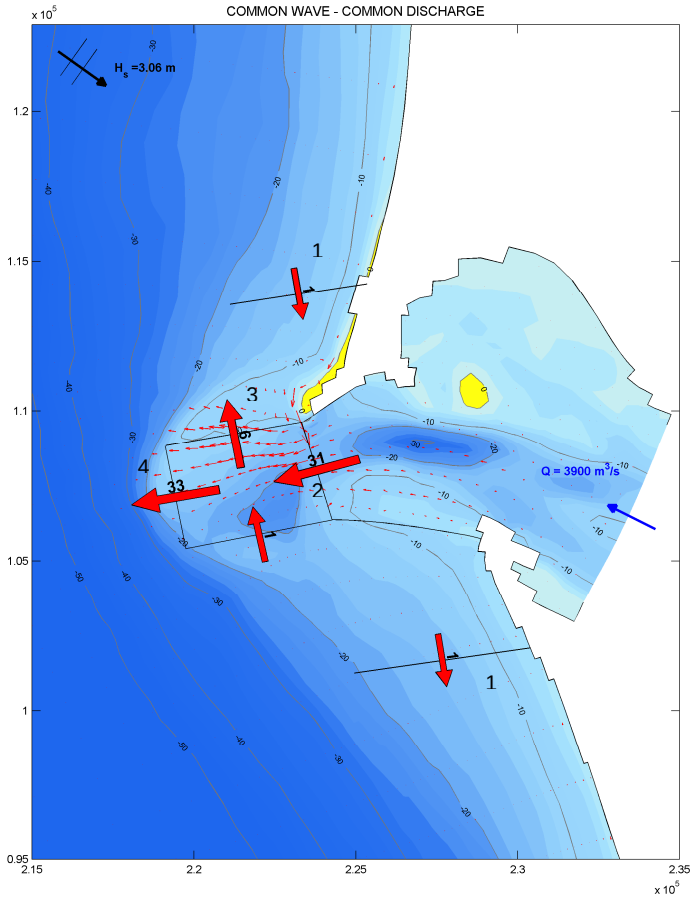

Figure 4.17 *Patterns of sediment transport and yearly transport through transects Common wave–Common discharge.*

From Figure 4.17 it shows that:

- Littoral sediment transport is limited under waves in the order of 3 meters and a direction of a little over 300 degrees (1).
- The yearly total transports through the mouth are about the same as for the previously analyzed condition of low waves and a high discharge (2). This could mean that the transport through the mouth is more dominantly influenced by the confined tidal flow than by the river discharge.
- Northward transport at the mouth is less as a result of the opposing waves force and a lower river discharge (3). Instead of being transported northward, the sediments are now transported further in offshore direction (4).

4.5.2.4 River discharge

The influence of the river discharge on the sediment transports at the mouth will be addressed by looking at the following three plots. In which an average wave of three meters from a western direction approaches the MCR under three different river discharge classes of 6000 m^3/s, 12500 m^3/s and 25000 m^3/s respectively.

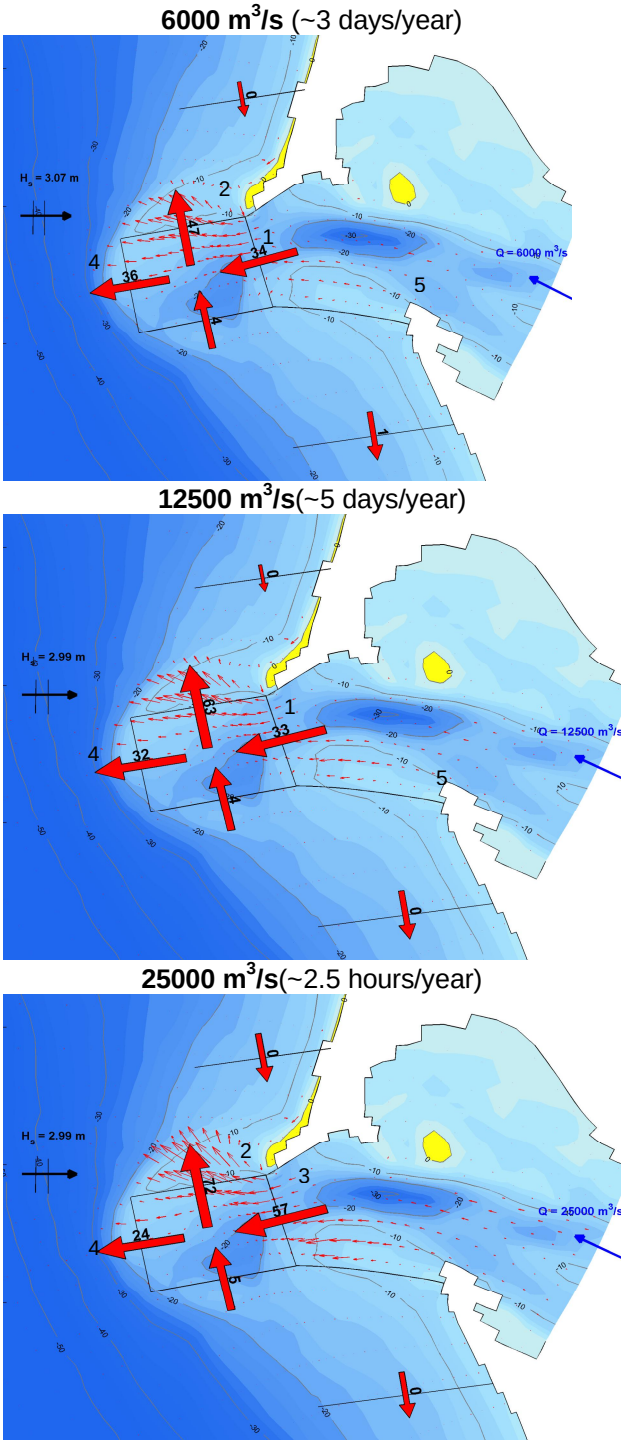

From Figure 4.18 it follows that:

- For a river discharge of 6000 m^3/s and of 12500 m^3/s, the transport through the mouth is about the same (1). The northward transport at the mouth however becomes larger under larger river discharge (2).
- For a river discharge of 25000 m^3/s the discharge starts to show its influence on the transports through the mouth (3). The previous dominant cause of sediment transport through the mouth, the tidal flow, becomes less dominant and allows for the river discharge to contribute.
- A high river discharge doesn't necessarily lead to sediment transport further offshore (4). It does however lead to a larger northern directed transport of sediment (2). The direction of the tidal propagation and the Coriolis force are addressed as possible causes for this northward transport.
- Higher river discharges lead to larger sediment transports inside the inlet (5).

Figure 4.18 Patterns of sediment transport and yearly transport through transects. Varying river discharge

4.5.2.5 *Dominant wave coming from the north, discharge 3900 m^3/s (~2 days/year)*

To show the general effect on sediment transports at the MCR for waves coming from a more northern direction, yearly total transports and mean total transport pattern are analyzed from Figure 4.19 for a high energy wave coming from the north under a more or less mean river discharge.

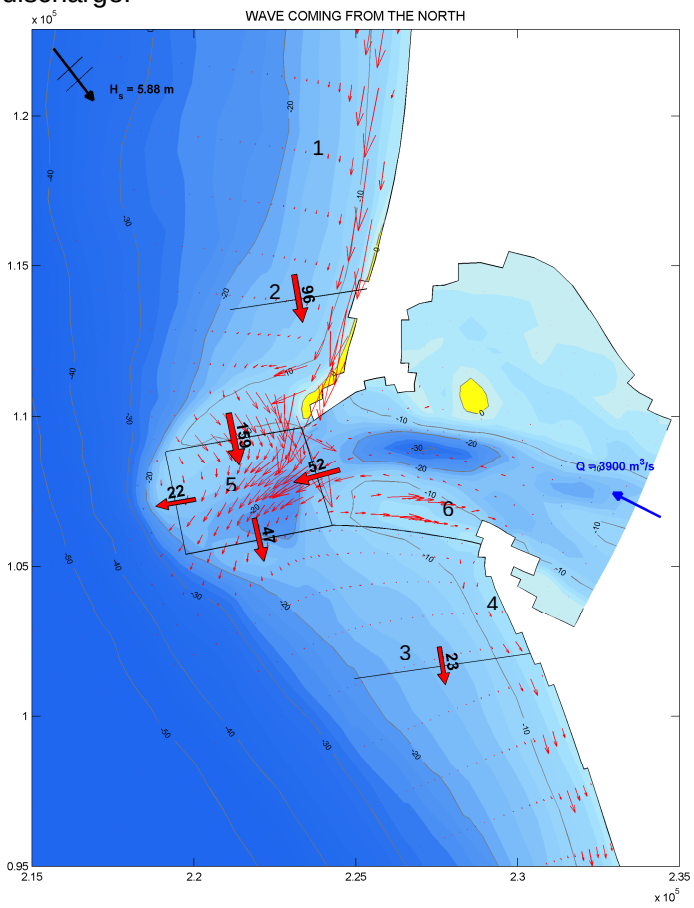

Figure 4.19 *Patterns of sediment transport and yearly transport through transects Dominant wave,northern direction–Common discharge.*

From Figure 4.19 it shows that:

- A strong southward littoral drift arises from relative high energy waves coming from a more northern direction (1).
- Year total transports through the cross-shore transect north of the mouth (2) are higher than transports through the transect south of the mouth (3). The shadowing effect of the orientation of the ebb-tidal delta and the refraction effect of the waves caused by the orientation and shallowness of the ebb-tidal delta will make this an area of lower energy and therefore less transport. The gradient in sediment transport that arises south of the South Jetty will lead to erosion (4).
- A summation of the year total transports within the ebb delta shows an importing behaviour (5). The supplied sediment from the southward littoral drift, the energy loss on the ebb delta due to wave breaking and the limited northward transport as a result of the limited river discharge and opposing waves are reasons for this.
- Import of sediment arises in the southern part of the inlet along the South Jetty (6).

4.5.2.6 *Wave coming from the south, discharge 3900 m^3/s (~5 days/year)*

The same analysis is done, now however for waves coming from a more southern direction.

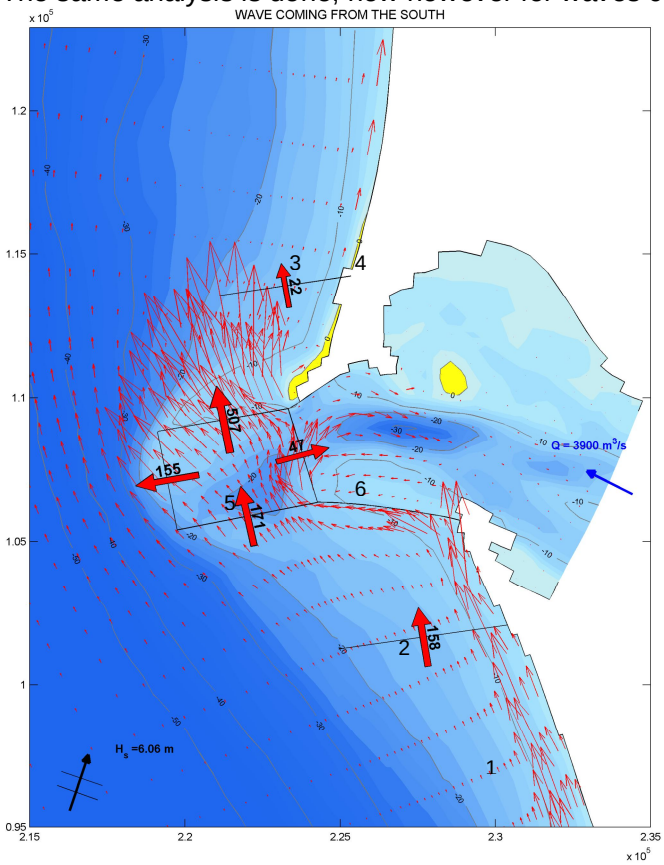

Figure 4.20 *Patterns of sediment transport and yearly transport through transects Dominant wave,southern direction–Common discharge.*

From Figure 4.20 it shows that:

- A strong northward littoral drift arises from relative high energy waves coming from a more northern direction (1). The fact that the northward littoral drift is stronger than the southward directed littoral drift is a consequence of a more oblique wave in northern direction.
- Year total transports through the transect south of the mouth (2) are higher than transports through the transect north of the mouth (3). The shadowing effect of the orientation of the ebb-tidal delta and the refraction effect of the waves caused by the orientation and shallowness of the ebb-tidal delta will make this an area of lower energy and therefore less transport. The gradient in sediment transport that arises north of the North Jetty will lead to erosion (4).
- A summation of the year total transports within the ebb delta leads to strong erosion (5). The fact that waves easily reach the outer lobe of the ebb-tidal delta due to the orientation of both the waves and the delta will cause waves to break just at the outer lobe. The sediment brought into suspension by this will transport out of the ebb delta as a result of the active overall northward littoral drift.
- Import of sediment through the mouth is possible as a result of the high energy and orientation of the waves (6).

4.5.2.7 General findings

- A strong littoral drift develops at the MCR for oblique incident waves of sufficient height.
- The orientation of the ebb-tidal delta has a shadowing effect on the total wave energy in trailing areas.
- Waves coming from a more southern direction lead to a more exporting pattern of the ebb tidal delta of the MCR.
- Waves coming from a more northern direction lead to a more importing pattern of the ebb tidal delta of the MCR.
- The tide dominates the sediment transport through the mouth of the MCR for limited wave conditions and limited river discharges. For high enough river discharges (> 25000m^3/s), the tidal flow allows for the contribution of the river discharge to the transport through the mouth as a result of limited stratification at the mouth.
- A higher river discharge doesn't necessarily lead to sediment transport further offshore. It does lead to a larger northward directed transport of sediment.
- Exports through the mouth are generally northward orientated as a result of tidal propagation and possibly as a result of the Coriolis Force.

5 Calibration

5.1 General

With the derived boundary forcing conditions (§3.3), various calibration steps need to be taken to optimize the performance of the model in simulating the observed morphological changes. The majority of the hydrodynamic settings emanate from the validated quasi real-time hydrodynamic and sediment transport pattern study of the MCR that was described in §3.2. The calibrated hydrodynamic settings are specifically kept unchanged as much as possible. An inevitable difference however is the application of the representative morphological tide at the water-level boundary. Lesser (2009) states that calibrated hydrodynamic settings may have unexpected results on long-term morphology when applied in a morphological feedback loop. On the other hand, changing the calibration settings potentially requires recalibration of the hydrodynamic boundary conditions and other settings. Since there are almost an infinite number of possibilities for “tuning” the morphological model, the hydrodynamic calibration settings are taken for granted and directly adopted from the quasi real-time hydrodynamic and sediment transport model. The simulation in the calibration phase therefore predominantly focuses on the morphodynamic settings of the model. The best resulting settings found in this calibration phase are used in the final long-term simulations of the MCR. The most important morphological calibration settings that remain available for optimization of the model are:

1 Bed schematization settings (§5.3)
2 Sediment transport calibration settings (§5.4)
3 Schematization morphological tide (§5.5)

The majority of the calibration simulations are set on a target of simulating five years of morphological change. A period of five years is considered long enough to simulate measurable changes and dominant patterns in the morphology at the mouth and still not be too time consuming. Five years of morphological change simulates the initial response of the area and further trend of development and is therefore considered sufficiently long for the calibration phase. The five year relative morphological development is compared to the measured 32 years of morphological change. Further development over time after the five-year simulation period obviously occurs, is variable and is kept in mind during calibration. The trend pattern that comes from the morphological development is analyzed and used to determine the long-term morphological performance of the model. From the calibration-runs a sound choice is made with respect to the bed schematization, the transport calibration settings and the schematization of the morphological tide. Basis for the calibration are the observed morphological changes between 1926 and 1958, as described by Buijsman (2003) and made applicable for the analysis with Delft3D from the derivation of post-processed measured data. By differencing bed elevations, patterns of sedimentation and erosion can be identified (Figure 5.1).

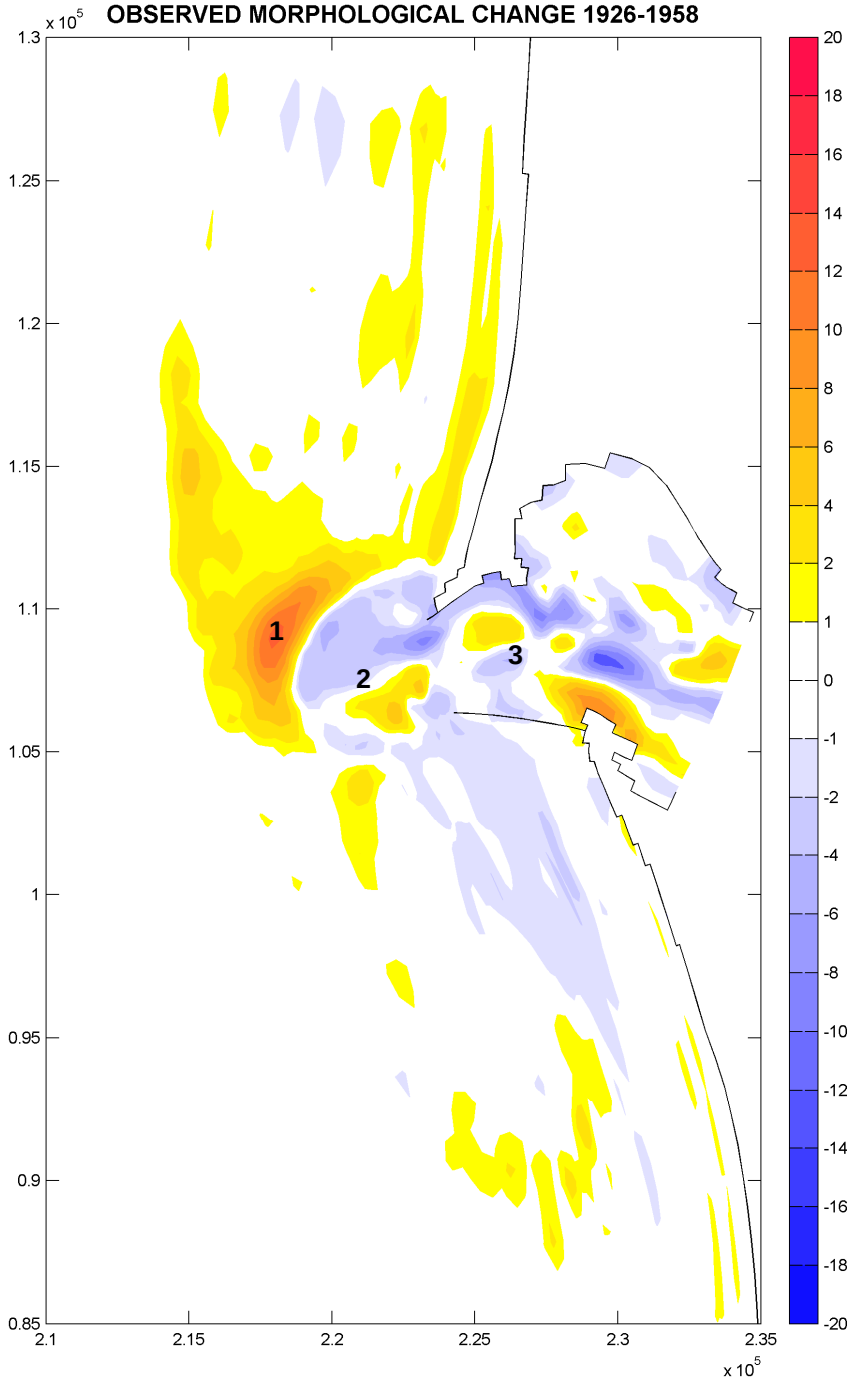

Figure 5.1 Observed morphological change MCR 1926-1958.

Focus in the calibration-runs is on the compartments of the outer (1) and inner ebb-tidal delta (2) and on the inlet (3).

In addition to the described calibration settings, another setting that is looked at in this chapter is the handling of the transition period between consecutive wave conditions in a simulation with varying MorFac and its influence on the total morphological change.

5.2 Boundary forcing conditions schematizations

The general morphological response to jetty construction is considered to be dominated by the tidal prism and the addition of the river discharge to this. Seasonal extreme values in the river discharge and the wave forcing might be able to alter this general pattern a bit but the residual development patterns are assumed to not be influenced much by these low probability disturbances. To be able to only calibrate the order of the general development of the morphology at the MCR of the various calibration settings, a basic schematized set of forcing conditions is considered to suffice. The river discharge at the model's boundary in the calibration phase is therefore schematized by an average year round value of around 6500 m^3/s. The wave climate consists out of more commonly applied basic schematization (see §3.3.5.1) of only four wave height classes and two directional classes.

5.3 Bed schematization

With the found optimal values for the variable morphological scale factors (§3.3.7) the main morphological related setting, the bed schematization of the model need to be calibrated. The following bed schematizations are tested:

- single sediment fraction of 200 µm [Run 1]
- single sediment fraction of 500 µm [Run 2]
- multiple sediment fractions 200+500 µm, stratified bed, well-mixed [Run 3]
- multiple sediment fractions 200+500 µm, stratified bed, spatially distributed [Run 4]

The choice of the four different schematizations are based on the present sediment gradations in the CRLC. The beaches and hereby the majority of the CRLC are primarily comprised of well-sorted medium to fine sand with an averaged grain-size of approximately 200 µm (Figure 1.10). The dominant presence of a grain-size of 200 µm therefore forms the initial bed schematization tested in this calibration phase. Fox et al. (1984) however showed that coarse to medium sized sand (D_{50} > 200 µm) dominates the inlet and the estuary. Therefore the situation where both 200 µm and 500 µm are present in a equal distributed well-mixed situation is also tested. Furthermore the morphological behaviour of the area under the presence of solely 500 µm is tested and finally a situation considered to be closest to reality, where a spatially distributed presence of both 200 µm and 500 µm is active is applied in the schematization of the bed. The spatial distribution of the sediment fraction in this latter case is determined by the model and thus the system itself. A simulation implemented with a layered bed of multiple sediment fraction with the morphological updating scheme of the bed switched off forms a base run and will re-distribute the sediment fraction to ultimately form a new equilibrium (§7.1). This internal re-distribution of sediments is subsequently applied to the initial bed schematization. Figure 5.2 shows the internal distribution of the sediment fractions in the first layer after a simulation of two hydrodynamic weeks, as applied.

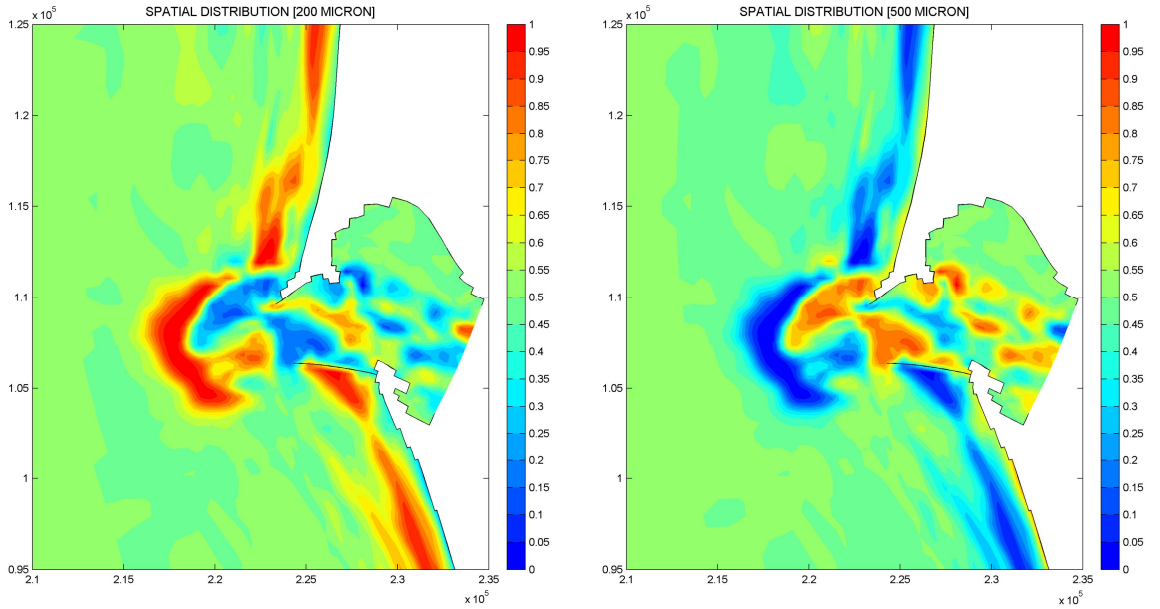

Figure 5.2 Model determined spatial distribution of 200 µm fraction (left) and 500 µm fraction (right).

At first, a quick visual comparison is done of the modelled five-year erosion/sedimentation patterns of the various bed schematizations to the observed 32 years of morphological change. Also a quantitative comparison of volumetric change per compartment is done. A trend in morphological development should be visual from these five-year morphological simulations and the continuing development rate should be able to be assessed. From this all a sound choice needs to be made for the schematization of the bed of the final long-term morphological simulation.

5.3.1 Visual analysis

The following plots show the erosion sedimentation patterns for the total observed morphological change between 1926 and 1958 (top left plot) and the modelled five years of morphological change for the various bed schematization calibration-runs (right column). What directly shows is that the model simulates the general patterns of development for the compartments of the outer ebb-delta and the inner ebb-delta quite well. Distinctive areas of morphological change are simulated. The order of the relative morphological changes of the simulations (five years) are however high in comparison to the total observed morphological changes (32 years). The simulation in which the bed is schematized by a single sediment fraction with a D_{50} of 500 µm is an exception on this. Polygons of the outer and inner ebb tidal deltas between the observed and modelled morphological changes differ slightly since the model seems to have a slightly different orientation of the development of the ebb tidal delta.

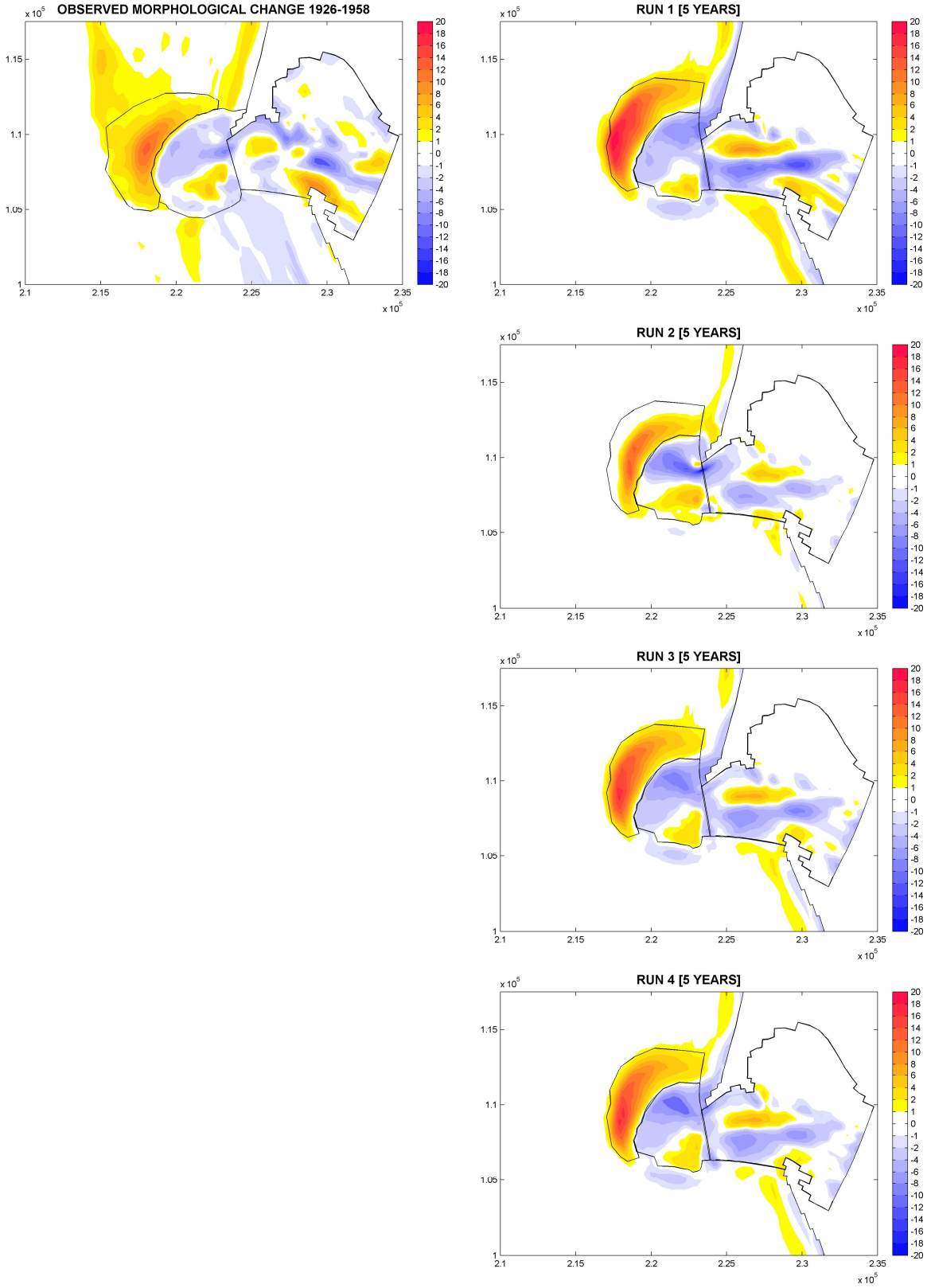

Figure 5.3 *Comparison observed (32 years) and modelled (5 years) morphological changes various bed schematizations.*

A more detailed comparison in bed level changes than the visual comparison is required to rightfully justify the application of a certain bed schematization. Therefore, a quantitative comparison of volumetric changes of the individual compartments over time of the observed 32 years of morphological change and the modelled five years of morphological change is given in the following paragraph. With an insight in the morphological development over time of the various bed schematization as better choice can be made for the final applied schematization of the bed in the model.

5.3.2 Quantitative analysis

The following three figures give the volumetric change over time for the three compartments of the inlet, the inner ebb-tidal delta and the outer ebb-tidal delta. Table 5. 1 at the end of this paragraph finally sums the total morphological change of the individual compartments.

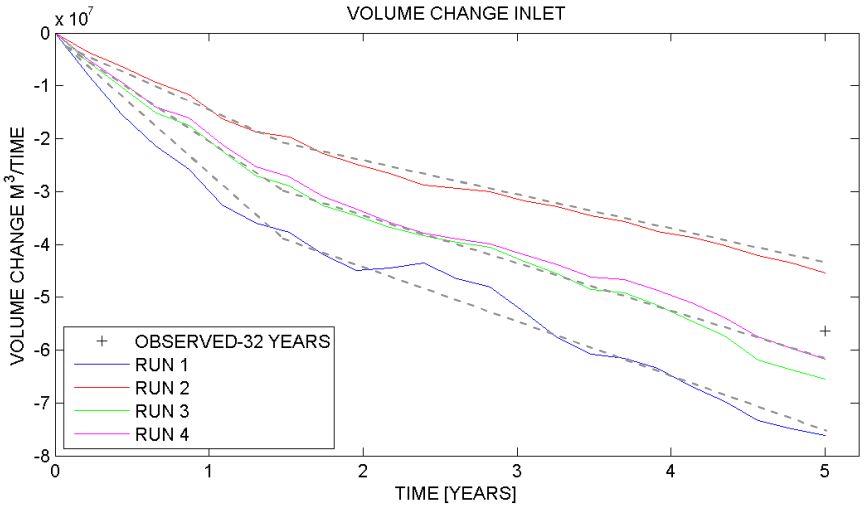

Figure 5.4 Comparison volumetric change Inlet.

Figure 5.4 shows that the morphological development rate (grey dotted lines) of the inlet area for all four of the schematizations in about the first two years of the morphological simulation is the largest. The volumetric change rates decrease slightly after this initial response period. Run 1 where solely a sediment fraction of 200 µm is applied, strongly overestimates the total observed morphological change. The modelled five years of morphological change of the single sediment fraction of 200 µm already surpassed the observed 32 years of morphological change by 35% (Table 5. 1). Also a stratified bed schematization consisting out of both 200 and 500 µm overestimates the total morphologic changes. An initial spatial distribution of multiple sediment fractions in the inlet however performs slightly better than a well mixed equal distribution of the sediments at the bed. The limited relative better performance however might be a result of the limited time over which the model performed the internal spatial distribution. The distribution seems to not have fully developed yet (Figure 5.2). It does however show that applying an initial spatial distribution is capable of reducing overall morphological change. Run 2, where solely a sediment fraction of 500 µm is implemented seems to better simulate the morphologic behaviour of the inlet. Fox et al, (1984) also state that the inlet and the estuary are dominated by sediments that are larger than 200 µm. However, if the volume change trend would be extrapolated further in time, than the application of a bed schematization consisting out of solely 500 µm would also overestimate the total morphological change. A general overestimation of the morphological change in the inlet compartment is thus present in the model.

Figure 5.5 shows the morphological development of the inner ebb-tidal delta of the four bed schematization calibration-runs in comparison to the total observed morphological change of the inner ebb-tidal delta. Figure 5.5 also shows a strong initial response and a decreasing development rate over time of the morphology for the four simulations. The total observed morphological change is again overestimated. The total modelled 5-years of morphological change for all four of the bed schematization calibration-runs already surpassed the observed 32 years of morphological change. The overestimation by Run 2, where solely a sediment fraction of 500 µm is implemented is the smallest. The bed schematization of Run 1 where solely a sediment fraction of 200 µm is implemented can under stronger wave action temporarily even turn around its general erosion rate into accretion. Figure 5.5 again shows that a spatial distribution of multiple sediment fraction in the inlet performs slightly better than a well mixed equally distributed sediment distribution. The reduced erosion effect is however limited. Again, the limited applied development time for the internal re-distribution of the sediment is addressed as the reason for this.

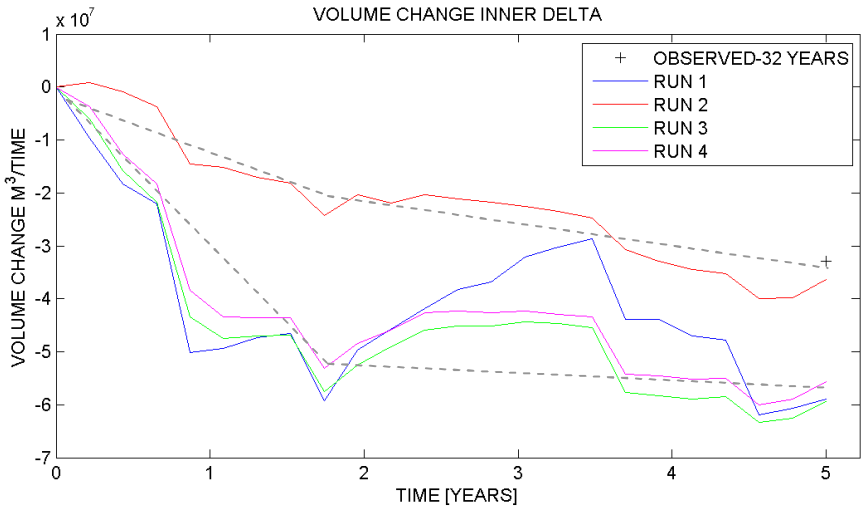

Figure 5.5 Comparison volumetric change Inner ebb tidal delta.

Figure 5.6 shows the morphological development of the outer ebb-tidal delta of the four bed schematization calibration runs in comparison to the total observed morphological change of the outer ebb-tidal delta. Also this figure shows a decreasing development rate over time of the morphology for the four simulations. Run 1, Run 3 and Run 4, where a sediment fraction of 200 µm is incorporated, overestimate the total morphological development. The modelled five years of morphological change again already surpasses the observed 32 years of morphological change. The overestimation in the five-year morphological simulations is already 37 to 78% higher than the total observed 32 years of morphological changes (Table 5. 1). From the continuing development rate of the volume of the outer delta, it shows that a morphological equilibrium has not yet been reached. Figure 5.6 and Table 5. 1 show that a spatial distribution of multiple sediment fractions in the outer delta performs slightly better than a well mixed equally distributed sediment distribution. It is noted that, the overestimation of the morphological development of the outer delta is partly be addressed to be a result of the earlier observed overestimation and continuing erosion of the inlet and inner delta.

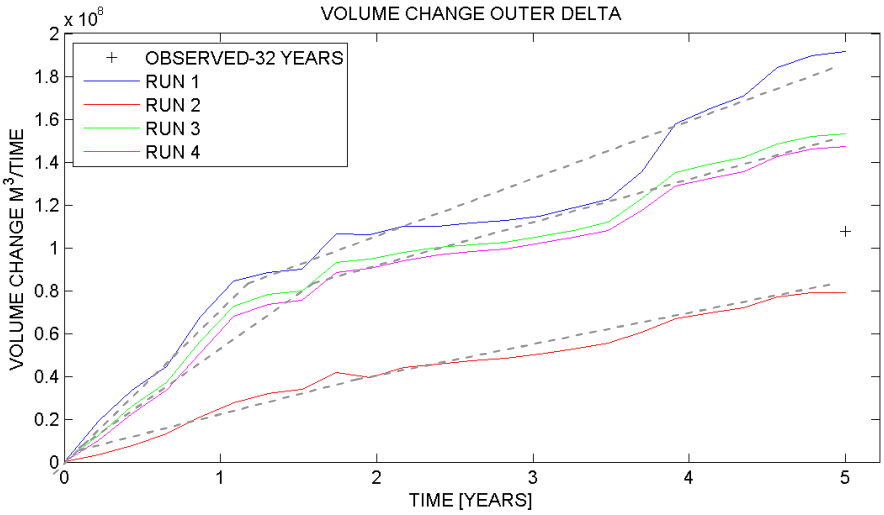

Figure 5.6 *Comparison volumetric change outer ebb tidal delta.*

Table 5. 1 *Quantitative comparison morphological change bed schematizations calibration runs.*

Compartment	Observed [m^3]	Run 1 [m3]	Run 2 [m^3]	Run 3 [m^3]	Run 4 [m^3]
Inlet	**$-5.634*10^7$**	$-7.609*10^7$ +35%	$-4.538*10^7$ -20%	$-6.555*10^7$ +16%	$-6.168*10^7$ +10%
Inner Delta	**$-3.290*10^7$**	$-5.887*10^7$ +79%	$-3.640*10^7$ +11%	$-5.937*10^7$ +81%	$-5.568*10^7$ +69%
Outer Delta	**$1.078*10^8$**	$1.915*10^8$ +78%	$7.898*10^7$ -27%	$1.532*10^8$ +42%	$1.474*10^8$ +37%
Total	**$1.856*10^7$**	$5.654*10^7$ +205%	$-2.800*10^6$ -85%	$2.548*10^7$ +37%	$3.004*10^7$ +62%

From the figures and table in this paragraph it shows that the model tends to overestimate the total morphological change. The strong initial morphological response of the inner delta and the inlet is seen as the main cause for the general overestimation of morphological change. Decreasing rates of development over time suggest that there is a clear initial response and a long-term trend in the development rate. Probably over time, the trend line will further stabilize and call the morphological development eventually to a halt. However, it is clear that the model under these bed schematizations will anyway strongly overestimate the total morphological change. The overestimation of the initial morphological response of especially the inner delta compartment (Figure 5.5) is considered to be the dominant cause for the general overestimation of morphological change in the model. An initial response of the morphology at the inner delta to the jetty construction as a result of the confined flow through the entrance is expected. However, in respect to the total observed morphological change [33Mm^3], the computed initial response [~50Mm^3] seems to be too high. Goal is therefore to reduce the initial response and thereby further improve the total computed morphological change. A bed schematization that is considered to be closest to reality and performed relatively best, was the bed schematization consisting out of a spatially distributed bed schematization of the dominant present sediment fraction of 200 µm and a coarser sediment fraction of 500 µm. However also here a strong general overestimation of the morphological change was present. To sufficiently decrease the initial morphological response of this bed schematization a fully developed distribution of the bed needs to be applied.

5.3.3 Fully developed spatial distribution of sediments

A fully developed distribution of sediment fractions at the bed is applied in the realization of reducing the initial morphological response. The afore applied limited developed spatial distribution showed to reduce the initial morphological response of the model to only a limited extent. Implementing a fully developed bed schematization is considered to be justified since in reality the system itself would also have determined an equilibrium spatial distribution of sediments at the bed considering the relatively stable state of the pre-jetty condition. The conditions for the model to determine the distribution of the bed differ slightly from reality since in the model the effect of the jetty construction is already taken into account. On the other hand, in reality the spatial distribution of the sediment fractions in the bed has had a longer time to develop Figure 5.7 shows the fully developed spatial distribution of both sediment fractions in the top layer of the bed. What shows is that both the inlet and inner delta compartment have developed to predominantly consist out of the coarser sediment fraction of 500 µm. Applying the coarser fraction as an initial condition will positively reduce the initial morphological response.

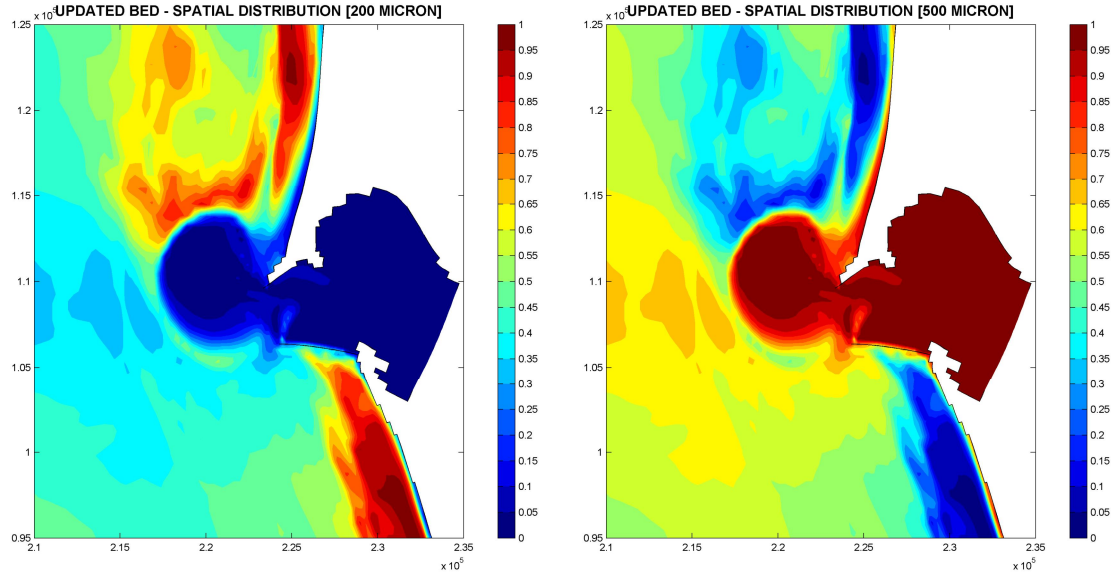

Figure 5.7 Spatial distribution 200 µm (left) and 500 µm (right).

Figure 5.8 handles the results of the application of the fully developed initial distribution of the sediments (black line) in comparison to a well-mixed distribution for the inlet compartment (red line) in a 30-year simulation.

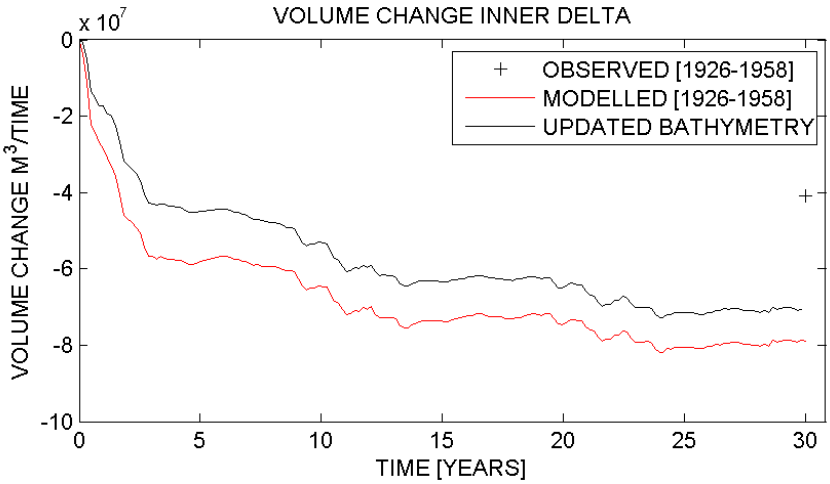

Figure 5.8 Influence spatial distribution of sediments and tidal reduction

From Figure 5.8 it clearly shows that the application of an initial fully developed spatial distribution of the sediments further improves the before strongly overestimated initial morphological response to the jetty construction. The total morphological change of the inner delta and directly linked, the outer delta will hereby positively be reduced. A general better morphological representation of the observation is hereby reached. However, still an overestimation of the total morphological change will be present.

As an extra measure to further reduce the general overestimation of the modelled morphological development of the MCR, the sediment transport calibration factors are lowered. Calibration results of which are looked at in the following paragraph.

5.4 Sediment transport calibration settings

User specified scaling factors (f*Sus*, f*Bed*, *fSusW* and *fBedW*) are available in the transport formulations of Delft3D for the bed load transport, current-related suspended transport and the wave related suspended and bed load transport (f*Bed*, f*Sus, fSusW* and *fBedW* respectively) to calibrate the sediment transports and resulting morphological development of the model. Default values are 1, which implies that the formulations represent physics of sand transport perfectly (van Rijn, 2004). Van Rijn (2004) further states that the lower and upper limits of the scaling factors *fBed* and *fSus* are 0.5 and 2.

As the wave-related suspended sediment transport is rather uncertain and since experience with this formulation is limited it seems that best results are obtained by ignoring the wave-related suspended transports (i.e. *fSusW*=0) or prescribing a strongly reduced factor in the range of 0.0 to 0.5. The calibration runs of the previous paragraphs are implemented with a bed load transport and a current-related suspended sediment transport factor of 1. Wave related suspended and bed load sediment transport factors were set on 0.3 and 0 respectively. As a result of the strong overestimation of the total morphological development in the afore calibration runs, both the bed load and current related suspended sediment transport are reduced to the lower limit of 0.5. The effect of this decrease in the sediment transport scaling factors is analyzed by comparing the best estimate calibration-run of the bed schematization (Run 4) for both cases of sediment transport calibration settings.

5.4.1 Analysis

The following figures show the morphological development over time for the compartment of the outer delta, inner delta and inlet in the application of upper and lower limit sediment transport calibration factors.

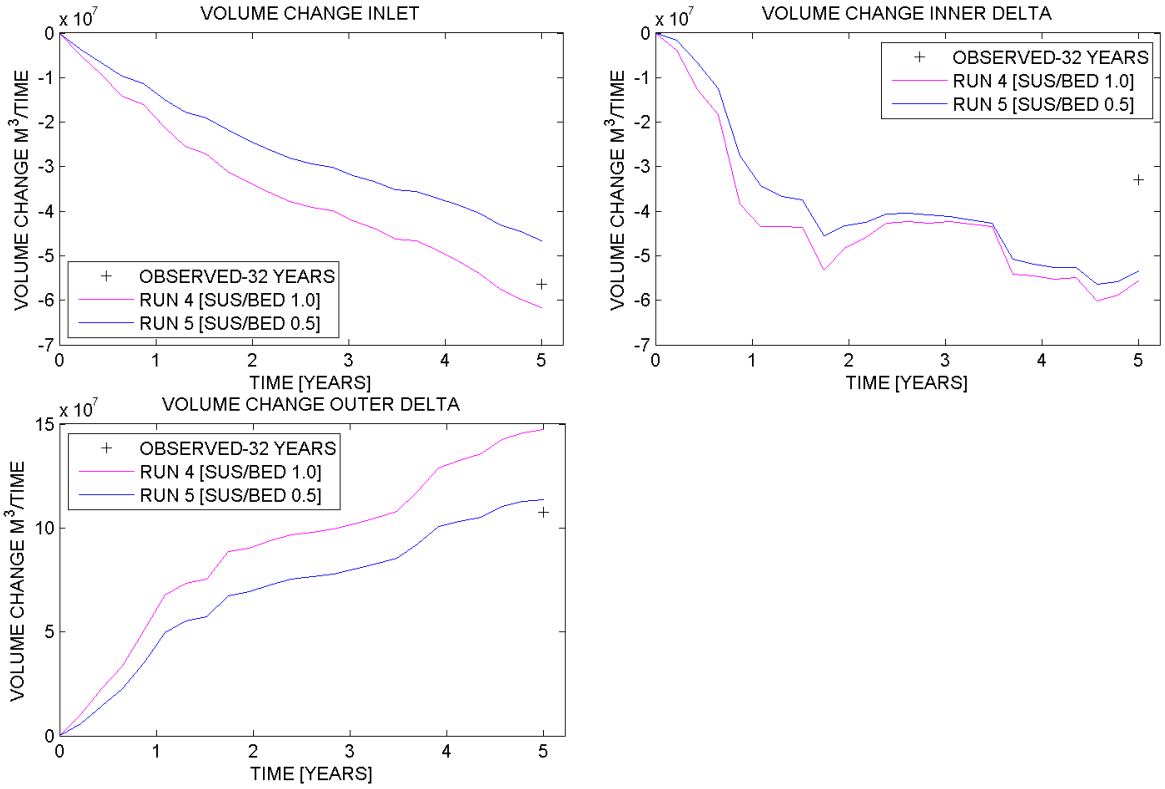

Figure 5.9 Influence sediment transport calibration factor

What shows from the figures is that, by applying sediment calibration factors that multipliy the bed load transport and the current related suspended sediment transports by a half does not lead to half of the total morphological change. For the outer ebb-tidal delta, the total volumetric change after five years of Run 5 is 77% of the volumetric change of Run 4. For the inner ebb-tidal delta this is 96% and for the inlet 76%. The compartment of the inner ebb-tidal is the area at which the greatest adjustment of the morphology to the jetty construction will arise. The confinement of the tidal flow through the entrance of the MCR will cause strong erosion effects. The dominant disturbance of the morphological behaviour due to jetty construction is apparently not hindered too much by the transport calibration parameters. However, a reduction of the total morphological change is reached. The final long-term morphological simulations will therefore be implemented with the lower limit transport calibration settings to reduce the total morphological change as much as possible and optimize the model in simulating the observed morphological changes.

5.5 Schematization morphological tide

Despite the application of lower limit sediment transport calibration factors, still an over prediction of the computed morphological changes is present. This is thought to partly be caused by the apparent over prediction of the schematization of the morphological tide.

In this study the work done by Lesser (2009) on the schematization of the tide for the neighbouring estuary of the Willapa Bay was directly adopted. In which a scaling factor of 1.08 has been applied to the tidal constituents that represent the 'morphological tide', namely M_2 and C_1 (§3.3.3). Figure 5.10 shows the relative high schematized morphological tide that followed from the application of the scaling factor of 1.08 with respect to the full astronomic tide. The tidal water levels of the morphological tide herein closely approach the tidal water levels of the spring tide. A tidal reduction is wanted to reduce tidal inflicted sediment transports and thereby the total morphological change of the model. A tide that is 10% higher than the average of the full-astronomic spring-neap tide is set to represent the desired tidal reduction of which the height is plotted in Figure 5.10. A re-adjustment of the scaling factor should allow for the morphological tide to represent the reduced tide. With the 10% above average tide representing a peak water level of about 1.24 meter and the morphological tide a peak water level of 1.34 meter, the scaling factor is reduced to 1.0. Also a reduction of the tide by applying a scaling factor of 1.06 to both the tidal constituents M_2 and C_1 following Equation 5.1 and the application of the scaling factor of 1.08 to only the tidal constituent M_2 according to Equation 5.2 are tested. The following paragraph handles the results on the morphology of the various tidal reductions.

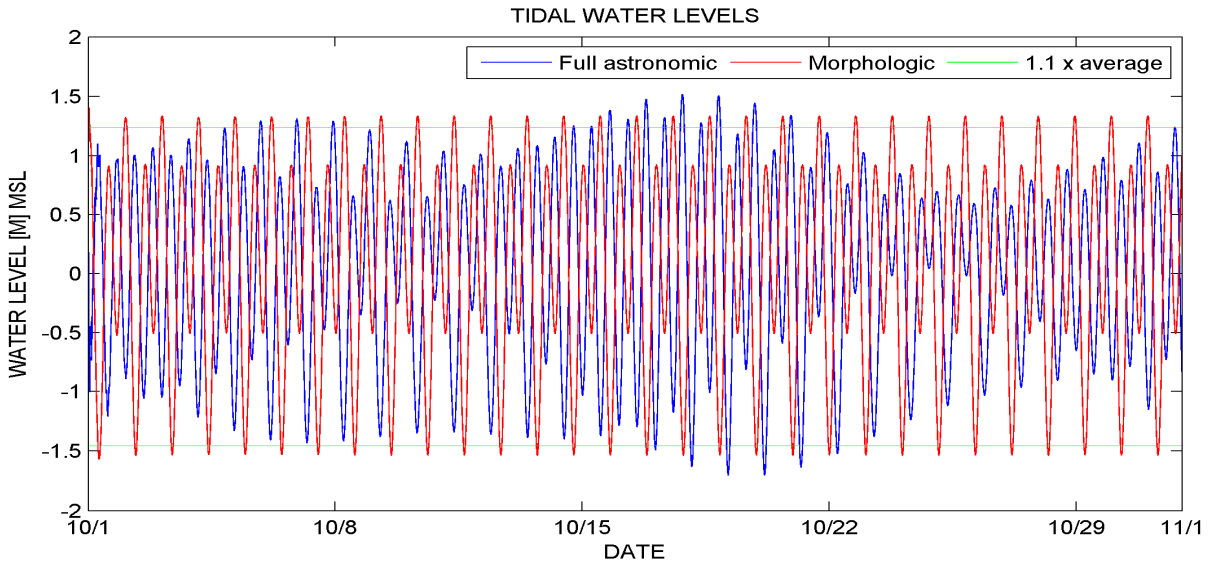

Figure 5.10 *Tidal offshore water levels, full astronomic (blue), morphologic (red) and 10% above average(green).*

5.5.1 Analysis

The volumetric changes over time for the compartments of the inlet, the inner delta and the outer delta for the reduced morphological tides are compared to the base case and the observations in Figure 5.11.

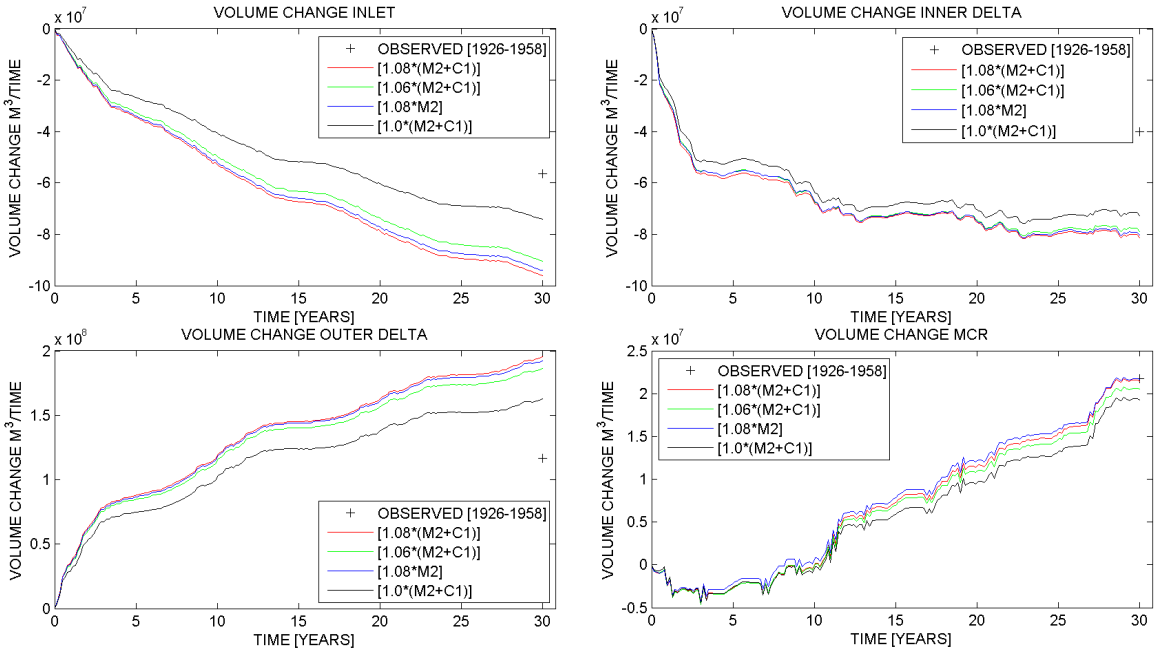

Figure 5.11 *Volumetric change over time reduced tide, inlet (top left), inner delta (top right), outer delta (bottom left) and total (bottom right)*

From Figure 5.11 it follows that the most significant relative reduction of the total morphological changes is reached by the application of a scaling factor of 1.0 to both the M_2 and C_1 constituent. The tide herein represents to be 10% higher than the average tide. In the inlet, an area of relative little wave influence, the effect of this tidal reduction increases over time. In the compartment of the inner delta where wave action becomes more dominant, the effect of the reduced tide over time is less. However, also here a total positive effect is gained in reducing the total morphological change. For the compartment of the outer delta, it holds that sediments that eroded from both the inlet and the inner delta end up in the compartment of the outer delta. With a total reduced morphological change of the inlet and an increasing positive effect of the total morphological change over time of the inlet, the morphological change of the outer delta is thus also positively reduced over time.

The application of a reduced morphological tide that represents to be about 10% higher than the average tide thus shows to positively further decrease the total morphological changes of the model and will be applied in the final long-term morphological simulations. Furthermore, from Figure 5.11 (bottom right plot) it shows that the total amount of volumetric change of the three compartments combined is accurately represented by the model. The area over which the individual polygons extend however has a strong effect on the level of accuracy in representing the total volumetric change. The area over which the outer delta polygon is chosen to be represented, especially determines the total amount of volumetric change for comparison between observations and computation. Tidal reduction is herein to a limited extent also capable of decreasing the overall import of sediment of the three compartments combined. The following figure shows the overall effect of tidal input reduction

on the total volumetric change of the estuary domain. What shows is that a reduced tide leads to less sediment removal from the estuary compartment and therefore a lower available supply of sediment to the compartments of the inlet, inner delta and outer delta. The overall reduction in volumetric change of the reduced tide is however limited (less than 3 Mm^3 in 30 years) as already showed from Figure 5.11.

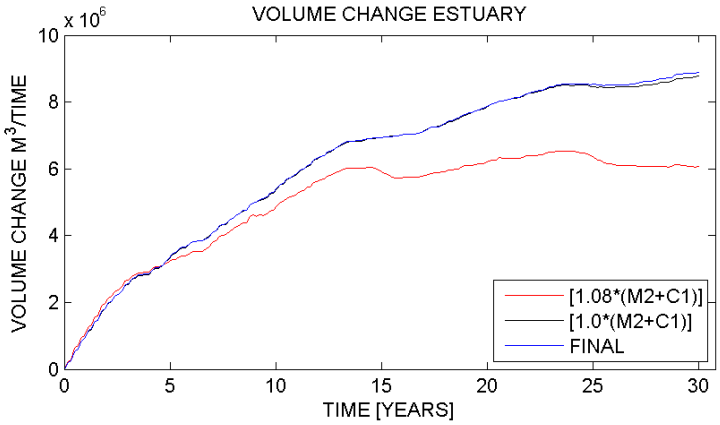

Figure 5.12 Volumetric change over time estuary compartment, influence tidal reduction

5.5.2 Background

Lesser (2009) states that a mean flow (non-tidal residual) causes enhanced residual transports in the presence of harmonic tidal velocity fluctuations due to the non-linear nature of sediment transports (sediment transport assumed being proportional to U^3). For a simplified tide to create the same residual sediment transport as a full astronomic tide in the presence of a non-tidal residual (i.e. wind and river flow) it is therefore important that the tidal energy is preserved in the simplified tide. A simplified tide of M_2+C_1 alone does not satisfy this requirement. Applying a scaling factor to the M_2 and/or C_1 constituents can however improve the preservation of total tidal energy. If applied to both M_2 and C_1 the required factor is limited by:

$$f_1 = \sqrt{\frac{(M_2^2 + S_2^2 + N_2^2 + O_1^2 + K_1^2 + P_1^2 + ...)}{M_2^2 + C_1^2}} \qquad (5.1)$$

If the factor is only applied to the M_2 constituent the factor is:

$$f_2 = \sqrt{\frac{(M_2^2 + S_2^2 + N_2^2 + O_1^2 + K_1^2 + P_1^2 + ...) - C_1^2}{M_2^2}} \qquad (5.2)$$

The application of the scaling factor is however not a perfect solution, as the scaling factor will also overstate the residual due to the M_2+O_1+K_1 interaction. Application of the scaling factor to just the M_2 component means that the error introduced to the M_2+O_1+K_1 residual will be linear with the amplification factor. This is preferable to applying the factor to both the M_2 and C_1 constituents which makes the error to the amplification factor cubed.

The factor to be applied furthermore depends on the mean residual flow. If U=0 then f_1=f_2=1.0. If U is large then f_2 should approach the limiting value. A pragmatic method to determine an optimum amplification factor is determinable through trial and error. For this study, the application of no scaling factor (f_1=1.0) showed to have a more

desirable effect in the total morphological changes than the application of an amplification factor of 1.08.

Despite the present mean residual flow as a result of the active river flow at the MCR a lower value amplification factor showed to benefit the computed total morphological changes in simulating the observed morphological changes. It is further noted that from the dependence of the scaling factor to the residual mean flow, it follows that an optimal scaling factor might possibly not be constant but should be river discharge determined and hence vary over time. This is a point of discussion and recommendation and will be further handles in §7.2.

5.6 Transition period variable MorFac

Lesser (2009) addressed the importance of choosing appropriate transition periods between consecutive wave conditions in morphological simulations where a variable MorFac is applied to avoid significant discontinuities in sediment mass. If the morphological scale factor changes while sediment is in suspension a sediment mass error could be introduced as soon as the sediment settles again under a changed MorFac, as a result of the fact that sediment fluxes to and from the bed are multiplied by MorFac. This problem can however be minimised by carefully choosing the start and end times of a morphological scale factor value so that suspended sediment concentrations are relatively low (i.e. around slack water) and/or approximately equal. Assurance of identical start and end times in the harmonic cycle per wave condition should minimise any discontinuity of sediment mass. A sufficiently long transition period where no morphological updating is active besides that should allow for the hydrodynamic and wave model to stabilise to the new boundary conditions. In consideration of the total computation time of the final long-term morphological model however, the transition period between consecutive wave conditions is wanted to be as short as possible. The effect of applying different transition periods on the total morphological behaviour of the MCR are verified together with a variation of the starting point of the morphological simulation within the harmonic tidal cycle. Again, a sound choice will be made for these model settings for the final long term morphological model.

Run 1, where a transition period of 15 minutes between consecutive forcing conditions is applied forms the most basic case in the comparison. Since waves are run in a stationary matter this limited transition period is considered not to impose a problem for the wave computation. Also the 15 minute transition period is considered to suffice for the relatively coarse sediment to settle down. The downfall of this schematization is that the start and end point of the various forcing conditions are different and random within the tidal cycle. A maximum gain in reducing the computation time is however reached.

In Run 2, the transition time has been extended from 15 minutes to a full morphological tide of 1490 minutes. Start and end times in the harmonic tidal cycle of consecutive forcing conditions are hereby identical and the model has more than enough time to stabilize to the new boundary conditions. The mixed semi-diurnal character of the tide determines the transition time of a full morphological tide in stead of for example half the morphological tide. The starting point within the tidal cycle of the morphological simulation of Run 2 is however still random as a result of the random starting point of the morphological simulation within the tidal cycle. Calculation times are almost doubled in comparison to Run 1.

In Run 3 finally, also the starting point of morphological updating is assigned at the starting point of the rising tide from the zero water level. The transition period is again a full morphological tide to guarantee an identical starting point for every consecutive forcing condition.

5.6.1 Analysis

Figure 5.13 shows the morphological development of the three calibration-runs of the handling of the transition period of consecutive wave conditions for the compartments of interest, the outer delta, the inner delta and the inlet.

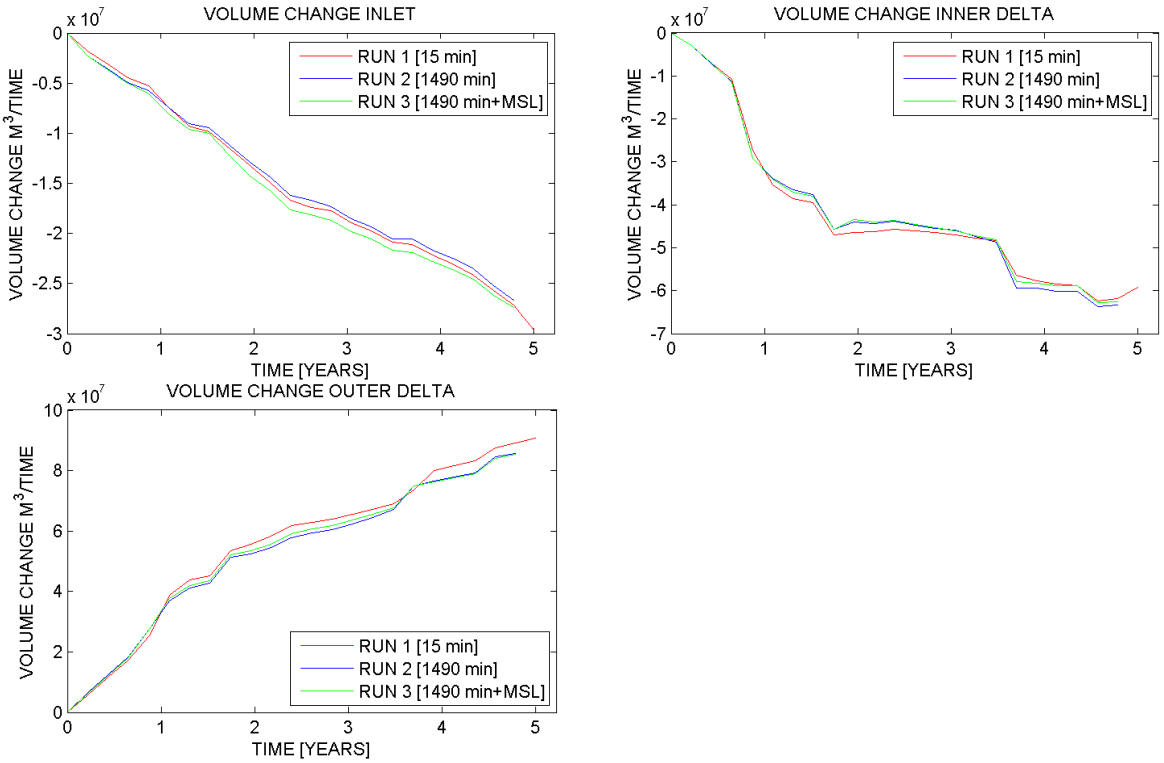

Figure 5.13 Comparison transition time and starting point of morphological simulation.

What shows from Figure 5.13 is that the sediment discontinuity and therefore the difference in modelled morphological change as a result of various transition periods is limited. Also the starting point of the morphological simulation within the tidal cycle does not seem to affect the morphological development much. From this analysis, therefore the application of the transition time most beneficial for the computation time is chosen for the final long-term morphological model, namely the application of Run 1, in which a transition period of 15 minutes is applied and the morphological simulation starts at a random point in the tidal cycle.

5.7 Discussion

From the calibration-runs, it showed that the model significantly overestimated the general observed morphological changes. Five-years of computed morphological change herein already surpassed the observed 32 years of morphological change. From the rates of morphological development it followed that an equilibrium situation was also no yet reached. The total computed morphological change would therefore strongly be overestimated. A significant initial response of the inner delta morphology to the construction of the entrance jetties was addressed as an import cause for the general overestimation. To reduce this initial response a fully developed (30 year) initial spatial distribution of sediments in which the inlet and the inner ebb-tidal delta predominantly formed to consist out of the coarser sediment fraction of 500 µm, showed to significantly reduce the initial response. The apparent general overestimation of the morphological changes at the MCR was further reduced by applying a relative reduced morphological tide and by reducing the sediment transport calibration settings to the lower limit.

All of these morphological change reducing settings are applied in the final long-term morphological model to reduce the total morphological change as much as possible and optimize the model in simulating the observed morphological changes.

6 Simulations

6.1 Period B 1926-1958

One of the main objectives of this study is to model (hind cast) the long-term morphological changes at MCR with Delft3D and compare the observed and computed bathymetric changes for the interval of 1926-1958. Focus is specifically on the MCR, namely on the compartments of the inlet, inner ebb-delta and outer ebb-delta. To address this objective, the modelled bathymetric evolution is compared to measured data (Figure 5.1) using bed level analysis, and deposition volumes.

6.1.1 Model set-up

In order to create a representative model, capable of simulating the observed morphological changes, the schematizations, calibrations and optimal model settings still have to be evaluated for the long-term morphological application of the 1926-1958 period.

The following section addresses this final model set-up. The *Opti-routine* (§4.2) is applied to reduce the vast amount of forcing conditions that followed from the schematization of the wave and river discharge climate. The f reduced set of conditions will be applied to the simulation of the 1926-1958 period. By applying the *Opti-routine*, the mean total transport pattern at the MCR for every combination of wave condition and river discharge times its probability of occurrence is summed to create a total mean transport pattern at the MCR (Figure 6.1 left). The number of forcing conditions is subsequently reduced by dominance and the alternation of weight factors to create a sufficiently accurate reduced set of conditions (Figure 6.1 right). This procedure cancels out forcing conditions relatively unimportant to the total morphological change. Either as a result of limited absolute morphological response of or as a result of a probability of occurrence that is too small to lead to high enough relative morphological change. The accuracy of the reduced set of conditions can be determined from the relative root-mean squared error. An optimal amount of conditions should however be found also taking into account computation time and a sufficient representation of both wave and river discharge conditions. The application of the *Opti-routine* led to a reduction of the in total 778 conditions to a representative set of eleven, given in Table 6.1.

Table 6.1 Reduced set of conditions from the Opti-routine.

Conditions	H_s [m]	T_p [s]	Dir [°]	V_{wind} [m/s]	Q [m^3/s]	P [-]	Duration [days/year]	No.# Mor.tides	MorFac [-]
1	5.50	5.50	202	12.54	3900	0.035	12.6	5	24.35
2	2.77	9.59	262	6.59	3900	0.054	19.7	4	47.58
3	5.18	11.86	270	7.90	3900	0.063	23.1	8	27.87
4	1.61	8.52	277	4.92	3900	0.534	194.7	20	94.10
5	4.05	10.95	287	6.57	3900	0.002	0.9	1	8.39
6	3.71	10.64	293	6.39	3900	0.030	10.9	3	35.25
7	2.29	8.71	308	5.66	3900	0.054	19.7	3	63.30
8	3.88	10.65	270	7.47	6000	0.008	3.0	2	14.44
9	2.03	8.42	260	5.70	7250	0.080	29.4	4	70.93
10	1.19	7.75	273	4.10	12500	0.081	29.5	3	94.97
11	2.99	9.60	273	5.86	12500	0.059	21.6	4	52.20
						1	**365**	**57**	

Figure 6.1 shows the comparison plots of the magnitude of the mean total transports at the MCR for the full set of conditions (left) and the reduced set of conditions (right). Figure 6.2 shows the vectoral differences between the full set of conditions and the reduced set to better show the relative difference. The relative weighted root-mean squared error of the mean total transport at the MCR of reducing the forcing conditions to 11 is 7.49% and considered to be within acceptable terms for the focus of this study.

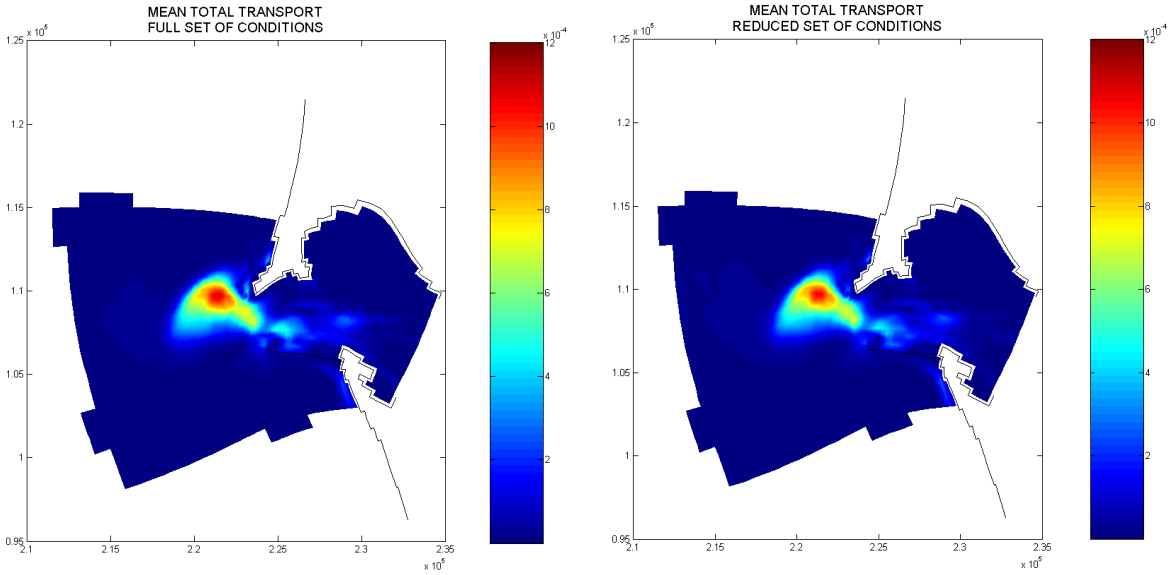

Figure 6.1 *Opti-routine results, full set of conditions and reduced set of conditions*

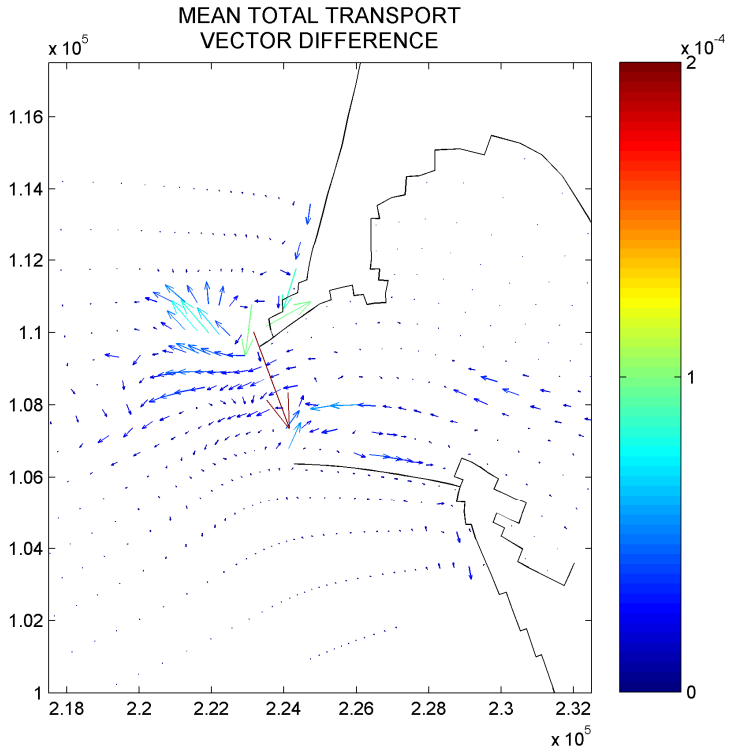

Figure 6.2 *Vector difference for mean total transport comparison*

The reduced set of conditions consists out of 6 wave conditions with a probability of occurrence of 76% coming from a more northern direction, 2 wave conditions coming from a western direction with a probability of occurrence of 7.1% and 3 wave conditions coming from a more southern direction of which the probability of occurrence is 16.9% (
Figure 6.3 left). This directional distribution of the reduced set of conditions agrees well with the directional distribution of all the wave data, in which 66.5% comes from a more northern direction, 10.4% from a western direction and 23.1% from a more southern direction (Figure 1.9).

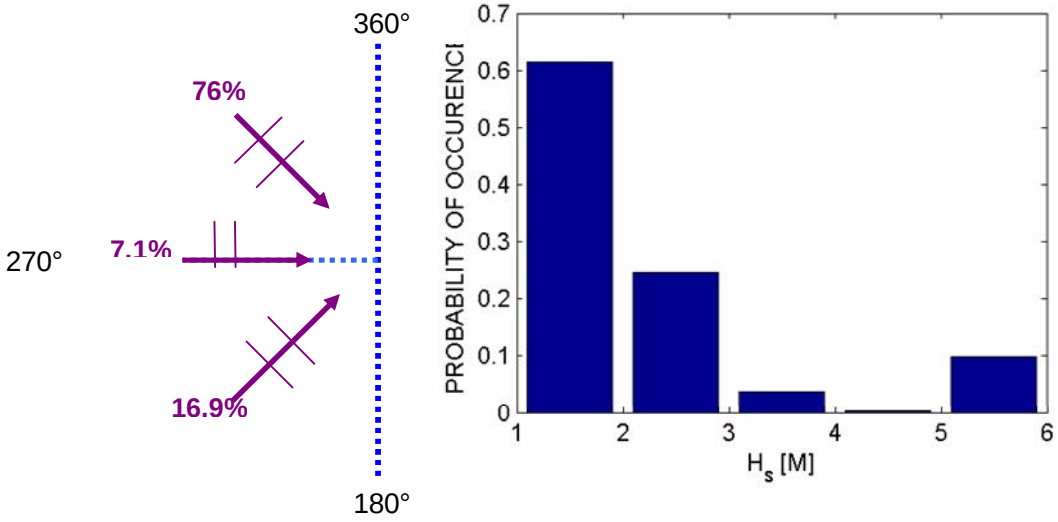

Figure 6.3 Distribution wave conditions resulting from Opti-routine

Figure 6.3 also shows the distribution of the wave heights. As a result of the low probability of occurrence of the individual peak wave conditions and therefore their relatively low contribution to the overall morphological change, wave heights only reach to the 5-6 meter range. Another important aspect of the wave climate schematization is that over 60% of the wave heights is in the 1-2 meter range, of which 90% is accounted for under the presence of a river discharge of 3900 m^3/s and 10% under a relative high river discharge of 12500 m^3/s. Figure 6.4 shows the total distribution of the discharge conditions that resulted from the *Opti-routine*. Also here holds that due to the low probability of occurrence of the peak river discharge conditions and therefore their relatively low contribution to the overall morphological change, the peak conditions do not appear from the reduction routine and the highest river discharge class is only 12500 m^3/s.

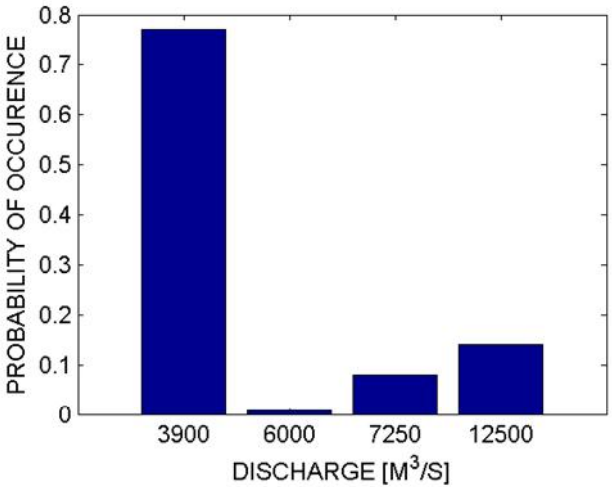

Figure 6.4 Distribution discharge conditions resulting from Opti-routine

Application forcing conditions

The dominant factor in the application of the forcing conditions to the model is the river discharge. Tide-induced and density driven flows are important for the generation of residual flows and sediment transports at the MCR. Elias and Gelfenbaum (2009) showed that sediment dynamics at the mouth are herein fully linked to the salt wedge. The development of the salt wedge is strongly influenced by the river discharge. The river discharge is however applied at the upriver boundary and alteration of the river discharge takes time to have its effect at the mouth. To limit the development time of the salt wedge as much as possible and hereby benefit the total computational time, it is chosen to let the river discharge be the determining condition of the total forcing conditions climate. The river discharge climate is implemented by gradually increasing the river discharge according to the derived conditions of Table 6.1. The gradual increase allows for the salt wedge to gradually develop and have its full effect on the morphology at the mouth. To simulate the 30 year morphological development and account for the seasonality of both the river discharge and the waves and still limit computation times, a repeating 10 year climate is developed in which at first the river discharge increases from 3900 m^3/s to 12500 m^3/s and subsequently decreases again to 3900 m^3/s. This climate is repeated three times to account for the total simulation time. In the transition between discharge classes an extra time period with the length of one morphological tide is implemented to give the salt wedge some extra development time.

The wave conditions follow the discharge conditions according to Table 6.1. Each wave conditions is run over full morphological tides. The number of morphological tides over which a single wave conditions is run depends on its total time of occurrence. An alternation between the lower and the higher wave conditions is applied to account for the variability and benefit the stability of the model.

To turn the representation of the wave conditions in a morphological simulation of the required length, a variable morphological scale factor is applied to each individual wave condition (Table 6.1). The application of a variable MorFac means that each wave (and thus also river discharge) condition is simulated for the duration of one morphological tide of fixed hydrodynamic duration (1490 minutes). A morphological acceleration factor specific to the wave conditions is applied so that the morphological duration of the wave condition matches its probability of occurrence (Lesser, 2009), to which now a maximum of the morphological scale factor of 150/Hs and a general maximum of 100 is allowed. The variable morphological scale factor is computed by:

$$f_{morfac} = \frac{p_{wc} * 5256000}{n * 1490} \quad (6.1)$$

Where p_{wc} is the probability of occurrence of the specific condition, *5256000* the number of minutes in the ten-year repeating simulation period, *1490* the hydrodynamic duration of the representative morphological tide and *n* the number of morphological tides that is needed to keep the morphological scale factor below the maximum allowed morphological scale factor. By applying the variable morphological scale factor, the hydrodynamic model can simply be run for the required number of morphological tides, one after another, and a different offshore wave boundary condition and corresponding morphological scale factor can be applied to each successive tide.

6.1.2 Basis for analysis

With the final derived schematization of the forcing conditions and the earlier derived bed schematization, transport calibration factors and general settings the simulation of the 1926-1958 period is performed. The performance of the model is attributed to the agreement with the observed 1958 bed level (Figure 6.5) and the observed morphological changes between 1926 and 1958 (Figure 6.6). The main and general observed morphological changes that occurred between 1926 and 1958 as described by Buijsman (2003) were:

- Erosion of the inlet
- Erosion of the inner ebb-tidal delta
- Accretion of the outer ebb-tidal delta

A more detailed description of the observed morphological behaviour of the MCR is however required to determine the actual performance of the model. Therefore, a detailed visual analysis of the morphological changes is given by analyzing spatial bathymetric and erosion-sedimentation patterns for both the observed and computed 1926-1958 period. This visual analysis is extended by looking at observed and computed cross-sectional bed level developments. In order to also be able to quantify the general performance of the model a comparison of the total observed and modelled volumetric change of the individual compartments of the inlet, the inner delta and the outer delta is done. The agreement of the model in simulating the observed morphological changes is subsequently analyzed, in which the strong and weak point of the model are outlined. A discussion and conclusion on the general performance of the model is finally formed, in which hypotheses for the deviating computed morphodynamics are addressed.

6.1.3 Observations

The observed morphodynamic changes are described by looking at the observed bed levels and erosion-sedimentation patterns of the 1926-1958 period (Figure 6.5 and Figure 6.6).

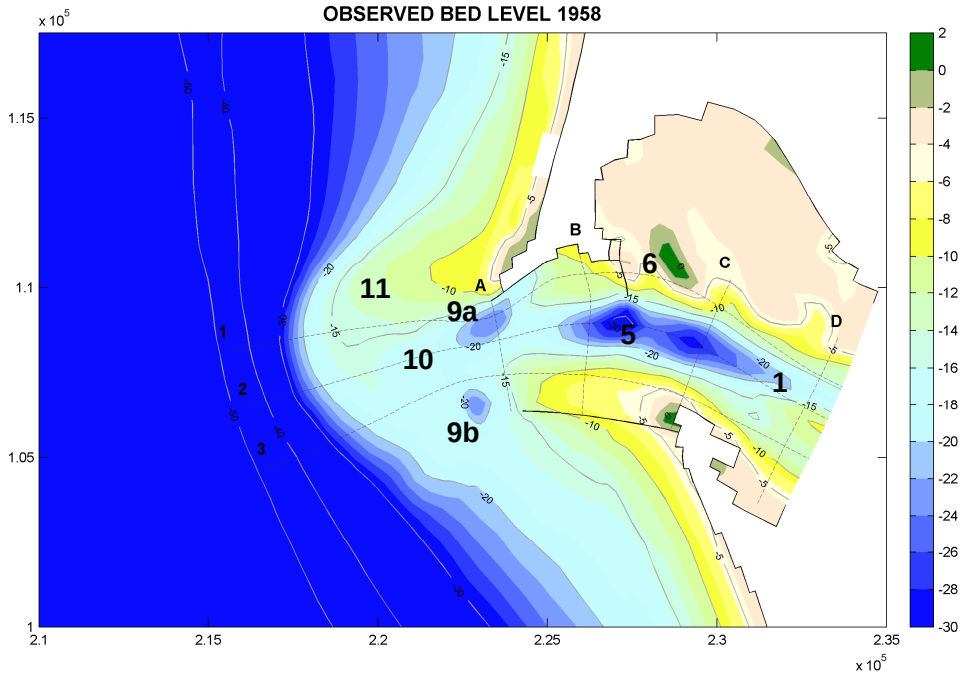

Figure 6.5 Observed 1958 bathymetry

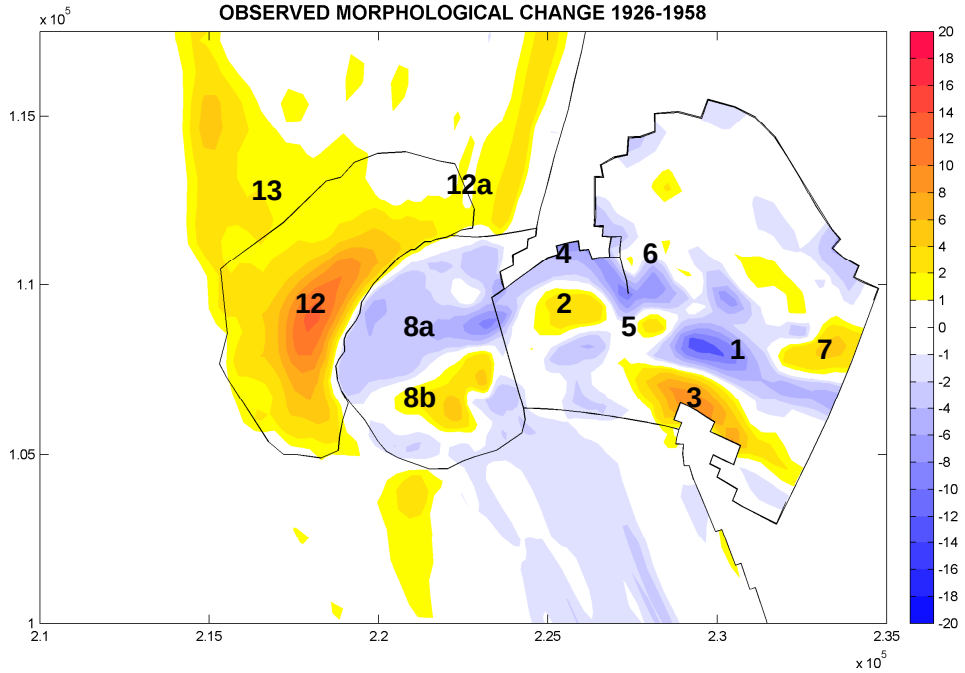

Figure 6.6 Observed erosion-sedimentation patterns 1926-1958.

Observed morphological changes 1926-1958

Inlet

In the readjustment of the morphology to the jetty construction the inlet eroded in which a predetermined and relatively stable single channel developed. The constant course of the flow through the main channel led to a fairly large extent of the channel well over 25 meters in depth The orientation of the channel is slightly to the north of the centre of inlet (1). In the areas of reduced energy adjacent to the channel, local bulges of sediment deposition arose (2 and 3). While along the inside of the North Jetty erosion was present (4). At (5), a local scour hole developed at the tip of the in 1939 constructed Jetty A, reaching over 30 meters in depth. The channel formation towards the marina of Ilwaco, Washington and Baker Bay (Figure 2.1) is visible at (6). At (7) a local area of sediment deposition is present.

Inner delta

The confined flow through the entrance pushed the existing pre-jetty ebb-tidal delta of the Columbia River further offshore into deeper water. Hereby effectively eroding the compartment of the inner ebb-tidal delta. The developed distinctive northern orientated ebb-tidal flow specifically caused erosion in the northern part of the ebb-tidal delta (8a). While in the southern section a accreting bulge of sediment arose (8b). The bathymetry shows that the tidal flow through the channel and out of the mouth slightly bends to the south just seaward of the mouth. Two distinctive scour holes developed at the tips of the North and South Jetty (9a,b). The majority of the inner delta developed into having a more or less uniform depth in the 16 to 20 meters region (10).

Outer delta

A distinctive northern orientated outer ebb-tidal delta (11) is observed. The confined flow through the entrance as a result of the jetty construction eroded the inner delta of the Columbia River and pushed the sediment further offshore into deeper water (12). Hereby contributing to the further off-shore development of the outer delta. Littoral drift re-distributed the sediment from the outer delta onto the adjacent shores (12a). The observations also show an offshore deposition of sediments northwest of the outer delta at (13).

6.1.4 Model results

Computed bed level and erosion-sedimentation patterns for the 1926-1958 period are shown in Figure 6.7 and Figure 6.8. By comparing the computed bed level and erosion and sedimentation patterns with the measured patterns allows for the determination of the performance of the model. Comparison of the development of the bed over several cross-section in both x and y direction are added to the analysis by looking at Figure 6.9 and Figure 6.10.

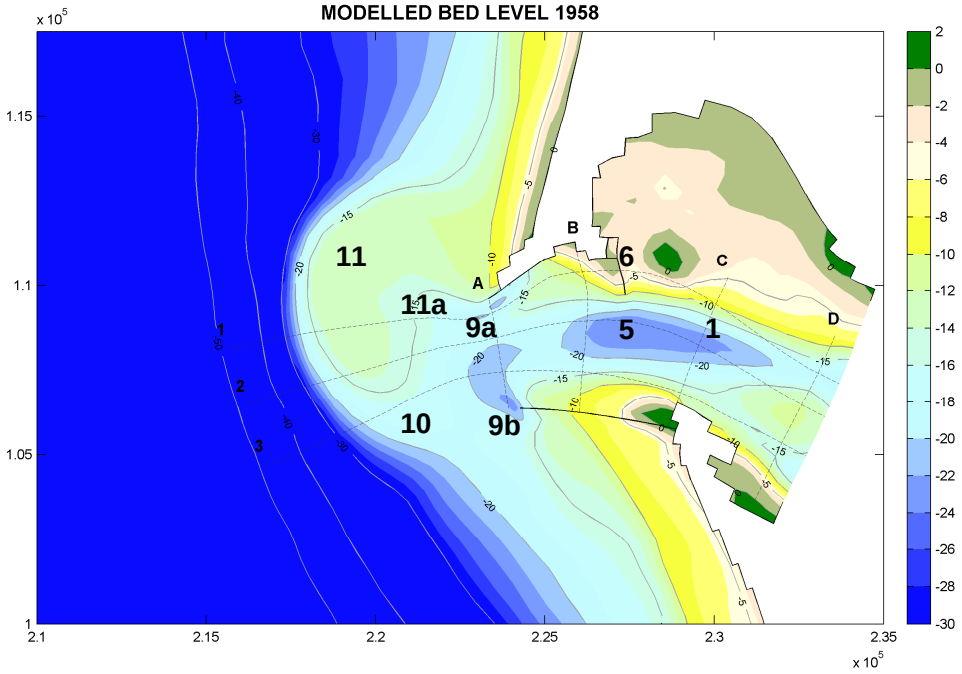

Figure 6.7 Modelled 1958 bathymetry

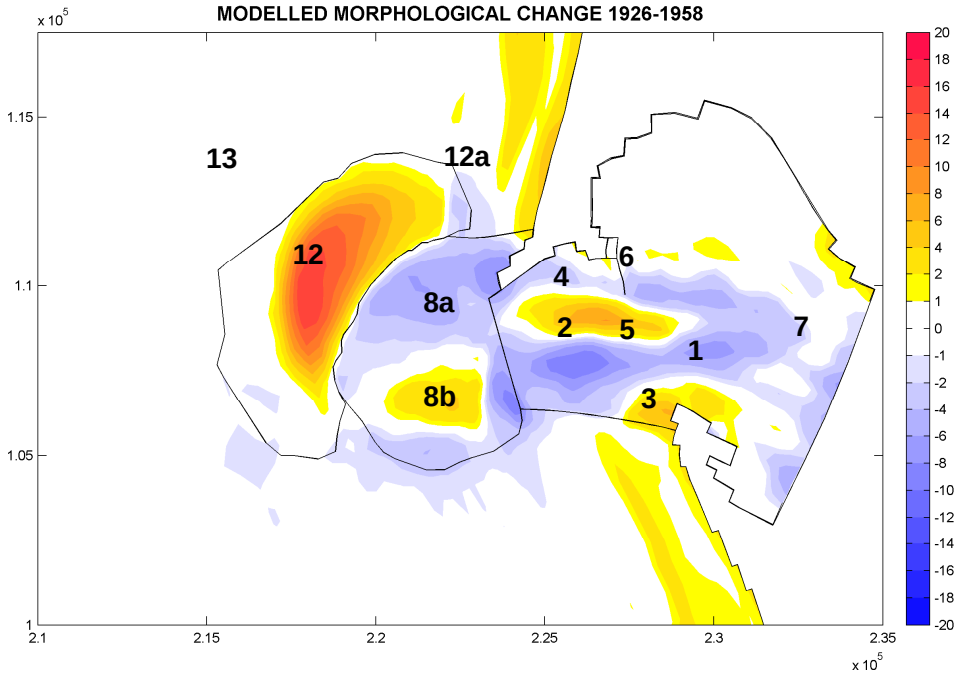

Figure 6.8 Modelled erosion-sedimentation patterns 1926-1958

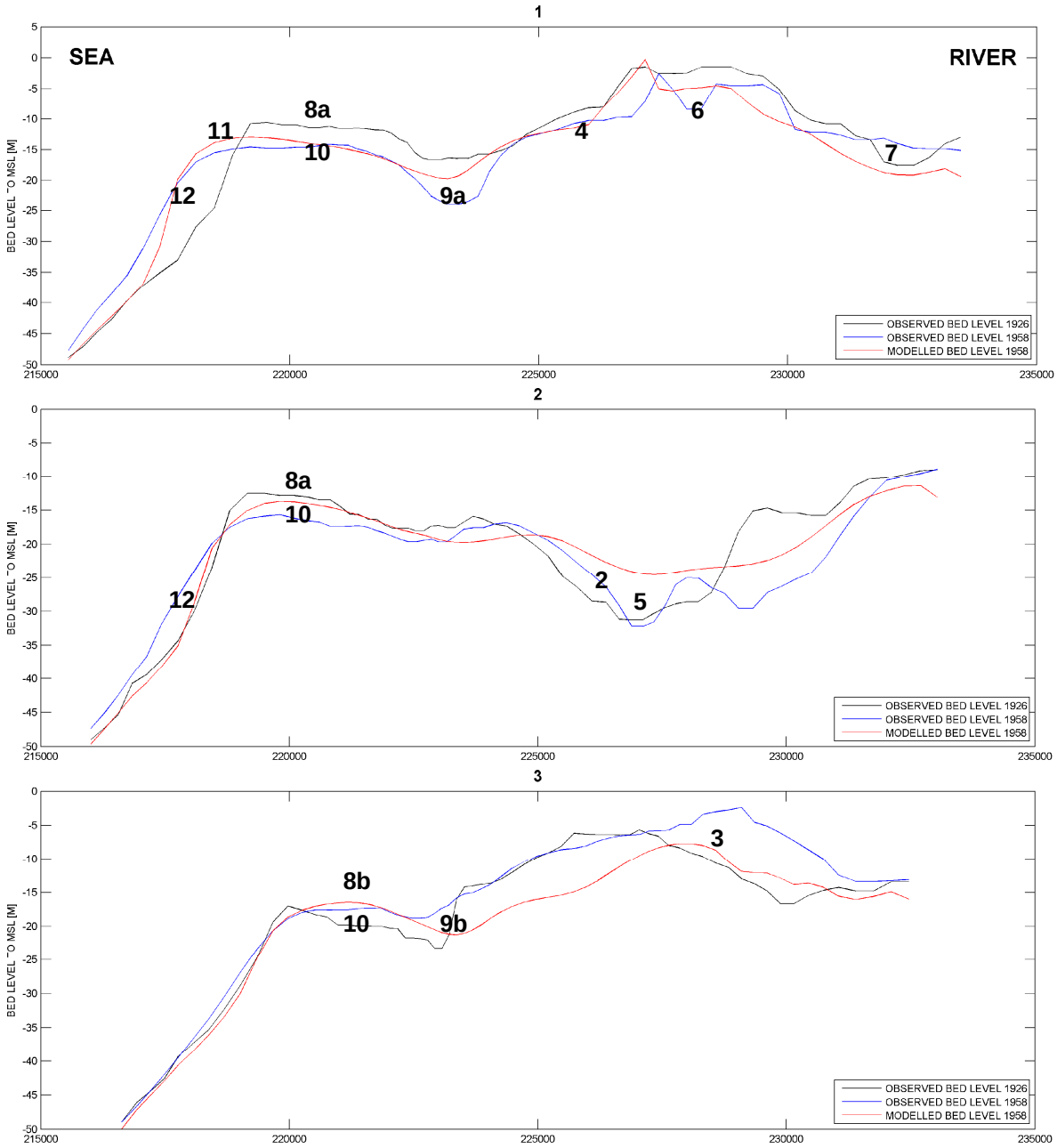

Figure 6.9 *Bed level cross-sections observed and modelled (x-direction).*

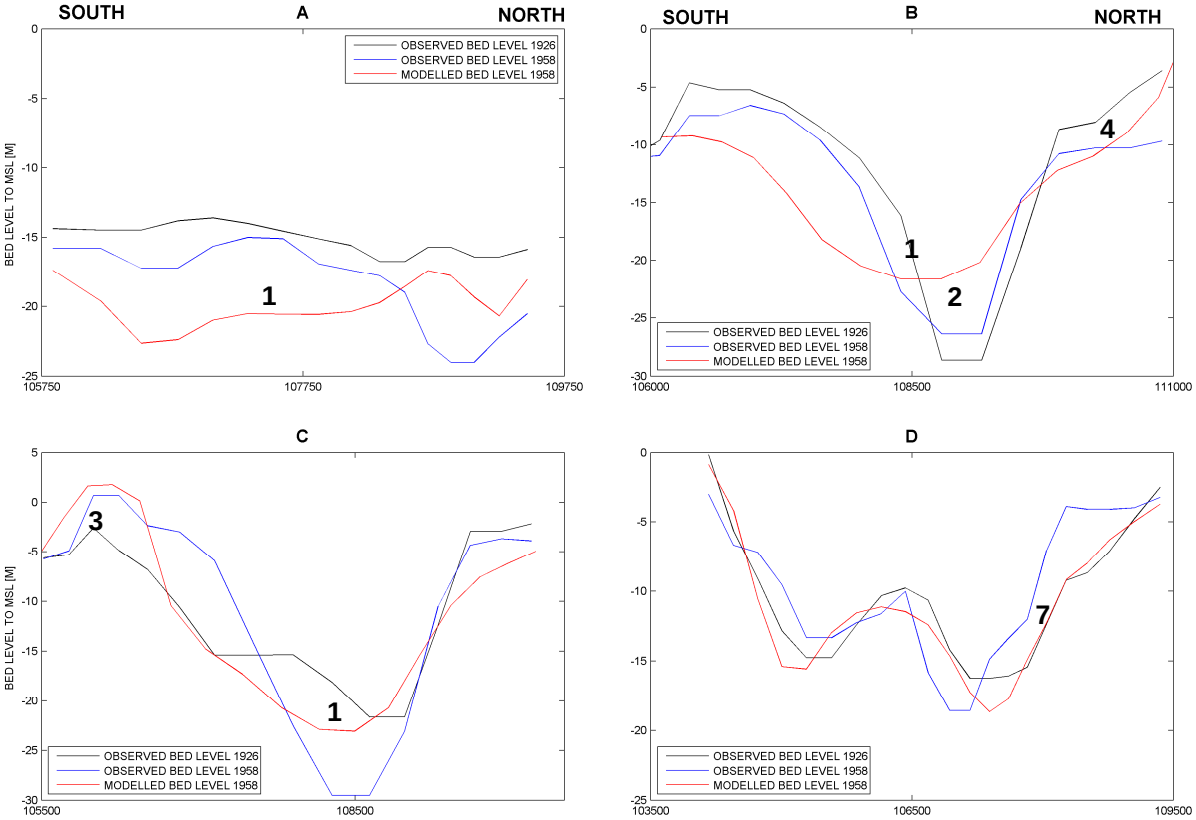

Figure 6.10 Bed level cross-sections observed and modelled (y- direction).

Modelled morphological changes 1926-1958

Inlet

In the readjustment of the morphology to the jetty construction the inlet eroded in which a fairly wide inlet channel developed in the model (1). Of which the general depth stays is not more than 25 meters. The channel development has a slight southern orientation with respect to the centre of the inlet. In the areas of reduced energy, adjacent to the channel local bulges of sediment accretion arose (2 and 3). Erosion is present along the inside of the North Jetty (4). A limited scour hole development is computed at (5). Also the development of the channel towards the Ilwaco marina and Baker Bay (6) is limited. The local deposition of sediment at (7) is not represented by the model.

Inner delta

A general computed erosional development of the inner delta is visible from (8a,b). While in the southern section a local accretion bulge arises (8b), the majority of the inner delta is dominated by erosion (8a). At the tips of the North and the South Jetty scour holes developed (9a,b). The majority of the inner delta developed into having a more or less uniform depth in the 16 to 20 meters region (10).

Outer delta

A distinctive northern-orientated outer delta is computed (11). At which directly at the northwest of the North Jetty a local relative deepening is present (11a). The rest of the outer delta has a more or less uniform bed level (11). The confined flow through the entrance allowed for the outer delta to develop further in off-shore direction (12). A limited northward transport of sediment from the outer delta to the adjacent shores is present in the model (12a). The off-shore deposition at (13) is not reproduced by the model.

Volumetric changes over time

Volumetric changes over time are also given in Figure 6.11 to allow for a more general quantitative analysis of the general morphological change of the model. From the rates of volumetric changes over time a judgement can also be made whether the morphology of the compartment is going towards an equilibrium or not. The subplots of Figure 6.11 show the volumetric change over time of the individual compartments, in which the black cross represent the total observed morphological change of the compartments, the red lines the computed development over time and the dashed lines the volumetric rates of change per 10 year section. Table 6.3 finally gives an overview of the total observed and computed morphological change of the compartments.

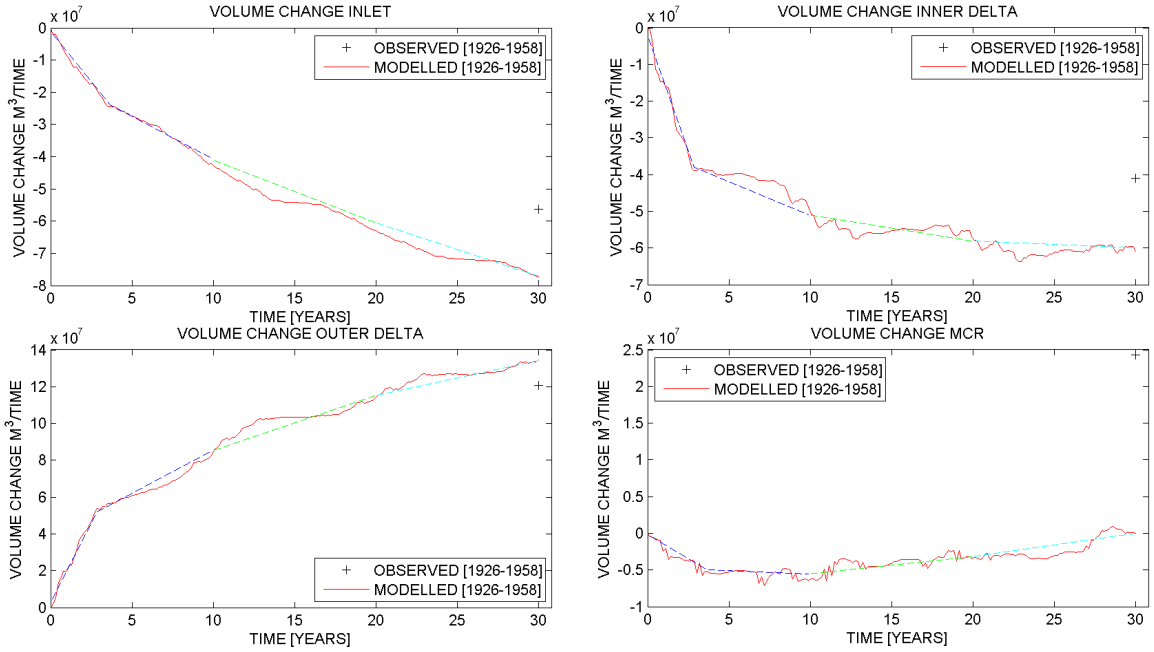

Figure 6.11 *Volumetric change over time, inlet (top left), inner delta (top right), outer delta (bottom left) and total (bottom right)*

Inlet

From the volumetric change of the inlet in the top left plot of Figure 6.11 it shows that in about the first three simulated years a strong initial response of the morphology of the inlet is computed. For the remainder of the first simulated 10 years, the morphological rate of change is strongly reduced. For the following two decades, the rate of morphological changes decreases further. However, from the fact that the morphological change rate has not yet approached zero, it can be said that no equilibrium in the morphological development of the inlet is reached in the simulation. The plot also makes clear that the total morphological change of the inlet compartment is overestimated by the model (Table 6.3). Even though strongly reduced sediment transport calibration factors (§5.4) are applied to the model.

Inner delta

From the volumetric change of the inner delta (top right subplot of Figure 6.11) also a strong initial response is present in about the first three years. The rate of morphological change reduces strongly for the following years in which the total morphological change seems to reach a more or less equilibrium state. The total modelled morphological change of the inner delta is however overestimated by about a 50% (Table 6.3).

Outer delta

The morphological change over time of the compartment of the outer delta (bottom left subplot of Figure 6.11) is also represented by a strong initial response in about the first three years and a decreasing morphological development rate over time for the following years. The compartment seems to go towards an equilibrium, however this will need some more time to fully develop. The total morphological change of the outer delta compartment is also overestimated by the model (Table 6.3) despite the reduced sediment transport calibration settings.

Total

The bottom right subplot of Figure 6.11 shows the computed total volumetric change over time for the three compartments combined in comparison to the observed total volumetric change. The observations show a small total overall sediment import of about 24 Mm^3. The computed total volumetric change of the three compartments combined is about 0 Mm^3. The difference is mainly attributed to the polygon over which the volumetric changes are calculated. E.g., in the observations, the polygon partly takes into account the offshore deposition of sediment northwest of the outer delta while in the computation this offshore deposition is not represented and therefore does not contribute to the total volumetric change. Furthermore, a possible inaccurate amount of erosion may have been taken into account in the polygon of the outer delta that decreased the overall accumulation of sediment in the outer delta.

Brier Skill Score

In order to make an objective assessment of the performance of morphodynamic models Sutherland et al (2004) suggest the use of the Brier Skill Score (BSS). For the MCR the BSS is defined as follows:

$$BSS = 1 - \frac{\left\langle (\Delta bed_{\mathrm{mod}} - \Delta bed_{meas})^2 \right\rangle}{\left\langle \Delta bed_{meas}{}^2 \right\rangle} \qquad (6.2)$$

In which:

Δbed_{mod} = *modelled bed level change compared to the initial bed [m^3]*

Δbed_{meas} = *measured bed level change compared to the initial bed [m^3]*

A BSS of 1 gives the perfect modelling result, whereas lower values suggest less adequate modelling. Van Rijn et al. (2003) further proposed a classification of BSS as follows:

Table 6.2 BSS classification

Model performance	BSS
Excellent	0.5-1.0
Good	0.2-0.5
Reasonable	0.1-0.2
Poor	0.0-0.1
Bad	<0.0

The bed level changes over time within the polygons of the inlet, the inner ebb-tidal delta and the outer ebb-tidal delta (Figure 6.11) are used for the assessment of the BSS.
Table 6.3 gives an overview of the total observed and modelled morphological change within the four polygons together with the classification of the Brier Skill Score.

Table 6.3 Quantitative comparison morphological changes 1926-1958 observed and modelled.

Compartment	Observed [Mm^3]	Modelled [Mm^3]	BSS
Inlet	-56.3	-77.2 +37.1%	-0.08
Inner Delta	-41.0	-60.8 +48.3%	0.24
Outer Delta	120.8	134.7 +11.5%	0.29
Total	24.3	0 -100%	0.13

From Table 6.3 it follows that according to the BSS the total morphological performance of the model is classified as reasonable. The morphological performance of the areas of the inner and outer delta are classified as good while the morphological change of the inlet is classified as bad.

6.1.5 Analysis

From the comparison of the model results with the observations, it follows that:

1 The general patterns of erosion and sedimentation and bed level change are represented fairly well by the model. Both the model and the observation show that jetty construction predominantly pushed sediments from the inlet and inner delta onto the outer delta.
2 Observed distinctive areas of sediment accumulation and erosion are simulated by the model. Example of which are, following the comparison of Figure 6.6 and Figure 6.8:
   - the development of the northern inlet bulge (2).
   - the development of the South Jetty inlet bulge (3).
   - the erosion along the inside of the North Jetty (4).
   - the erosional behaviour of the northern part of the inner delta (8a).
   - the accreted bulge of sediment in the southern part of the inner delta (8b).
   - the scour holes at the tips of the North and South Jetty (9).
   - the northern orientation of the outer ebb-tidal delta (11).
3 The offshore deposition (13) is not represented by the model.
4 The computed bed levels of the inlet channels are in the right order to the observed bed levels (Figure 6.9). However, a generally wider, shallower and more southern orientated inlet channel arises in the model (1, Figure 6.10).
5 Local deviations from the observed bed levels are present in the model. Examples of which are, following Figure 6.7, Figure 6.9 and Figure 6.10:
   - The local deepening at the computed outer delta north of the North Jetty (11a)
   - The limited representation of the local scour hole at the tip of Jetty A at (5).
   - The limited representation of the channel towards the Ilwaco Marina and Baker Bay (6).
   - The lack of representing the local accumulation of sediment in the upper part of the inlet at (7).
6 A limit representation of the northward littoral drift of sediment is present in the model.
7 Despite strongly reduced sediment transport calibration factors (§5.4), a general overestimation of the total morphological change is present (Table 6.3).
8 The overall morphological performance of the model is classified as reasonable according to the objective Brier Skill Score. In which the compartments of the inner and outer delta are classified as good and the compartment of the inlet is classified as bad.
9 The model underestimates the cumulative total amount of sediment supplied to the areas of interest (Figure 6.11). This could imply that sediment transports from the river and from both north and south of the MCR to the area under consideration are underestimated. However, from the comparison with the calibration runs of §5.5.1, in which a more accurate representation of the total volumetric change was reached, it shows that the areas over which the polygon of especially the inner delta and the outer delta extend are mainly responsible for the underestimation of the total volumetric change.

As a first approach in simulating the long-term morphological change of the complex and highly energetic area of the MCR, the model performs reasonably well. The general patterns of erosion and sedimentation as a result of jetty construction are represented by the model. The morphological model results are however still not perfect. Differences in both quantity and orientation are present between the observed and computed morphological changes. In which, a general overestimation of the morphological changes is present. The following paragraph continues discussing the observed differences of the model.

6.1.6 Discussion and conclusions

The model simulates the general observed bathymetry quite well. However, local bed level divergences, especially in the inlet compartment, the development of a less distinctive channel and an overestimation of the total morphological change are forthcomings of the model simulation.

The omission of pile dike structures (groynes) along the Sand Island of Baker Bay in the inlet and not taking into account the effect of dredging activities in the model are seen as important causes for some of the local divergences in the bed levels. The reason why the local pile dikes in the inlet are not taken into account is a result of the fact that they were not yet constructed until about halfway through the simulation period in 1939. Besides that, it was assumed that the morphological effect of these structures was limited in respect to the morphological effect of the entrance jetties and jetty A. The model however showed local bed level differences that are considered to be caused by the omission of the pile dike structures and dredging activities. The general considered effects of the omission the pile dikes structures at the Sand Islands and the dredging activities are:

- Together with the construction of Jetty A, the pile dike structures at the Sand Islands had an important influence in the final determination of the course of the flow. A northern orientated distinctive channel followed from this. Dredging activities on their hand maintained the channels in both location and depth. The omission of the pile dikes and the effect of dredging activities in the model led to a freer flow through the inlet and mouth, resulting in a wider, shallower and less northern orientated channel. Hereby effectively leading to local divergences of the bed. In general, a less erosional development in the northern part of the inlet and the mouth occur while a stronger erosional development occurred in the southern part.
- Jetty A, pile dike structures and dredging activities allowed for the development of a channel towards the marina of Ilwaco, Washington and Baker Bay.
- In the north-eastern section of the inlet (7, Figure 6.8.), the computed bed level is deeper than the observed bed level. This is contributed to the fact that there is less sediment accumulation due to the absence of the pile dike structures. The channel in the model is therefore capable of claiming this area as well.

In general, a wider, shallower and more southern orientated inlet channel arises in the model as a result of the omission of the pile dike structures and dredging activities in the model. Another possible explanation for the less pronounced channel formation might be the resolution of the grid cells in the inlet compartment in which only fourteen grid cells are applied to over span the inlet of three to four kilometres wide.

The total effect of the local bed level deviation and channel deviations on the morphodynamics at the mouth is however considered to be limited. The overall deviations in bed level as a result of the wider channel are the cause for the ‘bad’ BSS classification of the inlet compartment. The reduced erosion in the northern part of the inlet as a result of the widening and the increased erosion in the southern part of the inlet both contaminate the overall Brier Skill Score. It is therefore questionable whether a BSS assessment is the right method to objectively asses the morphological performance of the model in this particular case.

The schematization of the forcing conditions is seen as another cause for some of the computed deviations in morphodynamics. By schematizing the forcing conditions a reduced representative set of conditions is created, in which possible important conditions for the morphodynamics may have been cancelled out. The schematization of the wave climate for example resulted in wave heights not exceeding 5.5 meters while

observed wave heights can easily reach eight to ten meters and even more. The limited representation of these higher waves may for example to a limited extent bound the development of the outer delta. The area over which the area of the outer delta can spread out is hereby larger. The actual over development of the outer delta is however constrained in the model as a results of the application of the lower limit sediment transport calibration settings. Directly linked to the over development of the outer delta is a reduced supply of suspended sediment from the outer delta to the inner delta, leading to a possible overestimation of the erosion of the inner delta. Limited representation of high enough waves coming from a northern direction for example also limit the sediment supply to Clatsop Spit at the southern part of the inlet along the South Jetty as was found in §4.5.2. Especially from the vectoral comparison plot of the mean total transport for the full-set of conditions and the reduced set of conditions of Figure 6.2 the influence of the schematization of the forcing conditions is visible. Figure 6.2 shows the relative mean total transports that are not accounted for by the schematization. An apparent result from the unaccounted mean total transports shows from the differences in mean total transport, north-west of the North Jetty. The relative deepening of the outer delta in the model (11a, Figure 6.7) is seen to be caused by this.

Another forcing condition schematization related deviation of the model is the limited representation of the northward re-distribution of sediment by the littoral drift as a result of the limited extension of the area on which the *Opti-routine* focuses. *Opti-routine* was assigned to focus on the direct area of the mouth and to a limited extent on the adjacent shores (Figure 6.1). Hereby, possible only to a limited extent the forcing conditions responsible for northward transport are accounted for.

The lack of the representation of the offshore deposition as seen in Figure 6.8 is linked to be a possible cause of two process. First, the offshore deposition is possibly caused by a deposition from a plume of fine sediments released by the Columbia River as a result of the 1948 peak flow (Figure 1.8). The model does not represent either these fine sediments nor the peak flow. Another addressed possible cause for the offshore deposition may be a spring-tide enforced transport of sediments that deposited the sediment beyond the reach of the inlet circulation. In the schematization of the tide in the model, the spring-tidal effect is taken out of the simulation.

Even though the model represents the patterns of erosion and deposition fairly well, a significant deviation of the model is the general overestimation of the total morphological changes (Table 6.3). Despite several applied transport reducing settings, as the application of strongly reduced sediment transport calibration factors and a reduced morphological tide, the model still overestimates the observed morphological changes. This may imply that certain morphologically important physical processes may still be missing in the model. It is however also noted that, the overestimation of the outer delta is also directly linked to the overestimation of the compartments of the inlet and the inner delta and vice versa.

6.2 Period C 1958-1999

Following on the final simulation of the 1926-1958 period, in which the model proved to perform reasonably well, the model is validated in the simulation of the morphological changes of the period of 1958-1999. By doing so, more can be said about the general morphological performance of the model.

The continuing dam construction in the Columbia River basin in the 1958-1999 period however started to have a significant effect on the rivers hydrograph. Especially from 1973 on, river flow peaks eminently decreased. (Figure 1.8). In general, discharge peaks were reduced, discharge lows were increased and mean discharge values stayed more or less the same (Figure 6.12).

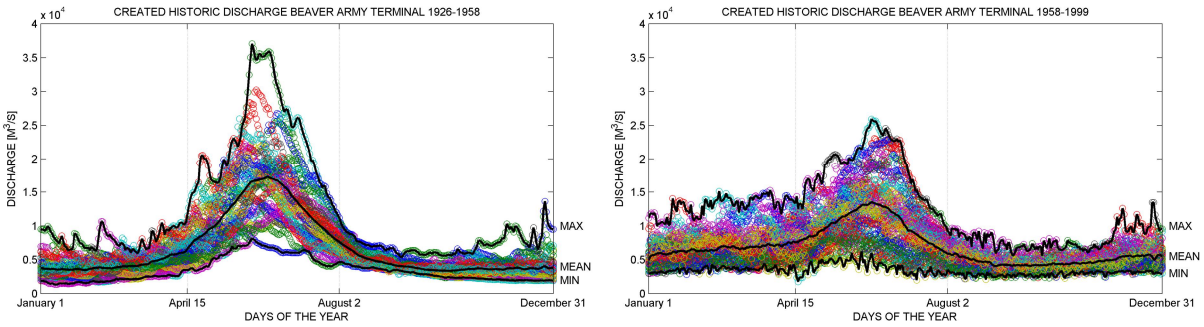

Figure 6.12 Comparison 1926-1958 discharge (right) and 1958-1999 discharge (left).

To somewhat account for the effect of dam construction on the river's hydrograph and not having to re-do the laborious and time consuming *Opti-routine,* a simple alternation of the derived probabilities of the river discharge and following wave conditions of the 1926-1958 climate was done. Unfortunately, this does not make up for the changed hydrograph in the most right order. It does however lead to a quick approach of the adjustments of the forcing conditions schematization to its respective simulation period. The procedure led to the following ten-year climate of the forcing conditions, in which reduced numbers are shown in red and increased numbers is green:

Table 6.4 Forcing conditions 1958-1999 period

Conditions	H_s [m]	T_p [s]	Dir [°]	V_{wind} [m/s]	Q [m^3/s]	P [-]	Duration [days/year]	No.# Mor.tides	MorFac [-]
1	5.50	5.50	202	12.54	3900	0.031	11.2	5	21.73
2	2.77	9.59	262	6.59	3900	0.048	17.6	4	42.46
3	5.18	11.86	270	7.90	3900	0.056	20.6	8	24.87
4	1.61	8.52	277	4.92	3900	0.476	173.8	20	83.98
5	4.05	10.95	287	6.57	3900	0.002	0.8	1	7.49
6	3.71	10.64	293	6.39	3900	0.027	9.8	3	31.46
7	2.29	8.71	308	5.66	3900	0.048	17.5	3	56.50
8	3.88	10.65	270	7.47	6000	0.020	7.5	2	36.09
9	2.03	8.42	260	5.70	7250	0.155	56.5	8	68.27
10	1.19	7.75	273	4.10	12500	0.080	29.1	3	93.61
11	2.99	9.60	273	5.86	12500	0.058	21.3	4	51.46
						1	**365**	**61**	

6.2.1 Observations

Limit bathymetric coverage

For the year 1999, limited bathymetric data is available of the MCR. The compartment of the inlet is almost entirely uncovered (2, Figure 6.13). The compartments of the inner and outer delta are fully covered by the data. It can however be stated that the adjustment of the morphology at MCR due to jetty construction continued in Period C. The inlet and inner delta continued to erode and the outer delta continued growing westward (Buijsman et al., 2003).

Dredging

In the 1958-1999 period dredging activities at the MCR became more and more significant. From around 1970 an average value of about 3.4 Mm^3 of sediment has been removed from the entrance channel per year. Figure 6.13 shows the locations of the dumpsites of the dredged material (1a-1e). Table 6.5 gives the total amounts of deposited sediment per dumpsite. In the model, dredging activities are not accounted for with the simulation being a simple first approach of simulating the continuing morphodynamic change. The local areas of sediment deposition will therefore not be represented by the model. Also the maintained alignment of the entrance channel as a result of the dredging activities will therefore probably only be represented to a limited extent.

Table 6.5 Deposition volumes

Area	Deposition [Mm^3]
1a	34.4
1b	7.2
1c	18.3
1d	43.5
1c	0.8

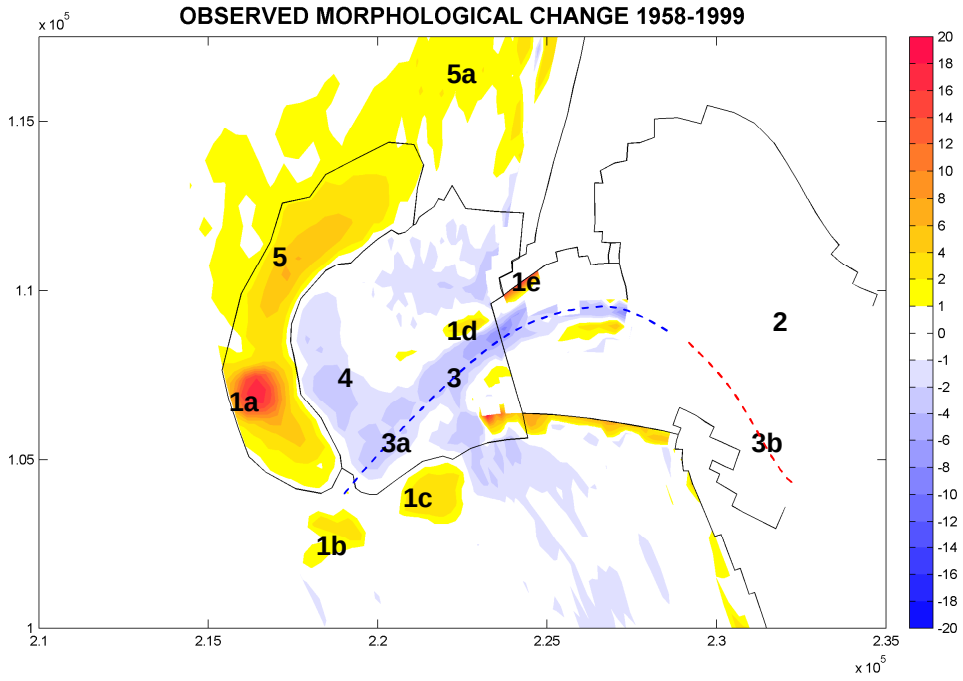

Figure 6.13 Observed morphological change 1958-1999

Observed morphological changes 1958-1999

Inlet
No bathymetric coverage is available for the majority of the inlet compartment (2). The alignment of the entrance channel is however visible (3).

Inner-delta
In the 1958-1999 period, erosion of the inner delta compartment continued (4). The significant volume of deposition (43.5Mm^3) in the northern part of the inner delta (1d) however limited the overall total erosion. Several deposition areas of dredged volumes are visible at 1c, 1d, and 1e.

Outer delta
Linked to the continuing erosion of the inner delta the development of the outer delta in north-western direction also continued (5). Sediments from the outer delta are subsequently re-distributed in northward direction by the littoral drift and herein supply the adjacent shore with sediment (5a).

Channel
By 1999, a distinct channel had developed across the entrance and inlet. Dredging activities maintained the alignment of the channel, which in seaward direction at first occupies the northern part of the inlet and as a result of the orientation of the outer delta turns in south-western direction at the mouth (3a). Present day bathymetric maps show that the channel at the uncovered inlet area, in landward direction also bends off towards the south (3b).

6.2.2 Model results versus observations

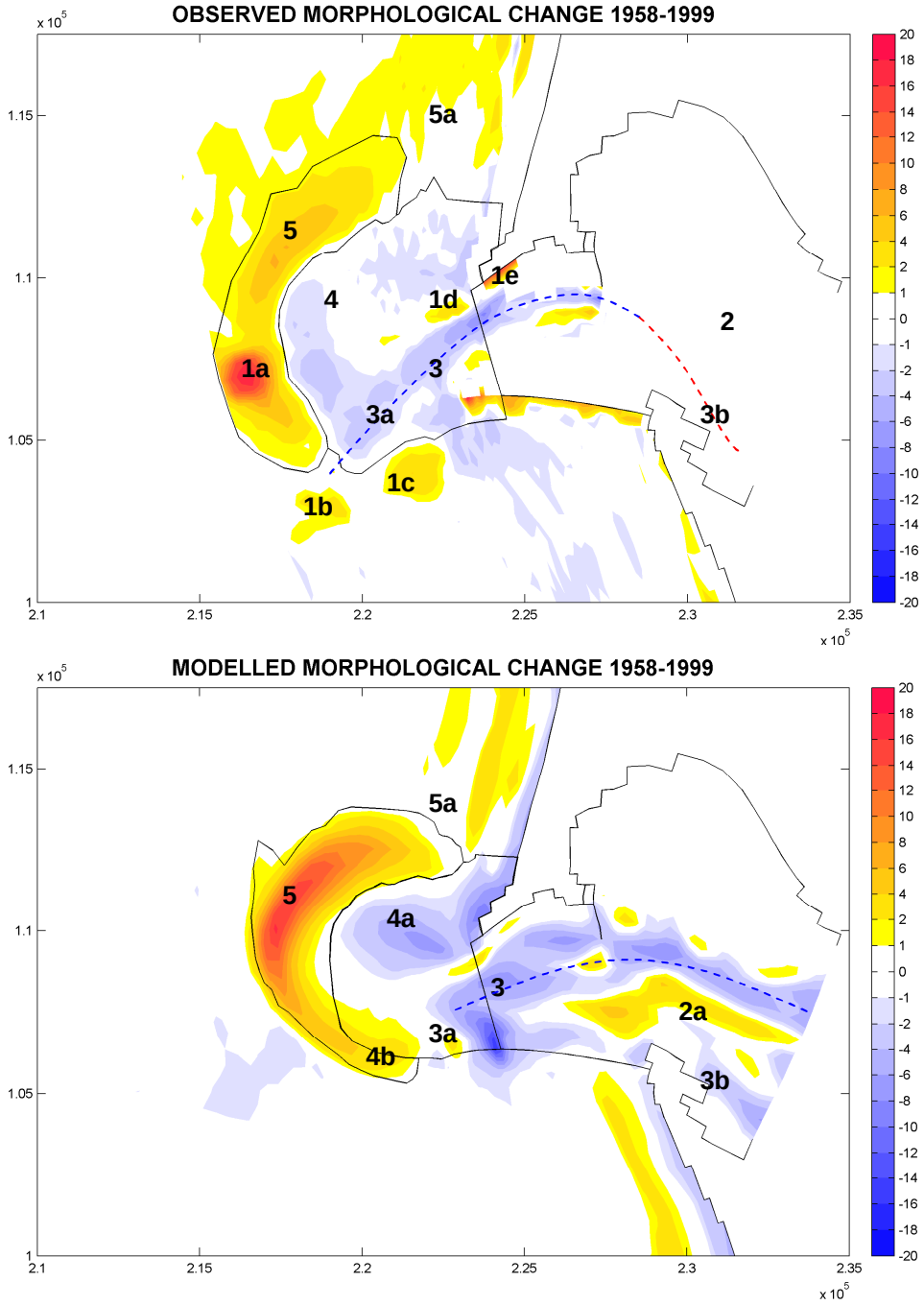

Figure 6.14 Observed and modelled morphological change 1958-1999

Modelled morphological changes 1926-1958

Inlet

An apparent continuing erosional development of the inlet is present in the model. The further development of the entrance channel in northern direction is apparent from the pattern of erosion and resulting channel alignment (3). Adjacent to which a local accumulation of sediment is present at (2a).

Inner-delta

In the modelled 1958-1999 period, general erosion of the inner delta compartment continued. Especially the northern part of the inner delta herein strongly continued to erode (4a) while in the southern section a local accretion of sediment was present that over time even connected (4b) to the outer delta (5). The overall erosion of the northern part of the inner delta in the observations was strongly reduced by a total deposition of dredged material of about 43.5 Mm^3. The southern part of the inner delta in the observation was artificially dredged and therefore did not develop in a local accumulation of sediment.

Outer delta

A strong continuing development of the outer delta is present in the model in north-western direction (5). The model however represents a limited distribution of sediment from the outer delta in northward direction to the adjacent shores (5a). Connection of the outer delta with the local accumulation of sediment in the southern part of the inner delta is visible at (4b).

Channel

A distinctive northern orientated single inlet channel arises in the model (3). In which a less pronounced bend towards the south at the landward side is present (3b). In seaward direction no distinct bend off towards the southwest is present (3a).

Volumetric changes over time

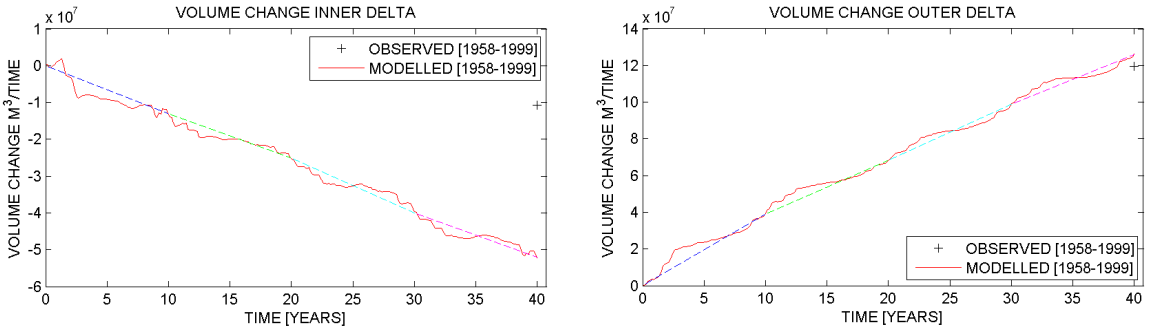

Figure 6.15 Volumetric change over time, inner delta (left), outer delta (right)

Inner delta

From Figure 6.15 it follows that the inner delta continues to erode. The model however strongly overestimates the total erosion (52 Mm^3 versus 11 Mm^3), despite the presence of a local accumulation of sediment in the model inner delta compartment. The difference in erosion can however for a large part be addressed to the omission of sediment deposition in the northern part of the inner delta. Without this deposition, the erosion of the inner delta in the observations would be 43.5 Mm^3 larger. From the volumetric change over time it can be stated that the adjustment of the morphology to the jetty construction has not yet reached an equilibrium by the end of the 1958-1999 period.

Outer delta

From Figure 6.15 it also follows that the development of the outer delta is overestimated. While the total volume change of the outer delta appears to be about the same in the model and the observations, it is noted that in the observations a sediment supply of about 34.4 Mm^3 to the outer delta compartment is incorporated in the total volume change and in the model this supply has not been accounted for. From the volumetric change over time it can also be stated that no morphological equilibrium has yet been reached in 1958-1999 period in the outer delta compartment.

6.2.3 Discussion and conclusions

Unfortunately, the performance of the model in simulating the morphological change of the interval of 1958-1999 is limited. Limited implementation of certain morphologically important aspect together with limited available data for comparison can be addressed as reasons for the limited performance. Limited bathymetric coverage of the 1999 bathymetry did not allow for an analysis of the morphological behaviour of the inlet compartment. Not taking into account dredging activities limited the overall morphological performance of the model. Sediment removal by entrance channel dredging and the re-deposition of dredged material in dumpsites within the area had a significant effect on the overall morphological change.

Significant dredging activities in which about 3.4 Mm^3 of sediment per year is removed from the channel strongly determined and maintained the alignment of the channel. An artificial channel developed in the south-western part of the inner delta (Figure 6.13). The northern part of the inner delta on the other hand accommodated the deposition of sediment from entrance channel dredging, in which from around 1970 about 43.5 Mm^3 of sediment has been deposited. The overall continuing erosion of the inner delta compartment has been artificially reduced by this vast amount of deposited sediment to the northern part of the compartment. The outer delta also harbours a dump site of dredged material. About 34.4 Mm^3 of sediment has been deposited here from around 1970 to present. The development of the outer delta has hereby artificially been increased. Dredging activities therefore strongly distorted the general morphological behaviour of the system.

Dredging processes were not taken into account in the simulation and as a result of this the morphological behaviour of the model strongly differs from the observed morphological behaviour. It can however be stated that the continuing erosion of the inner delta and the continuing development of the outer delta are simulated by the model. The erosion of the inner delta however has a stronger northern orientation in the model by the earlier addressed omission of entrance channel dredging and sediment deposition. The proclaimed general overestimation of the morphological changes in the model seems to still be present in the simulation of the 1958-1999 period. The limited representation of forcing conditions responsible for northward littoral drift also allows for the over-development of the outer delta.

In order for the model to perform better in simulating the observed morphological change of the 1958-1999 period, the overall morphology import dredging activities should therefore first be taken into account. This will not form part of this study, however it will form part of the recommendations.

6.3 Influence level of detail schematization forcing conditions

The complex and time-consuming process of schematizing the forcing conditions for the simulation of the long-term morphodynamics at the MCR and the morphological results from the calibration runs raised the question whether a lower level of detail in the schematizations of the forcing conditions could be used in the simulation of the morphodynamics of the MCR. The impact that the simulations of lower level of detail has on the total long-term morphological development should hereby be determined. To answer this question, the long-term morphological simulation of §6.1, in which a detailed schematization of forcing conditions is applied is compared to a simulation made up out of a simple schematization of the forcing conditions. In which the basic wave climate schematization of §3.3.6.1 and a constant mean river discharge are applied. Furthermore, both runs are implemented with earlier model settings in which no optimized morphological tide or fully developed bed are applied. A basic rather quick analysis of the influence of the level of detail of the schematization of the forcing conditions is made. The following page shows the model results of the 1999 bed levels and 1958-1999 erosion sedimentation patterns in comparison to the observations. In which *A* represents the detailed schematization of forcing conditions and *B* the basic schematization.

6.3.1 Results

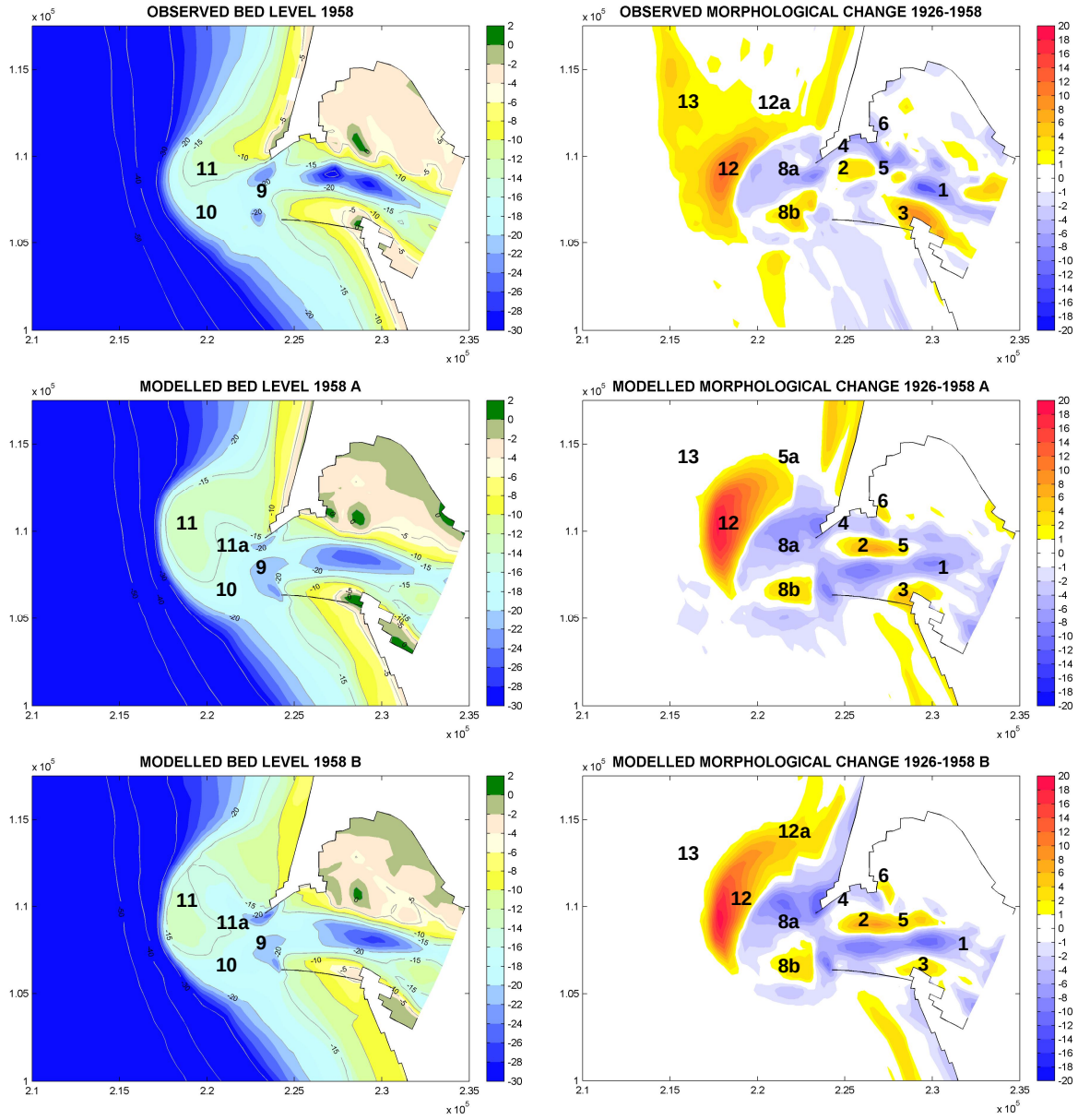

Figure 6.16 *Bed level and erosion/sedimentation patterns comparison of observed (top), high level of detail schematization A (middle), and low level of detail B (bottom).*

6.3.2 Analysis

What directly shows from Figure 6.16 is that the general patterns of morphological change as they were computed by the detailed schematization of forcing conditions (A) are also fairly well represented by the lower level of detail of schematization of the forcing conditions (B). The general development of the morphology resulting from the entrance jetty construction where sediments from the inlet and inner delta are pushed onto the outer delta is easily visible. Distinctive areas of sediment accumulation and deposition are herein just as well simulated by the lower level of detail in forcing conditions schematization. The development

of the northern inlet bulge (2), South Jetty inlet bulge (3), erosion along the inside of the North Jetty (4), the erosional behaviour of the northern part of the inner delta and the accretion of the southern part of the inner delta (8a/b), together with the scour holes at the tips of the North and South jetty (9), the northern orientation of the outer delta (11) and the general order of the bed level of the inner delta compartment (10) are all represented in about the same order. However, a more northern transport of sediment from the outer delta is computed in the simulation B (12a). Offshore deposition (13) was also not represented by the simulation B as a result of the previous addressed reasons (§6.1.6).

Volumetric changes over time

Volumetric changes over time are also given in Figure 6.17 to allow for a more quantitative comparison between the computed general morphological changes of the two levels of detail in the schematization of forcing conditions. Table 6.6 finally gives the relative quantitative volumetric difference between the two levels of detail in schematization.

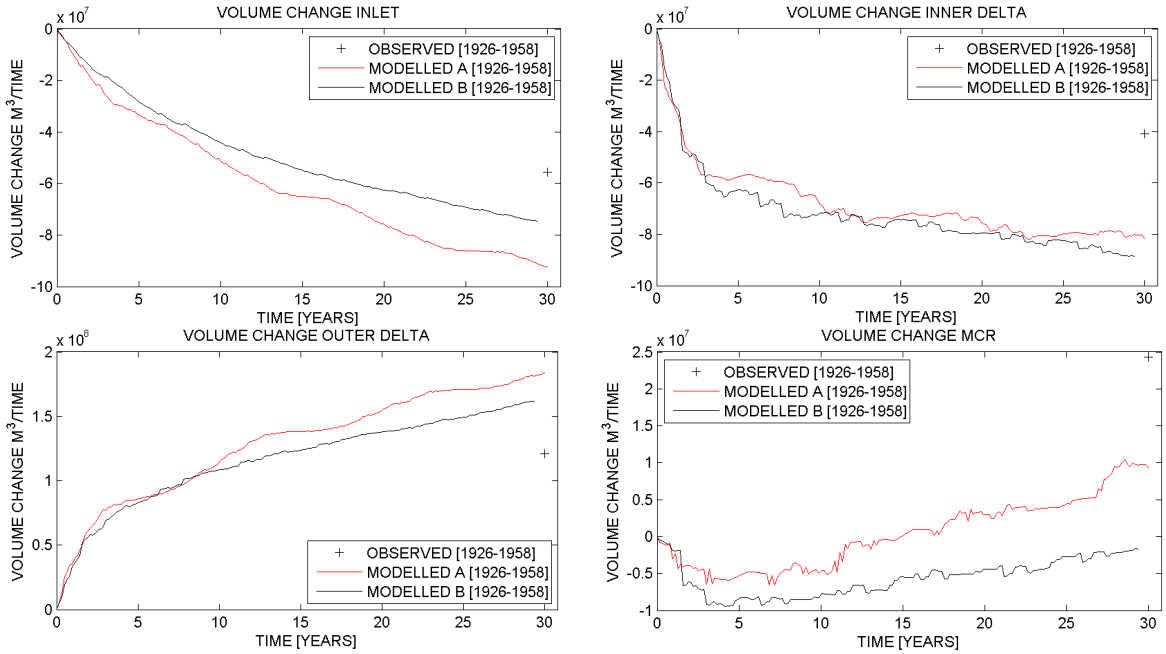

Figure 6.17 *Volumetric change over time comparison level of detail schematization of forcing conditions, inlet (top left), inner delta (top right), outer delta (bottom left) and total (bottom right).*

Inlet

From Figure 6.17 it follows that also quantitatively the morphological change of the inlet compartments is not much influenced by the level of detail of the schematization of the forcing conditions. A similar general development is present in the simulation B, in which the overall rate of morphological change decreases slightly stronger over time. The less variable forcing conditions as a constant river discharge may be the reason for this. §4.5.2.4 already showed that higher river discharge lead to larger sediment transports in the inner delta.

Inner delta

From Figure 6.17 it also follows that with respect to the inner delta compartment no significant difference in the volumetric change over time between the two levels of detail of the schematization of the forcing conditions is present. Both simulations result in a rather strong initial response of the morphology and over time the rate of morphological change decreases.

Outer delta

Inherently to the limited differences in the volumetric change over time of the inlet and inner delta compartments, the volumetric change over time of outer delta compartment for the two levels of detail of the schematization of the forcing conditions also does not differ all too much (Figure 6.17).

Total

In the summation of the three compartments, the differences in total morphological change between the two levels of detail in schematization of the forcing conditions start to show. A lower overall import of sediment to the three compartments is present in simulation B (Figure 6.17). Possible explanations for the import reduction may be the reduced supply of sediment form the river and estuary domain to the MCR as a result of the lower river discharge values but also the increased northward transport of sediment from the outer delta (12a, Figure 6.16). Another explanation may be the applied uniform polygon over which the volume change is calculated that may not take into account all the volumetric changes.

Table 6.6 Relative quantitative difference level of detail schematization of forcing conditions

Compartment	Observed [Mm^3]	Modelled A [Mm^3]	Modelled B [Mm^3]
Inlet	-55.6	-92.5	-74.6 -19.4%
Inner Delta	-41.0	-81.5	-88.6 +8.7%
Outer Delta	120.8	183.5	161.7 -11.9%

The maximum relative difference of the compartments of the inlet, the inner delta and the outer delta that shows from Table 6.6 is less than 20%. The relative difference for the three compartments combined is considered not to be right since the applied uniform polygon does not take into account all of the volumetric change for both of the simulations.

6.3.3 Discussion and conclusion

The application of a lower level of detail in the schematizations of the forcing conditions in the simulation of the long-term morphodynamics of the MCR, resulted in a more or less similar general morphological development as the higher level of detail of the schematization of the forcing conditions (lower than 20% differences). The application of a constant mean river discharge and a total of just eight wave conditions (four wave height classes and two mean directional classes) versus the application of a final of four different discharge classes and 11 wave conditions, varying in height and direction, of which the basis is a high resolution schematization of in total 788 conditions that takes into account the seasonal variations and joint-probability of discharges and waves, did not lead to significant long-term morphological differences.

From this result several conclusions can be drawn. The first one is that that the height of the river discharge on the morphological behaviour at the mouth seems to be limited. A constant mean river discharge versus a varying river discharge in which river discharge lows and peak are taken into account resulted in a similar morphological development. It must however be stated that, taking into account higher river discharge classes in the simulation might lead to a more significant effect of the river discharge on the morphology at the mouth. In the present situation, the chosen reduction of forcing conditions by the *Opti-routine* resulted

in a maximum river discharge of 12500 m^3/s while peak river discharges in the 1926-1958 period reached values of up to 35000 m^3/s.

In addition, the schematization of wave conditions of the two simulations did not lead to significant differences either, in both situation more or less the same wave height classes are also represented where wave height peaks are in the 5 to 6 meter range. A stronger northward directed transport of sediment is however present in the simulation of the lower level of detail in the schematization of the forcing conditions. This northward transport is also seen in the observations. The conclusion is drawn that even though wave conditions are more or less the same a slightly better representation of the waves responsible for northward transport is present in the lower level of detail of the schematization of the forcing conditions. Two single wave conditions is considered to be the reason for this deviation in northward littoral transport. In the high level of detail in schematization of the forcing conditions, a wave coming from the south of 5.5 meter in height is present while in the simulation of lower level of detail, a wave coming from the south of 6.10 meter in height is present. This height difference together with small directional differences is seen as an important possible cause.

The main driver of morphological changes therefore seems to be the tide. The confinement of the inlet as a result of jetty construction, increased the tidal currents through the mouth and resulted in a strong erosion of the inlet and inner delta compartments. The eroded sediment is stored in the outer delta and subsequently re-distributed to the adjacent shores by waves and currents.

From this all, it follows that a lower level of detail in the schematization of the forcing conditions is perfectly capable of representing the overall morphological change at the MCR. The dominance of the tide on the total morphological development seems to allows for a reduction of the level of detail in the schematization of the forcing conditions. However, an optimal representation of the forcing conditions should be found and taken into account to improve and optimize the morphological performance of the model.

7 Conclusion and recommendations

The main goal of this thesis was to develop a long-term morphological model and investigate methods and modelling approaches in simulating the complex morphodynamics of the Mouth of the Columbia River (MCR). The application of a process-based numerical model could provide a valuable insight in the understanding of the processes responsible for morphological change at the MCR. A better understanding of the morphodynamic behaviour could ultimately support predictive modelling, management of dredging strategies and coastal planning.

The primary task in long-term morphological modelling is the derivation of appropriate schematizations of forcing conditions. Especially in the complex and highly energetic area of the MCR this is a difficult task. Furthermore, input reduction and morphological acceleration techniques need to be applied to keep the simulations within practical time limits, in which the scale of interest of the model needs to be kept in mind. In the process of reaching the goal of developing a long-term morphological model specific objectives were set. The first paragraph of this chapter describes the conclusions of the study. The second paragraph discusses the model limitations and deficiencies. The chapter is concluded by giving several recommendations for model improvements and further research.

7.1 Conclusions

General conclusions

The main goal of this thesis was to develop a long-term morphological model and investigate methods and modelling approaches in simulating the complex morphodynamics of the Mouth of the Columbia River.

Highlighted summary

With this study, an important first step is taken in modelling the long-term morphodynamics of the MCR. A high-resolution schematization of the forcing conditions, in which the joint probability of occurrence of the river discharge and wave conditions is accounted for, forms the basis of the model. The general patterns of long-term morphological change are represented reasonably well by the model. Model results are however not yet perfect. Differences in both quantity and orientation are present between the observed and computed morphological changes. An important first step has however been taken in the goal of simulating the long-term morphological change of the complex coastal area of the MCR. The products of this study provide a valuable base for continuing research.

With this study, an important first step is taken in the goal of simulating the long-term morphological change of the complex and highly energetic coastal area of the Mouth of the Columbia River (MCR). The main focus was on simulating the morphological change for the interval of 1926-1958.

As a first approach in simulating the long-term morphodynamics for the MCR, the model is considered to perform reasonably well. The general patterns of erosion and sedimentation as a result of jetty construction are represented by the model. Both the model and observations show that jetty construction predominantly pushed sediments from the inlet and inner delta onto the outer delta.

The model is forced with a high-resolution schematization of the forcing conditions, in which the joint probability of river discharge and wave conditions is accounted for. The optimization/reduction process may however have cancelled out several forcing conditions important for long-term morphological development at the MCR. Optimization of the forcing conditions responsible for long-term morphological change at the MCR may therefore still be possible.

The model results are however not yet perfect. Differences in both quantity and orientation are present between the observed and computed morphological changes. In which, a general overestimation of the morphological change is computed. Furthermore, a general wider, shallower and more southern orientated inlet channel develops in the model. Relative large grid cell dimensions within the area of the inlet, as well as the omission of several small scale structures (groynes) and dredging activities are considered to be the reason for the less pronounced channel formation in the model. Considerable modelling efforts were however required to obtain the level of performance of the model and maintain the stability of the model.

A significant deviation of the model is the general overestimation of the total morphological changes. Despite the application of strongly reduced sediment transport calibration factors and a reduced morphological tide, the model still overestimates the observed morphological changes. This may imply that certain morphologically important physical processes may still be missing in the model. An inaccurate representation of forcing conditions as well as an inaccurate representation of other physical processes are examples.

Over time, anthropogenic influences as dredging activities and river damming that moderated the river's hydrograph and blocked sediment from reaching the mouth, started to have their influence on the overall morphological behaviour of the MCR. When modelling a particular era, the importance of these conditions on the overall morphodynamics should therefore be addressed and accounted for. The shift in dominance does not allow for an uniform approach for all time spans.

Even though model results in this study do not fully simulate the observed morphological changes of the MCR, it is felt that an important first step has been taken in the goal of simulating the long-term morphological change of the complex coastal area of the MCR. The products of this study will provide a valuable base for continuing research.

The individual objectives, model limitations, model deficiencies and areas for improvement, together with recommendations are addressed in the following sections.

Objective 1:

Verify appropriate schematizations of forcing processes responsible for long-term morphological change within the complex estuarine area of the MCR.

Highlighted summary

Basis for the model is a high-resolution schematization of the forcing conditions, in which the joint probability of occurrence of the river discharge and the wave conditions is accounted for. The main disadvantage of the applied method is the time-consuming nature.

From the model results, it followed that the applied schematizations of the forcing conditions (§3.3) performed reasonably well in simulating the observed morphological changes for the 1926-1958 period. A high-resolution schematization of the forcing conditions is taken into account in the schematization, in which the joint probability of river discharge and wave conditions is accounted for. The schematization however allows for further optimization. Both the area of interest as well as the representation of processes responsible for morphological change taken into account allow for optimization.

The main disadvantage of the applied method is the time-demanding nature. Every combination of forcing conditions (788 in total) needs to be simulated for the duration of a single morphological tide (1490 minutes). Having multiple computers at one's disposal for this vast amount of simulations (cluster) is therefore a must in the application of this method and not always self-evident.

Objective 2:

Model (hind cast) the long-term morphological changes at MCR with Delft3D and compare the observed and computed bathymetric changes for the interval of 1926-1958.

Highlighted summary

The model is considered to perform reasonably well in simulating the long-term morphological change for the interval of 1926-1958, however a general overestimation of the morphological change is present in the model together with the development of a general wider, shallower and more southern orientated inlet channel.

As a first approach, the model is considered to perform reasonably well in simulating the morphodynamic changes for the interval of 1926-1958. Despite some local deviations, distinctive areas of morphological change are represented fairly well by the model. Both the model and observations show that jetty construction predominantly pushed sediments from the inlet and inner delta onto the outer delta. The order of the bed level development is herein simulated particularly well. However, a general overestimation of the total morphological change is present in the model, despite the application of several sediment transport reducing calibration factors. This may imply that certain morphologically important physical processes are still missing in the model or are not sufficiently represented. Furthermore, a general wider, shallower and more southern orientated inlet channel develops in the model.

Objective 3:
Perform morphodynamic simulations for the interval of 1958-1999 and describe the overall performance of the model in the application of simulating long-term morphological changes.

Highlighted summary

The model showed to have a limited performance in simulating the observed morphological changes of the 1958-1999 period. Limited available data for comparison, insufficient representation of changed forcing conditions and not taking into account the significant morphological impact of dredging activities in the model are addressed as reasons for the limited performance. Validation of the model settings in the simulation of the morphology of the 1958-1999 period is in this phase of the model therefore not justified.

Limited performance of the model in simulating the morphological changes of the 1958-1999 period was reached. Incomplete bathymetric coverage of the area of interest, significant changing forcing conditions as regulated river flows by dam construction and not taking into account important dredging activities can be addressed as reasons for this overall limited performance. It can however be stated that the model is capable of simulating the continuing erosion of the inner delta and the continuing development of the outer delta. The model limitations that were addressed in the simulation of the 1926-1958, such as a general overestimation of the morphological change, local bed level deviations and limited representation of littoral drift are, as a result of the unchanged implementation of the model settings are still present in the simulation of the 1958-1999 period. Validation of the model settings in the simulation of the morphodynamic changes of the 1958-1999 period is therefore not justified. For the model to perform better, the overall morphological import dredging activities should therefore first be taken into account. Improving the other general model limitations will most probably further increase the performance of the model. More investigation is here for needed.

Objective 4:
Analyse the impact of different levels of detail in schematization of forcing processes on the long-term morphological development.

Highlighted summary

Jetty construction predominantly pushed sediment from the inlet and inner delta onto the outer delta. The dominance of the tidal flow in this morphological development allows for a certain reduction of the level of detail in schematization of the forcing conditions. However, for an accurate simulation of the total observed long-term morphological changes, an optimal representation of the forcing conditions should be accounted for.

From the comparison of the long-term morphological development of the MCR for two different levels of detail in schematization of river discharge and wave conditions, it showed that a lower level of detail in the schematization of the forcing conditions is to a certain level (less than 20% relative difference) capable of representing the general morphological change at the MCR (§6.3). The dominance of the tide on the total morphological development seems to allows for a reduction of the level of detail in the schematization of especially the river discharge and to a limited extent also the wave conditions. An optimal representation of the forcing conditions should however be found and taken into account to improve and optimize the morphological performance of the model. Sufficient representative forcing conditions responsible for the long-term morphological change at the MCR should be taken into account.

Objective 5:
Analysis of processes responsible for long-term morphological change at MCR. Give a detailed description of the system's behaviour.

The detailed interaction and quantitative influence of the processes responsible for the morphological change at the MCR are not fully understood nor proven. Chapter 4 handled a first analysis of processes responsible for long-term morphological change at the MCR. By looking at the relative influence of the variables of wave height, wave direction and river discharge on sediment transports an insight in the morphodynamic behaviour of these processes at the MCR is given together with the system's overall morphodynamic behaviour. The general findings with respect to the variables are:

Wave height
- Export through the mouth is generally larger for higher waves, however limited by wave breaking effects.
- Import at the mouth is only possible for high enough waves (H_s > 4 m), coming from a more southern direction (< 270 °).

Wave direction
- Import at the mouth is only possible for high enough waves (H_s > 4 m), coming from a more southern direction (< 270 °).
- Export through the mouth is generally the smallest for waves coming from a more southern direction. Export through the mouth is generally the largest for waves coming from a western direction.
- A strong littoral drift develops at the MCR for oblique incident waves of sufficient height.
- Waves coming from a more southern direction lead to a more exporting pattern of the ebb tidal delta of the MCR.
- Waves coming from a more northern direction lead to a more importing pattern of the ebb tidal delta of the MCR.

River discharge
- Influence of the river discharge on transports through the mouth is limited for discharges smaller than 12500 m^3/s.
- Export becomes larger when the river discharge becomes larger.
- The tide dominates the sediment transport through the mouth of the MCR for limited wave conditions and limited river discharges. For high enough river discharges (> 25000m^3/s), the tidal flow allows for the contribution of the river discharge to the transport through the mouth as a result of limited stratification at the mouth.
- A higher river discharge does not necessarily lead to sediment transport further offshore. It does lead to a larger northward-directed transport of sediment.

General findings
- Tidal flow is the most important process for morphological change as a result of jetty construction. The confinement of the entrance increased the tidal flow and had a strong and long-term effect on the morphology. The inlet and inner delta eroded and sediment accumulated in the outer delta.
- Waves are responsible for limiting the development of especially the outer delta and transporting sediment to the adjacent shores.
- The strong seasonality of the river discharge showed to have a limit effect on the morphological change.

Objective 6:
Describe methods used for long-term morphological modelling in this estuarine area of the MCR

The development of a (stable) model capable of simulating long-term morphological change in a highly dynamic delta area as the MCR showed to be a laborious and patience demanding task. This section summarizes the main methods applied that made the long-term morphological modelling possible. Methods, which hopefully benefit future modellers in the continuing research into long-term morphological modelling.

The main bottleneck in the process of long-term morphological modelling is the required computational time. In order to simulate the long-term morphological change at the MCR a number of input reduction and acceleration techniques therefore needed to be applied to keep the simulations within practical time limits. De Vriend et al. (2003) already addressed the importance of when attempting to model and hereby reduce the complexity of interaction of physical processes of a system, it is essential to keep in mind the scale of interest of the model. With respect to the MCR and this study, in which the long-term general morphological development of the MCR is desired to be modelled, a certain generalization of the forcing conditions was considered to suffice. The applied input reduction and acceleration techniques as applied in the model are summarized in the following section. Other case specific applied methods are also addressed.

Input reduction

Representative tide (§3.3.3)
Tidal input reduction replaces the complex time series of tidal water levels and current fluctuations with a simplified 'morphological' tide, under the condition that residual sediment transports of the representative tide most closely match the residual sediment transports for the entire spring-neap tidal cycle. This reduces the spring neap cycle to a single daily signal. The main advantage of which is that the application of the remaining forcing conditions subsequently can be applied to the model in a more uniform matter. The reduction of tidal components depends on the area being modelled. For the MCR model the created morphological tide consist out of two constituents, representing the dominant M_2 constituent and the interaction of the K_1 and O_1 constituents, which was found to be crucial for the residual transport pattern in the area of interest (Hoitink et al., 2003). For a simplified tide to create the same residual sediment transport as a full astronomic tide and herein preserve total tidal energy, an additional scaling factor should be applied to the tidal constituents of the morphological tide. The optimum scaling factor can be determined by trial and error of residual sediment transport between a morphological tide simulation and a full spring-neap astronomic simulation.

Morphological acceleration

(Variable) morphological scale factor (§3.3.8)
Morphological changes take place over much longer time periods than hydrodynamic changes. To overcome this problem a morphological acceleration factor (MorFac) is implemented in the Delft3D model. MorFac multiplies the sediment fluxes to and from the bed by a constant factor, thereby effectively extending the morphological development The application of MorFac implies that long term morphological simulations can be achieved using hydrodynamic simulations of only a fraction of the simulated duration.

The application of MorFac in combination with a morphological tide and the simulation of forcing conditions over full morphological tides strongly benefits the total

computation time of long-term morphological simulation. To account for the probability of occurrence of the wave and river discharge conditions considered, a variable MorFac is applied in the model. The hydrodynamic model is hereby run for the required number of morphological tides, one after another and a different offshore wave boundary and upriver river discharge and corresponding MorFac can be applied to each successive tide. The sequence of the wave classes follow the dominant order of the river discharge in which the seasonal distribution is accounted for.

Schematization forcing conditions

Classification river discharge (§3.3.5)
Elias and Gelfenbaum (2009) showed that sediment dynamics at the mouth are fully linked to the development of a salt wedge by tide-induced and density driven flows. Where dam construction in the Columbia River in the last century had a significant effect on the river flow by reducing discharge peaks and increasing discharge lows, mean river flows remained more or less the same (Figure 1.8). The historically different distribution of the river flow worked through in the development of the salt wedge and thus in the morphological development at the mouth. In simulating the historic morphological changes therefore also the historic river discharges should be taken into account. No historic river discharge is however available at the model's river boundary. An upriver station however does provide historic daily river discharges. To allow for this historic discharge data to be applied to the model's boundary a factor is applied to account for the contribution of downriver tributaries. The river discharge is subsequently simply distributed in several discharge classes according to their probability of occurrence. The classes at least represent a bin below the mean discharge, around the mean discharge, and an upper peak value discharge.

Equal energy distribution wave conditions (§3.3.6)
In the schematization of the wave climate, representative wave conditions are separated according to the concept of equal energy (Dobrochinski, 2009). Especially for morphological simulations this equal energy concept benefits the wave climate schematization. The influence of each wave conditions on the morphology is hereby considered to be more evenly distributed in comparison to the traditionally schematized wave climate. Wave conditions of relative low wave height carry limited energy and have generally limited influence on the morphodynamics. In the equal energy method more of the lower energy waves are combined to form a single wave condition of which the energy and morphodynamic influence is increased. The higher waves on the other hand that generally have a higher influence on the morphology are divided into more representative wave conditions. The wave climate coming from the equal energy distribution thus generally has a higher resolution of wave conditions with higher morphodynamic influence and a lower resolution of wave conditions with lower morphodynamic influence.

Model reduction

Domain decomposition (§3.3.1)
To speed up computations, domain decomposition has been applied by specifying three sub-domains: the sea-domain, the estuary-domain and the river-domain. Domain decomposition allows for parallel computation of each sub-domain. The computational time-consuming SWAN computations are solely applied to the sea-domain at hourly intervals.

Optimal grid cell sizes to solely represent processes of the scale of interest (§3.3.1)
Grid schematizations are a trade-off between the processes to be modelled and computational time. Grid cells should accurately represent the local hydrodynamic process and provide a sufficient description of the geometry to be modelled. As a result of this, the offshore grid cell sizes in the model reach values up to 3 kilometres while grid cell sizes at the mouth and in the estuary and river are about 250 meters in dimension. To accurately allow for the salt wedge to develop both the sea and estuary domain are resolved with nine vertical layers. The river domain consists out of a single vertical layer.

Case specific applied methods

Application of the joint probability of discharges and waves by splitting up the wave and river climate in distinctive seasons
Analysis of the wave and discharge data showed that both forcing conditions had a high alternating seasonal variability. The autumn/winter period is herein governed by high-energy wave conditions and lower river discharge conditions while in the spring/summer period it is the other way around with relatively low energy waves and high river flows. For a correct representation of the system's climate and with the alternating dominance having an import influence on sediment dynamics, the seasonal variation should be accounted for in the long-term morphodynamic simulation. The joint probability of discharges and waves is taken into account by separating both the river discharge and wave climate in two distinctive seasons. Combinations of forcing conditions for each season are hereby only taken into account in the analysis. By doing so, unrealistic combinations of forcing conditions as for example, extreme waves during peak river flows are taken out of the analysis and a better representation of the system's seasonal variation is accounted for.

Generic weighing and schematization of the forcing conditions by the application of the Opti-routine.
A Matlab based program developed by Deltares called *Opti* (Mol, 2007) is applied to reduce the vast amount of forcing conditions that followed from the schematization of the wave and river discharge climate and hereby reduce the computation time of the final long-term morphological simulations. The morphological simulation with the limited set of conditions should however lead to a similar outcome as the morphological simulation with the full set of conditions would. The vast amount of combinations of forcings conditions and also the joint probability of occurrence of waves and river discharge in the MCR made the application of *Opti* a necessity.

By applying the *Opti-routine*, the mean total transport pattern at the MCR for every occurring combination of wave conditions and river discharge times its probability of occurrence is summed to create a total mean transport pattern at the MCR for all the forcing conditions. The number of forcing conditions is subsequently reduced by dominance and the alternation of weight factors to create a sufficiently accurate reduced set of conditions with a similar total mean transport pattern. This procedure will cancel out forcing conditions relatively unimportant to the total morphological change. Either as a result of limited absolute morphological response of the condition or as a result of a probability of occurrence that is too

small to lead to high enough relative morphological change. The accuracy of the reduced set of conditions can be determined from the relative root-mean squared error. An optimal amount of conditions should however be found also taking into account computation time and a sufficient representation of both wave and river discharge conditions. The application of the *Opti-routine* led to a reduction of the in total 778 conditions to a representative set of just 11 conditions.

Bed schematization
No detailed distribution of sediment of the system was available. It was however known that the beaches and hereby the majority of the CRLC are primarily comprised of well-sorted medium to fine sand with an averaged grain-size of approximately 200 µm (Ruggiero et al., 2005). Fox et al. (1984) showed that coarse to medium sized sand (D_{50} > 200 µm) dominates the inlet and the estuary. The sediment distribution of the model was ultimately chosen to be implemented with two sediment fractions, one of 200 µm and a relatively coarse sediment fractions of 500 µm. The coarse sediment fraction of 500 µm will play an important part in limiting the overall morphological change (§3.3.9.1). A situation considered to be closest to reality, where a spatially distributed presence of the two sediment fractions is active is ultimately applied in the schematization of the bed. The spatial distribution of the sediment fractions is determined by the model and thus the system itself. A simulation implemented with a layered well-mixed bed of the two sediment fractions with the morphological updating scheme of the bed switched off forms a base run and will re-distribute the sediment fractions to ultimately form a new equilibrium. This internal re-distribution of sediments is subsequently applied as initial bed schematization. In reality, the system itself would also have determined an equilibrium spatial distribution of sediments at the bed.

Sediment transport calibration factors
User-specified scaling factors are available in the transport formulations of Delft3D to calibrate the sediment transports and resulting morphological development of the model. The calibration simulations showed a general overestimation of the total morphological change. To reduce the total morphological change and optimize the model in simulating the observed morphological changes lower limit transport calibration settings were applied in the final long-term simulations to reduce the total morphological change as much as possible and optimize the model in simulating the observed morphological changes. However, despite the application of the lower limit sediment transport calibration factors still an overestimation of the total observed morphological change was present in the model. This may imply that certain morphologically important physical processes may still be missing in the model.

7.2 Model limitations, deficiencies and improvements

This section discusses the limitations, deficiencies and areas for improvement of the model and should benefit future research into the area with respect to the model.

Overestimation general morphological development
One of the most import limitations of the model is the general overestimation of the morphological change. Despite the application of lower limit sediment transport calibration factors, a general overestimation of the total morphological change is still present. This may imply that certain morphologically important physical processes may still be missing in the model. Numerous amount of examples can be addressed for this, inaccurate representation of sediment characteristics, inaccurate schematization of forcing conditions (of especially the tide and waves), limited interaction with adjacent shores, taking into account dredging activities and small scale structures amongst many others.

Schematization of forcing conditions

In the schematization of the forcing conditions, the final amount of forcing conditions supplied to the model is reduced from almost 800 to just 11. In this reduction certain morphological important forcing conditions may have been cancelled out. For example, forcing conditions responsible for northward transport of sediment or particular wave conditions that limit the outer delta development, to name a few. The focus area of the applied *Opti-routine* herein also has a limited coverage. It focuses directly on the mouth and only to a limited extent on the adjacent shore. The Opti-routine also has a danger of cancelling out peak conditions with a low probability of occurrence. The relative effect on the mean total transport patterns is limited of these conditions. However, they could have certain morphological important influences. Optimization of the schematization of forcing conditions in better capturing all of the processes relevant to long-term morphological change at the MCR and adjacent shores is therefore possible.

Interaction with adjacent shores

The analysis of the simulations for both the 1926-1958 period and the 1958-1999 period showed that the model had a limited interaction of the MCR with the adjacent shores. The previous addressed focus area of the *Opti-routine* is addressed as possible reason for this. Furthermore, grid sizes dimensions are not designed to accurately represent shoreline evolution. Model improvements may be gained in this area.

Channel representation

A limited representation of the main inlet channel, in both location and size is represented by the model. A generally wider, shallower and more southern orientated channel was computed. The omission of several small scale structures in the inlet area (groynes) and not taking into account dredging activities may be play a role. The other cause may be that the resolution of the grid cells at the inlet is too large for accurate channel representation. The effect on absolute morphological change at the mouth is however uncertain and possibly limited. However, it might be an area of improvement.

Morphological tide

A rather quick and straightforward schematization of the tide is applied in the study. An adoption of the work done by Lesser (2003) for the neighbouring estuary is applied to which a simple calibration is applied to optimize the performance (5.5.2). The factor to be applied depends on the mean residual flow. A pragmatic method to determine an optimum amplification factor is determinable through trial and error. For this study, the application of no scaling factor (f_1=1.0) showed to have a more desirable effect in the total morphological changes than the application of an amplification factor of 1.08. An important note in this is that from the dependence of the scaling factor to the residual mean flow, it follows that an optimal scaling factor might possibly not be constant but should be river discharge determined and hence vary over time. Also, especially in the application of a morphological tide in the case of an estuary, further investigation with respect to the justification of this application is needed. The river flow schematization according to the morphological tide method is namely not mathematically proven. Higher order components may have a significant effect on the tidal flow at the river boundary.

Sediment supply

In the model no additional sediment concentration is applied to the river inflow. The supply of sediment to the model from the river is determined as an equilibrium concentration from the point of inflow. The effect of this omission is uncertain.

Wind

Wind is applied as a time-varying, spatially uniform shear stress. Wind data resulted from the measurements at the offshore buoy 46029 and herein directly followed the wave conditions. The spatially uniform application may have unrealistic effects on the morphology, though this effect is thought to be small. Also the equal energy method in which the wave and wind conditions of the forcing climate were determined led to mean wind speed values flowing the wave conditions. A large standard deviation from these mean values makes the justification of this application uncertain.

Dredging activities

A significant influence on the morphology at the MCR showed to be the dredging activities in which large amounts of sediment are removed from the area. Particularly in the simulation of the 1958-1999 period the effect of the omission of these dredging activities became to dominant. Therefore, in the simulation of the post-jetty conditions dredging activities should be accounted for.

Boundary problems

A deficiency of the model arose in the representation of the flow velocities at the boundary, resulting in large flow velocities at the boundary. No solution has really been found to this problem. Effects at the MCR and on the wave field were limited and therefore the deficiency was taken for granted. The representation of the tidal amplitude and/or phases may play a role. Further investigation is needed. Switching the Thatcher-Harleman time lags to negative values to a limited extent solved the problem. However, on the long-term this led to salinity problems, in which an overall decrease of the salinity occurred. The influence of the salinity decrease has stronger effects on the morphology at the mouth and therefore this ‘solution’ has not been applied in the final runs.

Salt wedge development

Tide-induced and density driven flows are important for the generation of residual flows and sediment transports at the MCR. Elias and Gelfenbaum (2009) showed that sediment dynamics at the mouth are herein fully linked to the salt wedge. The development of the salt wedge is strongly influenced by the river discharge. The river discharge is however applied at the upriver boundary and alteration of the river discharge takes time to have its effect at the mouth. Therefore, in the transition between discharge classes an extra time period with the length of one morphological tide is implemented to give the salt wedge some extra time to develop. The applied transition period between discharge classes of one morphological tide may possibly be extended and optimized to improve its representation.

7.3 Recommendations

To improve the performance of the model the following recommendations are given:

1 Further analyse the schematization of forcing conditions in capturing the processes relevant for long-term morphological change at the MCR and adjacent shores
With the model not capturing the morphological change to its full extent, optimization of the forcing conditions responsible for morphological change may be possible. The final reduced set of forcing conditions (11 conditions) may not sufficiently represent all of the processes relevant for long-term morphological change at the MCR. Certain low-probability, high-energy conditions may have been cancelled out by the applied Opti-routine as well as forcing conditions responsible for alongshore sediment transport. Optimization may lead to better model results.

2 Look into the interaction of the mouth with the adjacent coast
The interaction of the model with the adjacent coast seems to be limited. Forcing conditions responsible for sediment transport to the adjacent shores are represented to a limited extent only. The limited area taken into account in the Opti-routine (Figure 6.1) may be an import reason for this. An addition of sediment transport through a transect in the Opti-analysis may also benefit the problem.

3 Study the effect of inlet structures, grid cell dimensions at the inlet area and dredging activities
Local bed level differences may be caused by the omission of the several small scale pile dike structures (groynes) along the Sand Island of Baker Bay in the inlet, not taking into account dredging activities and the resolution of the grid cells in the inlet compartment. As a result of this, a general wider, shallower and more southern orientated inlet channel arises in the model as a result of this. The effect of the inlet structures, grid cell dimensions and dredging activities on the morphology should be looked at.

4 Take into account dredging processes in more-present day modelling
Maintenance dredging of the entrance channels began already in 1903. At that time however, the amount of dredged volumes in comparison to the overall morphological change was limited. From around 1970, dredging activities began to play a significant role in the morphological behaviour of the area. Dredging activities should therefore be taken into account in more present day modelling.

5 Further look into the application of a morphological tide in an estuary
A rather quick and straightforward schematization of the tide is applied in the study. A direct adoption of the work done by Lesser (2003) for the neighbouring estuary is applied to which a simple calibration with a constant scaling factor is applied to optimize the performance. An optimal scaling factor might possibly not be constant but should be river discharge determined and hence vary over time. Higher order components may also have a significant effect on the tidal flow at the river boundary.

6 Take the model towards predictive modelling
Ultimately, the model should be taken towards more present-day modelling and predictive modelling. A more accurate model may support management dredging and coastal planning.

References

d'Angremond, K., Pluim-Van der Velden, E.T.J.M., 2001, Introduction to Coastal Engineering. *Lecture notes CT 4300, Delft University of Technology*

Bottom, D. L., C. A. Simenstad, J. Burke, A. M. Baptista, D. A. Jay, K. K. Jones, E. Casillas, and M. H. Schiewe (2005), Salmon at river's end: The role of the estuary in the decline and recovery of Columbia River salmon. *NOAA Tech. Memo., NMFS-NWFSC-68, U.S. Deptartment of Commerce.*

Booij, N., Ris, R.C. and Holthuijsen, L.H., 1999. A third-generation wave model for coastal regions. Part 1: Model description and validation. *Journal of Geophysical Research, 104(C4), 7649–7666.*

Buijsman, M.C., Sherwood, C.R., Gibbs, A.E., Gelfenbaum, G., Kaminsky, G.M., Ruggiero, P., Franklin, J., 2003b. Regional sediment budget of the Columbia River littoral cell, U.S.A.. United *States Geological Survey, Open-File Report 02-281.*

Deltares, 2010a. Delft3D-Flow User Manual. Version 3.14 Revision 11214, Delft.

Deltares, 2010b. Delft3D-Wave User Manual. Version 3.04 Revision 11114, Delft.

Dobrochinski, J.P.H., 2009. Wave climate reduction and schematization for morphological modeling. MSc thesis, Universidade do Vale do Itajaí & Delft University of Technology, Delft.

Elias, E., Gelfenbaum, G., 2009. Modeling processes controlling sediment transport at the mouth of the Columbia River. *Proceedings of Coastal Dynamics 2009, pp 1-14.*

Fox, D.S., Bell, S., Nehlsen, W., Damron, J., 1984. Atlas of Physics and Biological Characteristics. *Columbia River Estuary Data Development Program.*

Gelfenbaum, G., Sherwood, C.R., Peterson, C.D., Kaminsky, G.M., Buijsman, M.C., Twichell, D.C., Ruggiero, P., Gibbs, A.E., Reed, C., 1999. The Columbia River littoral cell: a sediment budget overview. *Proceedings of Coastal Sediments '99. ASCE, pp 1660-1675.*

Gelfenbaum, G., Buijsman, M.C., Sherwood, C.R., Moritz, H.R., Gibbs, A.E., 2001. Coastal evolution and sediment budget at the mouth of the Columbia River, USA. *Proceedings of the Conference* American Society of Civil Engineers, Coastal Dynamics, 2001, Lund, Sweden, *pp. 818-827.*

Gelfenbaum, G., Roelvink, J.A., Meijs, M., Buijsman, M.C., Ruggiero, P., 2003. Process-based morphological modelling of Grays Harbor inlet at decadal timescales. *Proceedings of Coastal Sediments '03.*

Gelfenbaum, G., Kaminsky, G.M., 2010. Large-scale coastal change in the Columbia River littoral cell: An overview. *Marine Geology, pp 273, 1-10.*

Grunnet, N.M., Walstra, D.J.R., Ruessink, B.G., 2004. Process-based modelling of a shoreface nourishment. *Coastal Engineering, Vol 51, pp 581-607.*

Hoitink, A.J.F., Hoekstra, P., van Maren, D.S., 2003. Flow asymmetry associated with astronomical tides: Implications for the residual transport of sediment. *J. Geophysical Research, 108(C10), 3315.*

Jay, D.A., 1984. Circulatory processes in the Columbia River Estuary. *Columbia River Estuary Data Development Program.*

Jay, D.A., Giese, B.S., Sherwood, C.R., 1990. Energetics and sedimentary processes in the Columbia River Estuary. *Progress in Oceanography 25 (1/4), pp 157-174.*

Kaminsky, G.M., Ruggiero, P., Gelfenbaum, G., 1997. Long-term coastal evolution and regional dynamics of US Pacific Northwest littoral cell. *Proceedings of Coastal Dynamics '97. ASCE, pp 614-623.*

Kammerer, J.C., 1990. Largest rivers in the United States. *Water fact sheet, United States Geological Survey, Open-File Report pp 87-242.*

Latteux, B., 1995. Techniques for long-term morphological simulations under tidal action. *Marine Geology 126, pp 129-141.*

Lesser, G.R., Roelvink, J.A., van Kester, J.A.T.M. and Stelling, G.S., 2004. Development and validation of a three-dimensional morphological model. *Coastal Engineering, 51(8-9), 883-915.*

Lesser, G.R., 2009. An approach to medium-term coastal morphological modelling. PhD thesis, UNESCO-IHE & Delft University of Technology, Delft. *CRC Press/Balkema. ISBN 978-0-415-55668-2.*

Mol, A.C.S., 2007. Reduction of Boundary Conditions with Opti H4959.10. *Deltares*

Pawlowicz, P., Beardsley, B., Lentz, S., 2002. Classical tidal harmonic analysis including error estimates in MATLAB using T TIDE. *Computers & Geosciences 28 pp. 929-937.*

Reniers, A.K,H.M., Roelvink, J.A., Thornton, E.B., 2004. Morphodynamic modelling of an embayed beach under wave group forcing. *Journal of Geophysical Research 109 (C01030).*

Rijn, van L.C., 2004. Description of TRANSPOR2004 and Implementation in Delft3D-ONLINE Z3748.00. *Deltares*

Rijn, van L.C., Walstra, D.J.R., Grasmeijer, B., Sutherland, J., Pan, S., Sierra, J.P., 2003. The predictability of cross-shore bed evolution of sandy beaches at the time scale of storms and seasons using process-based profile models. *Coastal Engineering 47, pp 295– 327.*

Roelvink, J.A., Walstra, D.J.R., 2004. Keeping it simple by using complex models. *6th International Conference on Hydroscience and Engineering, Advances in Hydro-Science and Engineering, Brisbane, Australia.*

Roelvink, J.A., 2006. Coastal morphodynamic evolution techniques. *Coastal Engineering, 53(2-3), 277-287.*

Ruggiero, P., Kaminsky, G.M., Gelfenbaum, G., Voigt, B., 2005. Seasonal to Interannual Morphodynamics along a High-Energy Dissipative Littoral Cell. Journal of *Coastal Research, 21(3), 553-578.*

Sherwood, C.R., Jay, D.A., Harvey, R.B., Hamilton, P., Simenstad, C.A., 1990. Historical changes in the Columbia River Estuary. *Progress in Oceanography 25 (1/4), pp 299-352.*

Sherwood, C.R., Creager, J.S., 1990. Sedimentary geology of the Columbia River Estuary. *Progress in Oceanography 25 (1/4), pp 15-79.*

Sutherland, J., Peet, A.H., and Soulsby R.L., 2004, Evaluating the performance of morphological models. *Coastal Engineering*, *51 (8-9), pp 917-937.*

Vriend, de H.J., Zyserman, J., Nicholson, J., Roelvink, J.A., Pechon, P., and Southgate, H.N., 1993, Medium-term 2DH coastal area modelling. *Coastal Engineering*, *21 (1-3), pp 193-224.*

Appendices

Appendix A Delft3D Model settings

The following Delft3D Model settings are applied to the main simulation of §6.1, where the 1926-1958 morphological changes are simulated.

Table A.1 Delft3D-MDF setting sea.mdf

Data group	Parameter	Description	Value
Domain	*Grid parameters*	*Grid*	sea.grd
		Enclosure	sea.enc
		Grid points-M	89
		Grid points-N	78
		Latitude	46.25 [°]
		Orientation	0
		Layers	9 (2,5,10,22,22,22,10,5,2)
	Bathymetry	*File*	sea.dep
	Dry Points	*n.a.*	
	Thin dams	*File*	sea.thd
Time Frame		*Reference date*	25 09 1997
		Simulation start time	26 09 2001
		Simulation stop time	11 04 2002
		Time step	1 [min]
		Local time zone	0 (+GMT)
Processes	*Salinity*		
	Sediments		
	Wind		
	Wave		
	Online Delft3D-WAVE		
Initial conditions		*File*	tri-rst.rsea.3900
Boundaries	*North*	*M1*	2
		M2	59
		N1	78
		N2	78
		Type	Neumann
		Forcing	Harmonic
		Thatcher-Harleman	Surface 1490
			Bottom 1490
	Sea	*M1*	1
		M2	1
		N1	2
		N2	77
		Type	Water level
		Reflection parameter	100 [s2]
		Forcing	Harmonic
		Thatcher-Harleman	Surface 1490 [min]
			Bottom 1490 [min]

	South	*M1*	2
		M2	83
		N1	1
		N2	1
		Type	Neumann
		Forcing	Harmonic
		Thatcher-Harleman	Surface 1490
			Bottom 1490
Physical parameters	*Constants*		
	Hydrodynamic	*Gravity*	9.81 [m/s^2]
		Water density	1025 [kg/m^3]
		Air density	1 [kg/m^3]
		Temperature	15 [°C]
	Wind drag coefficients	*First breakpoint*	0.0025 [-] 0 [m]
		Second breakpoint	0.0289 [-] 100 [m]
	Roughness	*Chezy (Uniform)*	U = 65 V= 65
		Stress formulation	Van Rijn 2004
		Wall roughness	Free
Viscosity	*Background*	*Hor. eddy viscosity*	1 [m^2/s]
		Hor. eddy diffusivity	1 [m^2/s]
		Vert. eddy viscosity	9.9999997e-5 [m^2/s]
		Vert. eddy diffusivity	9.9999997e-5 [m^2/s]
		Model 3D turbulence	k-Epsilon
Sediment		*File*	sea.sed
Morphology		*File*	sea.mor
Wind	*Uniform*	*File*	sea.wnd
		Interpolation	linear
Numerical parameters	*Drying and flooding*		Centres and faces
	Depth specified at		Grid cell corners
	Depth at centre		Max
	Depth at faces		Mor
	Threshold depth		0.1 [-]
	Marginal depth		-999 [-]
	Smoothing time		0 [-]
	Advection scheme	*Momentum*	cyclic
		Transport	cyclic
	Forester filter	*Horizontal*	True
		Vertical	False
	Correction for sigma		True
Additional parameters	*Cstbnd*		#YES#
	BarocP		#N#
	TraFrm		#vrijn04.frm#
	Gammax		0.55 [-]
	ubcom		#yes#
Output	*Storage*	*Map results start*	26 09 2001
		Map results stop	11 04 2002
		Interval	1505 [min]
		History interval	10 [min]
		Map results start	26 09 2001

		Map results stop	11 04 2002
		Interval	60 [min]
		Restart interval	14900 [min]

Table A.2 Delft3D- Sediment parameter setting sea.sed

Data group	Parameter	Description	Value
Sediment overall		*Csoil*	1e+6 [kg/m^3]
		IopSus	0 [-]
	Sediment 1	*SedType*	sand
		RhoSol	2650 [kg/m^3]
		SedDia	2e-4 [m]
		CDryB	1600 [kg/m^3]
		IniSedThick	sand.sdb
		FacDSS	1 [-]
	Sediment 2	*SedType*	sand
		RhoSol	2650 [kg/m^3]
		SedDia	5e-4 [m]
		CDryB	1600 [kg/m^3]
		IniSedThick	sand.sdb
		FacDSS	1 [-]

Table A.3 Morphology input file sea.mor

Data group	Parameter	Description	Value
Morphology		MorFac	#mor.mft#[1]
		MorStt	15 [min]
		Thresh	0.02 [m]
		MorUpd	True
		EqmBc	True
		DensIn	True
		AksFac	1 [-]
		RWave	2 [-]
		Rouse	False
		AlfaBs	10 [-]
		AlfaBn	15 [-]
		Sus	0.5 [-]
		Bed	0.5 [-]
		SusW	0.0 [-]
		BedW	0.3 [-]
		SedThr	0.25 [m]
		ThetSD	0.4 [-]
		HMaxTH	0 [m]
		FWFac	0.1 [-]
		EpsPar	False
		IopKCW	[1]
		RDC	0.01 [-]
		RDW	0.02 [-]
		Espir	1 [-]
		ISlope	2 [-]
		AShld	0.85 [-]

		BShld	0.5 [-]
		IHidExp	1 [-]
		UpdInf	True
Underlayer		IUnderLyr	2 [-]
		ExchLyr	False
		TTLForm	1 [-]
		ThTrLyr	0.1 [m]
		MxNULyr	10 [-]
		ThUnLyr	5 [m]
		IniComp	sea.ini
Output		AverageAtEachOutputTime	True
		Dm	True

Note[1]: mor.mft defines the variable MorFac (§3.3.8)

Table A.4 Delft3D-MDF setting est.mdf

Data group	Parameter	Description	Value
Domain	*Grid parameters*	*Grid*	est.grd
		Enclosure	est.enc
		Grid points-M	88
		Grid points-N	37
		Latitude	46.25 [°]
		Orientation	0
		Layers	9 (2,5,10,22,22,22,10,5,2)
	Bathymetry	*File*	est.dep
	Dry Points	*n.a.*	
	Thin dams	*n.a.*	
Time Frame		*Reference date*	25 09 1997
		Simulation start time	26 09 2001
		Simulation stop time	11 04 2002
		Time step	1 [min]
		Local time zone	0 (+GMT)
Processes	*Salinity*		
	Sediments		
	Wind		
	Wave		
	Online Delft3D-WAVE		
Initial conditions		*File*	tri-rst.rest.3900
Boundaries	*n.a.*	*n.a.*	*n.a.*
Physical parameters	*Constants*		
	Hydrodynamic	*Gravity*	9.81 [m/s^2]
		Water density	1025 [kg/m^3]
		Air density	1 [kg/m^3]
		Temperature	15 [°C]
	Wind drag coefficients	*First breakpoint*	0.0025 [-] 0 [m]
		Second breakpoint	0.0289 [-] 100 [m]
	Roughness	*Chezy (Uniform)*	U = 58 V= 58
		Stress formulation	Van Rijn 2004
		Wall roughness	Free
Viscosity	*Background*	*Hor. eddy viscosity*	1 [m^2/s]

		Hor. eddy diffusivity	1 [m^2/s]
		Vert. eddy viscosity	9.9999997e-5 [m^2/s]
		Vert. eddy diffusivity	9.9999997e-5 [m^2/s]
		Model 3D turbulence	k-Epsilon
Sediment		*File*	est.sed
Morphology		*File*	est.mor
Wind	*Uniform*	*File*	sea.wnd
		Interpolation	linear
Numerical parameters	*Drying and flooding*		Centres and faces
	Depth specified at		Grid cell corners
	Depth at centre		Max
	Depth at faces		Mor
	Threshold depth		0.1 [-]
	Marginal depth		-999 [-]
	Smoothing time		0 [-]
	Advection scheme	*Momentum*	cyclic
		Transport	cyclic
	Forester filter	*Horizontal*	True
		Vertical	False
	Correction for sigma		True
Additional parameters	*Cstbnd*		#YES#
	BarocP		#N#
	TraFrm		#vrijn04.frm#
	Gammax		0.55 [-]
	ubcom		#yes#
Output	*Storage*	*Map results start*	26 09 2001
		Map results stop	11 04 2002
		Interval	1505 [min]
		History interval	10 [min]
		Map results start	26 09 2001
		Map results stop	11 04 2002
		Interval	60 [min]
		Restart interval	14900 [min]

Table A.5 Delft3D- Sediment parameter setting est.sed

Data group	Parameter	Description	Value
Sediment overall		*Csoil*	1e+6 [kg/m^3]
		IopSus	0 [-]
	Sediment 1	*SedType*	sand
		RhoSol	2650 [kg/m^3]
		SedDia	2e-4 [m]
		CDryB	1600 [kg/m^3]
		IniSedThick	0 [m]
		FacDSS	1 [-]
	Sediment 2	*SedType*	sand
		RhoSol	2650 [kg/m^3]
		SedDia	5e-4 [m]
		CDryB	1600 [kg/m^3]
		IniSedThick	20 [m]

		FacDSS	1 [-]

Table A.6 Morphology input file est.mor

Data group	Parameter	Description	Value
Morphology		MorFac	#mor.mft#
		MorStt	15 [min]
		Thresh	0.02 [m]
		MorUpd	True
		EqmBc	True
		DensIn	True
		AksFac	1 [-]
		RWave	2 [-]
		Rouse	False
		AlfaBs	10 [-]
		AlfaBn	15 [-]
		Sus	0.5 [-]
		Bed	0.5 [-]
		SusW	0.0 [-]
		BedW	0.3 [-]
		SedThr	0.25 [m]
		ThetSD	0.4 [-]
		HMaxTH	0 [m]
		FWFac	0.1 [-]
		EpsPar	False
		IopKCW	[1]
		RDC	0.01 [-]
		RDW	0.02 [-]
		Espir	1 [-]
		ISlope	2 [-]
		AShld	0.85 [-]
		BShld	0.5 [-]
		IHidExp	1 [-]
		UpdInf	True
Underlayer		IUnderLyr	2 [-]
		ExchLyr	False
		TTLForm	1 [-]
		ThTrLyr	0.1 [m]
		MxNULyr	10 [-]
		ThUnLyr	5 [m]
		IniComp	est.ini
Output		AverageAtEachOutputTime	True
		Dm	True

Table A.7 Delft3D-MDF setting riv.mdf

Data group	Parameter	Description	Value
Domain	*Grid parameters*	*Grid*	riv.grd
		Enclosure	riv.enc
		Grid points-M	136
		Grid points-N	11

		Latitude	46.25 [°]
		Orientation	0
		Layers	1
	Bathymetry	*File*	riv.dep
	Dry Points	*n.a.*	
	Thin dams	*n.a.*	
Time Frame		*Reference date*	25 09 1997
		Simulation start time	26 09 2001
		Simulation stop time	11 04 2002
		Time step	1 [min]
		Local time zone	0 (+GMT)
Processes	*Salinity*		
	Sediments		
	Wind		
	Wave		
	Online Delft3D-WAVE		
Initial conditions		*File*	tri-rst.rriv.3900
Boundaries	*BeaverArmyTerminal*	*M1*	136
		M2	136
		N1	8
		N2	2
		Type	Time series
		Forcing	Harmonic
Physical parameters	*Constants*		
	Hydrodynamic	*Gravity*	9.81 [m/s^2]
		Water density	1025 [kg/m^3]
		Air density	1 [kg/m^3]
		Temperature	15 [°C]
	Wind drag coefficients	*First breakpoint*	0.0025 [-] 0 [m]
		Second breakpoint	0.0289 [-] 100 [m]
	Roughness	*Chezy (Uniform)*	U = 48 V= 48
		Stress formulation	Van Rijn 2004
		Wall roughness	Free
Viscosity	*Background*	*Hor. eddy viscosity*	1 [m^2/s]
		Hor. eddy diffusivity	1 [m^2/s]
		Vert. eddy viscosity	9.9999997e-5 [m^2/s]
		Vert. eddy diffusivity	9.9999997e-5 [m^2/s]
		Model 3D turbulence	k-Epsilon
Sediment		*File*	riv.sed
Morphology		*File*	riv.mor
Wind	*Uniform*	*File*	riv.wnd
		Interpolation	linear
Numerical parameters	*Drying and flooding*		Centres and faces
	Depth specified at		Grid cell corners
	Depth at centre		Max
	Depth at faces		Mor
	Threshold depth		0.1 [-]
	Marginal depth		-999 [-]
	Smoothing time		0 [-]

	Advection scheme	*Momentum*	cyclic
		Transport	cyclic
	Forester filter	*Horizontal*	True
		Vertical	False
	Correction for sigma		True
Additional parameters	*Cstbnd*		#YES#
	BarocP		#N#
	TraFrm		#vrijn04.frm#
	Gammax		0.55 [-]
	ubcom		#yes#
	Filbc0		#NetRiverDischarge.bcr#[1]
Output	*Storage*	*Map results start*	26 09 2001
		Map results stop	11 04 2002
		Interval	1505 [min]
		History interval	10 [min]
		Map results start	26 09 2001
		Map results stop	11 04 2002
		Interval	60 [min]
		Restart interval	14900 [min]

Note[1]: #NetRiverDischarge.bcr# defines the variable river discharge

Table A.8 Delft3D- Sediment parameter setting riv.sed

Data group	Parameter	Description	Value
Sediment overall		*Csoil*	1e+6 [kg/m^3]
		IopSus	0 [-]
	Sediment 1	*SedType*	sand
		RhoSol	2650 [kg/m^3]
		SedDia	2e-4 [m]
		CDryB	1600 [kg/m^3]
		IniSedThick	0 [m]
		FacDSS	1 [-]
	Sediment 2	*SedType*	sand
		RhoSol	2650 [kg/m^3]
		SedDia	5e-4 [m]
		CDryB	1600 [kg/m^3]
		IniSedThick	20 [m]
		FacDSS	1 [-]

Table A.9 Morphology input file riv.mor

Data group	Parameter	Description	Value
Morphology		MorFac	#mor.mft#[1]
		MorStt	15 [min]
		Thresh	0.02 [m]
		MorUpd	False
		EqmBc	True
		DensIn	True
		AksFac	1 [-]
		RWave	2 [-]
		Rouse	False

		AlfaBs	10 [-]
		AlfaBn	15 [-]
		Sus	0.5 [-]
		Bed	0.5 [-]
		SusW	0.0 [-]
		BedW	0.3 [-]
		SedThr	0.25 [m]
		ThetSD	0.4 [-]
		HMaxTH	0 [m]
		FWFac	0.1 [-]
		EpsPar	False
		IopKCW	[1]
		RDC	0.01 [-]
		RDW	0.02 [-]
		Espir	1 [-]
		ISlope	2 [-]
		AShld	0.85 [-]
		BShld	0.5 [-]
		IHidExp	1 [-]
		UpdInf	True
Underlayer		IUnderLyr	2 [-]
		ExchLyr	False
		TTLForm	1 [-]
		ThTrLyr	0.1 [m]
		MxNULyr	10 [-]
		ThUnLyr	5 [m]
Output		AverageAtEachOutputTime	True
		Dm	True

Appendix B Overview sediment distribution Columbia River estuary